國立臺灣大學理學院海洋研究所

博士論文

Institute of Oceanography
College of Science
National Taiwan University
Doctoral Dissertation

龜山島淺海熱泉系統中烏龜怪方蟹共生體之環境互動與適應機制

Environmental Interactions and Adaptive Mechanisms of the *Xenograpsus testudinatus* Holobiont in Kueishan Island Shallow-Water Hydrothermal Vent System

邱　翎

Ling Chiu

指導教授: 魏志潾 博士

曾庸哲 博士

Advisor: Chih-Lin Wei, Ph.D.

Yung-Che Tseng, Ph.D.

中華民國 114 年 3 月

March 2025

doi:10.6342/NTU202500809

國立臺灣大學博士學位論文

口試委員會審定書

DOCTORAL DISSERTATION ACCEPTANCE CERTIFICATE
NATIONAL TAIWAN UNIVERSITY

龜山島淺海熱泉系統中烏龜怪方蟹共生體之環境互動與適應機制

Environmental Interactions and Adaptive Mechanisms of the *Xenograpsus testudinatus* Holobiont in Kueishan Island Shallow-Water Hydrothermal Vent System

本論文係 **邱 翎 D10241002** 在國立臺灣大學 **海洋研究所** 完成之博士學位論文，於民國 114 年 3 月 18 日承下列考試委員審查通過及口試及格，特此證明。

The undersigned, appointed by the **Institute of Oceanography** on 18 March 2025 have examined a Doctoral Dissertation entitled above presented by **Ling Chiu, D10241002** candidate and hereby certify that it is worthy of acceptance.

口試委員 Oral examination committee:

魏志偉 (指導教授 Advisor)　　葉昌哲 (指導教授 Advisor)　　藤平晉

湯森林　　呂良忠

系（所、學位學程）主管 Director: 黃千芬

doi:10.6342/NTU202500809

誌謝

三年半的博士生涯，首先要感謝我的指導老師，曾庸哲老師以及魏志潾老師，因為有兩位老師亦師亦友的陪伴，學生在這個階段的研究才得以順利完成，還有參與口試的湯森林老師、藤井賢彥老師、吳貫忠老師、黃鵬鵬老師、于宏燦老師。每一位老師的鼓勵與建議都給予我非常多的想法與幫助，如同我對於學術研究的忠旨，來自不同領域的看法與專業都讓我受益良多，所有看法與討論都將成為日後精益求精的養分。

時間真的過得很快，進入中興生科恍如昨日。說起進入魚類生理研究，是在李宗翰老師引領下展開，因為小莊，我才有機會認識李宗翰老師，進入到這個水生生物研究的大家庭，父親般的關心、嚴師的標準是李老師給我的第一印象，也讓我在大學最後四個月，參與了人生第一篇國際期刊的發表。碩士班雖然曲折離奇，但多虧于宏燦老師、黃鵬鵬老師的指導，讓我能順利完成碩士研究，延續了我對魚類及各種水生生物研究的熱忱與興趣，也與小莊一起完成了黃老師夢想中的許多研究，成果陸續發表在相當不錯的國際期刊。

因為黃鵬鵬老師的推薦，加上我對不同領域知識的渴望，與曾庸哲老師多次~~把酒言歡~~討論後決定在臨海研究站以熱泉怪方蟹共生體作為主題進行博士班的研究。在魏志潾老師的幫忙以及蕭仁傑老師、周銘翊老師、鍾明宗老師的監督下順利完成博士班資格考。之後的一年半除了與林子皓老師實驗室合作持續進行龜山島怪方蟹的研究外，也與楊姍樺老師實驗室有非常多微生物研究的交流，吳貫忠老師也根據自身專業與經驗給予我論文上非常多的想法與建議。

學生研究生涯終於結束，要感謝的人很多，我太太小莊，不管是在研究還是陪伴上都給予我最多的愛與支持，也是我這輩子最感謝的人，希望我們能一直一起快樂的走下去。大顧，在臨海如孤島般的生活中，如我身心靈消毒的一抹光芒，祝你身體健康萬事如意。龜山島團隊：敏真、文爰、蘇淮，還要特別感謝藍船長與金陵大發，還有盧教練兄弟，沒有大家的幫忙，採樣無法如此順利。還有臨海 B106 及細生所 R144 的各位，期間也要感謝李宗翰老師、李龍緣老師、于宏燦老師時常的關心，所有人的幫忙與支持都是我不斷前進的動力。

最後，再次感謝小莊，一直以來對我的支持與包容，還有學術上的交流與合作，要找到興趣相投的伴侶真的不容易。感謝我的父母，感謝你們從小到大的照護、支持與鼓勵，此篇獻給所有愛我的人，以及我愛的人，謝謝你們。

邱 翎 謹誌於 臺灣台北

民國 114 年 3 月

doi:10.6342/NTU202500809

摘要

近年來，淺水熱泉因其複雜的特性，受到越來越多的關注，這些特性受到多種表層海洋因素的影響，如日照、潮汐、水流和季節性變化，與深海熱泉有明顯的差異。台灣東北方宜蘭海域的龜山島，同時擁有淺水熱泉及珊瑚生態系統，相當適合作為研究熱泉環境相互作用的自然實驗室。通過監測水質及聲景特徵，我們觀察到熱泉區的間歇性熱液排放，硫化物 (HS^-/S^{2-})、溶解無機碳 (dissolved inorganic carbon, DIC) 和 pH 值為區分龜山島周圍棲地的重要指標，尤其在活躍期展現了熱泉活動在淺海環境中時間與空間的動態變化。

烏龜怪方蟹 (*Xenograpsus testudinatus*) 作為龜山島熱泉系統最優勢其中一種動物，已發展出能存活於熱泉極端環境中的生理機制來維持體內恆定。然而，其共生菌與環境變化之間的相互作用仍未完全了解。利用全長 16S rRNA 基因定序和 Alpha 多樣性分析，我們觀察到水中細菌群落與熱泉相關的水質參數有相關性。在綱 (class) 的階層下，Campylobacteria 和 Gammaproteobacteria 的相對豐度有相反的變化趨勢，其中，一種硫還原菌 *Thioreductor* 是 Campylobacteria 中相對豐度最高的菌屬，而 Gammaproteobacteria 中最豐富的菌屬則是一種硫氧化菌 *Thiomicrorhabdus*，說明環境變動與微生物的物質利用之間可能密切相關。而對怪方蟹 *X. testudinatus* 來說，鰓的菌群與水質化學變化的相關性高於殼表的細菌，儘管 Campylobacteria 中的 *Sulfurovum* 在鰓和殼表都是優勢菌屬，但殼表的菌群有更高的多樣性。螢光原位雜交 (fluorescence in situ hybridization, FISH) 支持鰓中 *Sulfurovum* 的優勢地位。功能預測分析顯示菌群主要進行硫氧化 (sulfur oxidation) 及脫硝作用 (denitrification)，相關反應可能由 *Sulfurovum* 主導。由於在海水中 *Sulfurovum* 並不是豐度較高的菌屬，怪方蟹的鰓可能為其及相關硫氧化菌 (sulfur-oxidizing bacteria, SOB) 提供了一個適合定殖 (colonization) 的微棲地 (microhabitat)，進而幫助宿主乃至共生體的硫解毒機制 (sulfide detoxification) 及有機物質的提供。

熱泉的間歇性使得 *X. testudinatus* 反覆暴露於一般海水與極端環境之間。為了研究牠們的適應機制，我們將實驗室馴化的 *X. testudinatus* 回放到原熱泉棲地，採樣並透過定序技術分析鰓的細菌微生物群 (bacterial microbiota)、轉錄體 (transcriptome)，同時測定其氨基酸及脂肪酸組成。在回放轉移後的 0, 1, 2, 4 小時 (H) 期間，細菌多樣性在 2H 時觀察到的屬數量 (observed genus taxa number) 和

doi:10.6342/NTU202500809

Chao 1 顯著下降，*Sulfurovum* 在 1H 豐度最高，並伴隨著異營性功能 (heterotrophy) 的減少和氮代謝及硫化物代謝的增加，同時轉錄組顯示宿主組織中 GTPase 活性和肌動蛋白骨架重構 (actin cytoskeleton remodeling) 相關的路徑被上調，而幾丁質和外骨骼的形成 (chitin and cuticle formation) 受到抑制。在之後的 2H 和 4H，硫化物代謝有逐漸增強的趨勢，與硫化物解毒相關的氨基酸牛磺酸 (taurine) 也顯著減少，而與氮代謝相關的組氨酸 (histidine)、精氨酸 (arginine) 和谷氨酰胺 (glutamine) 則在 2H 及 4H 時累積，同時與上述胺基酸相關的代謝酵素基因如谷氨酰胺酶 (glutaminase)、組氨酸氨基水解酶 (histidine ammonia-lyase) 及丙氨酸轉氨酶 (alanine transaminase) 也被上調。抗氧化防禦 (antioxidant defense) 則藉由穀胱甘肽過氧化酶 (glutathione peroxidase) 及麩胱甘肽轉移酶 (glutathione S- transferase) 的旁系同原體 (paralogs) 在回放過程中持續進行，說明抗氧化機制對烏龜怪方蟹適應熱泉環境的重要性。此外，脂肪酸含量雖然並沒有顯著變化，相關性和倍數差異 (fold change) 分析顯示不飽和脂肪酸可能比飽和脂肪酸對環境的反應更加明顯，脂肪酸的累積與消耗可能與細胞結構的維持及抗氧化物的調節相關。

上述結果顯示 *X. testudinatus* 熱泉共生體棲息於一個比以往認知更為複雜的動態環境中，我們的研究透過多方面的分析，包含環境變量、細菌群時間性變化以及宿主生理代謝反應，探討不同層面之間的交互作用及相互依賴關係。研究熱泉共生體為我們提供了生命在挑戰性環境中所展現出韌性的相關見解，並且揭示了極端條件下跨域共演化 (inter-domain evolution) 的奧秘。

關鍵字:甲殼類細菌共生體、微生物組、轉錄組、代謝物組、硫氧化菌、硫解毒、脫硝作用、抗氧化防禦

doi:10.6342/NTU202500809

Abstract

Shallow-water hydrothermal vents have garnered growing attention due to their complex characteristics, influenced by various epipelagic factors such as insolation, tides, currents, and seasonal changes, in contrast to their deep-sea analogues. Kueishan Island, which harbors both shallow-water hydrothermal and coral ecosystems, provides an exceptional natural laboratory for investigating hydrothermal environmental interactions. We captured sporadic fluid discharges at the vent site by monitoring water quality and soundscape features. Sulfide (HS^-/S^{2-}), dissolved inorganic carbon (DIC), and pH levels were identified as key indicators for habitats differentiation around Kueishan Island, especially during active venting periods, which highlights the profound spatial and temporal dynamics of hydrothermal activity in shallow water marine environments.

The brachyuran vent crab *Xenograpsus testudinatus*, a dominant metazoan inhabiting Kueishan Island hydrothermal vent system, has developed robust physiological mechanisms to sustain homeostasis in this extreme environment. However, the interactions between its symbiotic bacteria and environmental fluctuations remain incompletely understood. Through the application of full-length 16S rRNA gene sequencing and alpha diversity analysis, we observed strong correlations between water bacterial community and hydrothermal-associated physicochemical parameters at the vent site. The relative abundances of Campylobacteria and Gammaproteobacteria exhibited inverse temporal patterns, where *Thioreductor*, a sulfur-reducing bacteria, was the most abundant genus within Campylobacteria, while the sulfur-oxidizing *Thiomicrorhabdus* predominated among Gammaproteobacteria, indicating a potential link between environmental dynamics and microbial resource availability. In *X. testudinatus*, gill-associated bacteria showed greater correlations with water quality

doi:10.6342/NTU202500809

compared to those present on the carapace surface. While *Sulfurovum* (Campylobacteria) was predominant in both the gills and carapace surface, the carapace surface demonstrated higher bacterial diversity. Furthermore, fluorescence *in situ* hybridization (FISH) and functional prediction analysis supported the branchial predominance of *Sulfurovum*, which performs sulfur oxidation and denitrification processes. Given that *Sulfurovum* is not abundant in the ambient seawater, the gills may serve as an enclave for sulfur-oxidizing bacteria (SOB) such as *Sulfurovum*, facilitating sulfide detoxification and organic production to the host.

The intermittent nature of hydrothermal venting repeatedly exposes *X. testudinatus* to transitions between normal seawater and extreme environmental conditions. To investigate their adaptive responses, we reintroduced lab-acclimated *X. testudinatus* to their native habitat and analyzed their gill tissue for bacterial microbiota, transcriptome, amino acid compositions, and fatty acid profiles. During the period, 0, 1, 2, and 4 hours (H) post-reintroduction, bacterial diversity showed a significant reduction in observed taxa numbers and Chao 1 estimates at the genus level at 2H. *Sulfurovum* had the highest abundance at 1H, coinciding with elevated nitrogen and sulfide metabolism and reduced heterotrophy-associated functions. Meanwhile, transcriptomic analysis revealed upregulation of GTPase activity and actin cytoskeleton remodeling in the host tissue, while chitin and cuticle formation pathways were suppressed. At subsequent time points (2H or 4H), both sulfide metabolism and stress responses showed progressive enhancement. Taurine, crucial for sulfide detoxification, significantly depleted at 2 and 4H. Additionally, nitrogen metabolism-related amino acids, histidine, arginine, and glutamine, accumulated at the later time points, accompanied by upregulation of related enzyme genes, including glutaminase, histidine ammonia-lyase, and alanine transaminase. During the reintroduction, fatty acid levels did not show significant

doi:10.6342/NTU202500809

changes; however, correlation and fold change analyses revealed that unsaturated fatty acids had more pronounced responses to environmental transition compared to saturated fatty acids.

These analyses demonstrate that *X. testudinatus* holobiont exists in a dynamic environment, more complicated than previously acknowledged. Our study provides a multi-faceted examination of environmental variables, bacteria community dynamics, and the crab host's physiological responses, elucidating their intricate interactions and interdependencies. Exploring hydrothermal-endemic holobionts provides valuable insights into the remarkable resilience of life in a challenging environment, shedding light on the mechanisms of inter-kingdom coevolution under extreme conditions.

Keywords: Crustacean-bacteria symbiosis, microbiome, transcriptome, metabolome, sulfide-oxidizing bacteria, sulfide detoxification, denitrification, antioxidant defense

doi:10.6342/NTU202500809

Contents

doi:10.6342/NTU202500809

doi:10.6342/NTU202500809

Background and Aims

Hydrothermal vent (HV) systems are renowned as some of the world's most extreme marine environments, characterized by underwater volcanic activity (Lonsdale, 1977; Glowka, 2003). The chemical-rich fluids that gush from the vents create acidic and high temperature environments (Elderfield and Schultz, 1996; Fisher et al., 2007), which are home to unique microbiota (Van Dover and Trask, 2000; Glowka, 2003). The mixing of reduced vent fluids recharging from the magma chamber with subterranean oxidized seawater substantially impacts the chemistry and biological distribution in the venting area (McDermott et al., 2020). Diverse microorganisms in HVs form a biological bridge between these extreme environments and metazoans, serving as primary biomass sources for food webs that support endemic species of crustaceans, polychaetes, echinoderms, coelenterates, and mollusks (Little and Vrijenhoek, 2003). While deep-sea smokers have been the primary focus of much research since the discovery of HVs on the Galapagos rift (Tarasov et al., 2005; Yucel et al., 2013; Lough et al., 2019), several shallow-water HV systems have been successively identified in recent years, including those off Panarea, Aeolian Island, Italy (Maugeri et al., 2009), Milos Island, Aegean Sea, Greece (Thiermann et al., 1997), and Showa Iwo-jima, Kagoshima, Japan (Oda et al., 2022). Although shallow-water HV systems are partly distinguished from their deep-sea counterparts due to epipelagic and photic junctures, they provide valuable opportunities for exploring organisms and environments influenced by hydrothermal activities.

Located at the rifting end of the Okinawa Trough, the shallow-water HV system off Kueishan Island is situated northeast of Taiwan (Jeng et al., 2004). This HV system consists of several smokers that discharge highly acidic (pH 1.75-4.60), sulfidic and hot fluids (65-116°C), resulting in relatively low pH (5.4-7.3) and dissolved oxygen (3.9-4.9

doi:10.6342/NTU202500809

mg/L) levels compared to normal seawater (Jeng et al., 2004; Han et al., 2014; Chan et al., 2016). Previous studies have identified brachyuran crab species, *Xenograpsus testudinatus*, as the dominant metazoan near these hydrothermal vents, along with 13 mollusk species (Jeng et al., 2004; Chen et al., 2018a). These vent-endemic crabs have been reported to possess strong acid-base regulatory abilities to cope with low pH challenges (Hu et al., 2016; Allen et al., 2020). In addition, symbiotic fungi and bacteria have been found in *X. testudinatus* (Yang et al., 2016; Shaumi et al., 2021), suggesting that *X. testudinatus* functions as a holobiont inhabiting this extreme environment.

To understand how this *X. testudinatus* holobiont adapts to the shallow-water hydrothermal vent system, we aimed to investigate the interactions between the environment, the microbiome, and the crab host. Kueishan Island, located within 10 km of the coastline, serves as an accessible platform for this research. The experiments were designed to achieve three major objectives:

1. To characterize the spatial and temporal effects of shallow-water hydrothermal vents on the submarine environments surrounding Kueishan Island (**Chapter 1**)
2. To investigate the bacterial communities involved in the interactions between the hydrothermal vent environment and the endemic crabs *X. testudinatus* (**Chapter 2**).
3. To examine the responses of *X. testudinatus* holobiont to hydrothermal venting, focusing on the microbiome, transcriptome (RNA-seq), and metabolome (including amino acids and fatty acids) (**Chapter 3**).

doi:10.6342/NTU202500809

Chapter 1

Spatial and Temporal Effects of Shallow-Water Hydrothermal Venting on the Surrounding Environments

doi:10.6342/NTU202500809

1.1 Introduction

Since the first discovery of HV on the Galapagos rift (Tarasov et al. 2005), deep-sea smokers were the primary focus within the majority of related research (Lough et al. 2019; Yucel et al. 2013). Broadly, knowledge of HV systems is primarily based on deep-sea or short-term observations (Price and Giovannelli, 2017), leaving much to be studied about how venting dynamics spatiotemporally influence the submarine environments around shallow-water HVs. With epipelagic and photic junctures, shallow-water HV systems potentially support both chemosynthetic and photosynthetic communities (Price et al., 2013; Chang et al., 2018). Insolation, tidal variation, wave effects, atmospheric precipitation, and air-sea exchange are important factors differentiating them from their deep-sea counterparts (Price and Giovannelli, 2017; Vaucher et al., 2021). Therefore, the natural settings in the traits of primary producers and biological composition may distinguish shallow-water and deep-sea HV systems in certain respects, such as basal resource utilization and trophic structures (Tarasov et al., 2005). The abiotic-biotic interaction between vent fluids, prokaryotes, and eukaryotes serves as a driving force of hydrothermal activity, establishing a specialized biota through incorporative processes and evolution (Perner et al., 2011). While some studies have depicted the geochemical and biological characteristics of shallow-water HV systems, further observations are still needed to assess spatial and temporal variations in environmental conditions influenced by chemically enriched vent fluids (McKenna et al., 2021).

Hydrothermal emissions fundamentally shape oceanic chemistry, crust-lithosphere interactions, and the development of unique chemosynthetic ecosystems (Kadko et al., 1995). These systems exhibit remarkable diversity in geological settings and biological distributions (Tunnicliffe, 1991), creating complex environmental gradients at spatial

doi:10.6342/NTU202500809

scales. The physicochemical conditions within these systems are dynamically influenced by interactions between vent fluids and the up-flow system, as well as the precipitation of minerals, which collectively drive organic production and nutrient cycling (McCollom and Shock, 1998; Martín-Díaz et al., 2024). These geochemical processes regulate the flux of dissolved elements and gases, establishing chemical gradients that characterize hydrothermal fields. Furthermore, temporal variability in chemical constituents often results from phase separation during hydrothermal venting, which can be identified through characteristic fluctuations in temperature, pH, dissolved oxygen, metal ion concentrations, and sulfide levels (Von Damm et al., 2003). Investigating the spatiotemporal dynamics of vent fluids is essential for understanding the evolution of hydrothermal geochemistry and its broader impact on oceanic and lithospheric processes (Matabos et al., 2022).

Aside from commonly used biochemical indicators, sound has been adopted as one of the essential ocean variables (Howe et al., 2019). Sounds from all living organisms (biophony), atmospheric or geophysical events (geophony), and human activities (anthrophony) create a soundscape, which reflects the overall state of an ecosystem (Pijanowski et al., 2011; Erfanian et al., 2019). Investigating soundscapes has emerged as a tool to complement conventional surveys of bioecological and geochemical parameters in difficult-to-access marine ecosystems (Staaterman et al., 2014; Bertucci et al., 2016). Owing to their great speed and distance traveled in water, sounds, compared to other chemical, optic, or physical cues, are particularly effective in the study of marine ecosystems, “speaking out” for marine organisms and environments (Duarte et al., 2021; Minello et al., 2021). Soundscape research has been conducted in various marine ecosystems such as reefs, estuaries, submarine canyons, and seamounts (Kasaya et al., 2015; Putland et al., 2017; Havlik et al., 2022), but remains limited in HV

doi:10.6342/NTU202500809

systems. To fully interpret the environmental dynamics of HVs, sound recording offers a non-invasive method to assess both the biotic and abiotic components (Lin et al., 2019; Chen et al., 2021), which complement the measurement of water quality in our research.

At Kueishan Island, vents located offshore the southeastern tip create one of the most extreme marine environments in the world. In contrast, the submarine areas around the western tip of the island exhibit a non-reefal coral ecosystem with relatively high biodiversity (Chan et al., 2016). Active volcanic features, climate disturbances from typhoons, winter monsoons, and the Kuroshio currents make this island a unique natural laboratory. The shallow-water HV field and surrounding habitats act as an exceptional platform to study the impacts of hydrothermal activity on ambient environments. Here, we investigated the physicochemical and acoustic parameters of Kueishan Island waters on a quarterly basis. Measuring water quality allowed us to understand subsurface mixing driven by atmospheric and geodynamic forces, while characterizing habitat-specific soundscapes revealed the bio-geophysical interactions between HV and coral ecosystems. The spatiotemporal analysis demonstrated the environmental variability associated with shallow-water hydrothermal venting.

doi:10.6342/NTU202500809

1.2 Materials and Methods

Study locations and data collection

Seawater samples and audio data were collected by SCUBA divers from Kueishan Island during daytime. Between August 2020 and October 2022, seawater samples were collected from six sampling sites, including VN (site near the vent), VF (site farer from the vent), C (CO_2 vents without sulfide), S (south), N (north), and T (tail) sites (Fig. 1). Physicochemical conditions were assessed according to temperature, pH value, dissolved oxygen (DO), sulfide (HS^-/S^{2-}) concentration, alkalinity (Alk), and dissolved inorganic carbon (DIC). Temperature, pH, and DO were measured using a multi-parameter meter (Multiline® Multi 3620 IDS, WTW, Weilheim, Germany) equipped with an IDS pH electrode (SenTix® 940, WTW) and an optical IDS dissolved oxygen sensor (FDO® 925, WTW). Alkalinity was determined by following a previously published method (Sarazin et al., 1999). Sulfide concentration was measured by a spectrophotometric method modified from a previous study (Cline, 1969), using a mixed diamine reagent specific for sulfide sulfur, containing N, N-Dimethyl-p-phenylenediamine sulfate and ferric chloride in 50% hydrochloric acid. DIC was analyzed using an analyzer (AS-C3, Apollo SciTech, Newark, DE, USA) and quantified via a non-dispersive infrared (NDIR) CO_2/H_2O analyzer (LI-7000, LI-COR, Lincoln, NE, USA). Bicarbonate (HCO_3^-) and carbonate (CO_3^{2-}) concentrations were calculated using a CO2SYS module within Microsoft Excel according to DIC, temperature, and pH (Pierrot, 2006).

A SoundTrap recorder (ST300 STD, Ocean Instruments, New Zealand) was used in audio data collection. The recorder has a built-in hydrophone with a sensitivity of -175 dB re 1 V/μPa and a working bandwidth of 20 Hz to 60 kHz (±3 dB), which is ideal for capturing most underwater sounds from biological and environmental sources. The

doi:10.6342/NTU202500809

SoundTrap recorder was set to continuous operation with a frequency of 96 kHz, providing broadband recordings at up to 48 kHz. Metrics of sound pressure levels (SPLs) were extracted to characterize soundscapes. At first, we manually listened to the recordings and removed any fragments that were heavily interfered with by noises generated from divers and passing vessels. After noise removal, recordings were divided into 90-sec fragments. Each fragment produced a spectrogram using a discrete Fourier transform with a window size of 9600 without overlapping and subsequently converted to a spectrum by finding the median for each frequency bin. Based on the median spectrum, we calculated frequency band-specific SPLs by integrating the power spectral densities from frequencies 20-200 Hz, 200-2k Hz, and 2k-20k Hz. This approach ensures that our acoustic data accurately reflects the biophonic and geophonic sounds that dominate the local soundscapes and ignore the influence of high-intensity transient signals, such as rare biological sounds or tapping noises produced during fish-instrument interactions (Lin et al., 2021). For each survey, three 90-sec recording fragments were randomly selected from each site to ensure a consistent sampling effort with the physicochemical data.

Spatiotemporal analysis

Firstly, to evaluate the variability of hydrothermal activity, we used the *breakpoints* function from the R package *strucchange* (Zeileis et al., 2002), examining temporal changes in pH levels at the VN site, which has been identified as a tracer for HV fluids (Le Bris et al. 2001). The trend line was estimated for each time interval by applying ordinary least squares regression.

Due to the measurement of multiple parameters, we applied dimension reduction algorithms to analyze the physicochemical and acoustic datasets across time and

doi:10.6342/NTU202500809

sampling sites. DIC, Alk, HCO_3^-, CO_3^{2-}, and S^{2-}, which have right-skewed distributions, were transformed to logarithmic scales. During the logarithmic transformation, CO_3^{2-} and S^{2-} values were increased by one to avoid issues with zero values. After the data transformation, both physicochemical and audio datasets were normalized to a scale of zero to one according to the minimum and maximum values of each parameter. Principal component analysis (PCA) was then conducted to identify the key parameters contributing to the observed environmental fluctuations, using the Python package *pca*. The density distribution of PC1 was presented for the entire, active, and silent periods. The first two principal components, PC1 and PC2, which typically explain most of the total variance, were used in permutational multivariate ANOVA (PERMANOVA) based on Euclidean distances, incorporating the factors Period (active vs. silent), Site, and MonthYear, using the *adonis2* function from the R package *vegan* (Dixon, 2003). A total of 999 permutations were performed to determine the significant contribution of each factor to the PCs.

Uniform manifold approximation and projection (UMAP) was applied to visualize spatiotemporal dynamics of physicochemical and soundscape conditions, projecting the multidimensional dataset into a two-dimensional space while retaining information for exploring data structure (McInnes et al., 2018). The analysis was performed using the Python package *umap*, with a correlation distance metric and a large neighborhood (n_neighbors=100) to learn the global data structure. UMAP coordinates were modeled by using cubic smoothing splines, and the coordinates from different sites were fitted separately to ensure the reconstruction of variations in each sampling site. Equal weight was assigned to all data points, and smoothing parameters were automatically determined using the *csaps* function of the MATLAB Curve Fitting Toolbox.

doi:10.6342/NTU202500809

1.3 Results

Geographical settings and characterizations

Kueishan Island is situated approximately 10 km off the coast of Yilan County, Taiwan (Fig. 2A). A shallow-water HV system is to the southeast of the island (Fig. 2B). The island's name, "Kueishan," literally "Turtle Mountain" in mandarin, is derived from its shape, which resembles a turtle (Fig. 2C). The easternmost tip of the island resembles a turtle's head, while the westernmost tip forms the tail. The vent site (V; 24°50′29.9″N, 121°56′17.2″E, 15-17 m depth) is the primary sampling site for collecting hydrothermal characteristics and the non-vent site, located offshore the western "tail" (T; 24°50′02.4″N, 121°57′42.7″E, 8-10 m depth), serves as the control site for comparing normal water conditions (Fig. 2B). White sulfur plumes are visible on the sea surface around the V site (Fig. 2C), emanating from subsurface vents (Fig. 2D). In the vicinity of the vents, aggregations of HV crabs (*X. testudinatus*) inhabit the area (Fig. 2E), with a white biofilm observed on their carapace surfaces (Fig. 2F)

Physicochemical parameters of the water quality of the whole sampling period

From 2020 to 2025, temporal variations in several physicochemical parameters at the vent site (V) and the tail site (T) offshore Kueishan Island were measured from August 2020 to September 2024 at intervals of 1 to 3 months (Fig. 3). According to our long-term monitoring, the water conditions at the V site were relatively dynamic compared to those at the T site. The parameter with the most similar trend was temperature, which exhibited seasonal variations at both study sites, with a distinct summer peak observed each year around August, ranging from 18.4 to 30.3°C (Fig. 3A). The dissolved oxygen (DO) levels at the T site tended to increase at lower temperatures, and the DO levels at the V site were generally lower than those at the T site (Fig. 3B).

doi:10.6342/NTU202500809

Additionally, baseline DO levels in the waters surrounding Kueishan Island have shown slight shifts over the past few years of monitoring. The highest dissolved oxygen (DO) level measured was 9.25 mg/L at the T site and 8.93 mg/L at the V site, while the lowest levels were 6.19 mg/L and 4.84 mg/L, respectively (Fig. 3B). The pH levels at the V site were lower than those at the T site throughout our monitoring (Fig. 3C). The pH levels at the T site remained around 8.2, while the lowest recorded pH at the V site dropped to 5.8 (Fig. 3C). At the T site, almost no sulfide was measured. In comparison, sulfide concentrations at the V site were recorded above 1000 μM on three occasions: 1185 μM in August 2020, 3480 μM in November 2020, and 1256 μM in April 2022 (Fig. 3D). For the CO_2 metrics, dissolved inorganic carbon (DIC), partial pressure of CO_2 (pCO_2), and alkalinity (Alk) were measured. DIC levels at the T site were consistently around 2000 μM, while two peaks, reaching 3000 μM, were observed at the V site in November 2020 and April 2022 (Fig. 3E). Due to the large range, pCO_2 (μatm) was log10-transformed for display (Fig. 3F). Several extremely high pCO_2 readings were recorded at the V site, with the highest being 22511 μatm (log10 value: 4.35) in April 2022 (Fig. 3F). In contrast, pCO_2 at the T site fluctuated from tens to hundreds of μatm, once reaching the low thousands but not exceeding 2000 μatm (log10 value: 3.30). Lastly, the alkalinity (Alk) at the V site was lower than at the T site for about half of the monitoring period (Fig. 3G). The highest Alk values were 2813 μM at the T site and 2712 μM at the V site, while the lowest Alk values were 1989 μM and 1425 μM, respectively.

Physicochemical and acoustic investigations surrounding Kueishan Island

From August 2020 to October 2022, we investigated the physicochemical and acoustic conditions surrounding Kueishan Island at intervals of 1 to 3 months. During this period, apart from the V and T sites, the study also included the south (S), north (N),

doi:10.6342/NTU202500809

and CO_2 (C) sites. Additionally, a site farther from the main vents (approximately 15 m away) was added and named the VF site, and the original V site was renamed the VN site, which is nearer to the vents (Fig. 1). In addition to the previously mentioned parameters, bicarbonate (HCO_3^-), carbonate (CO_3^{2-}), and sound pressure levels (SPLs) across three different frequencies 20–200 Hz, 200–2 kHz, and 2 kHz–20 kHz were also recorded. The comparison of water conditions between the VN and T sites is shown over time (Fig. 4), and comparisons for the other sites are also provided, although some data are missing (Fig. 5). As pH serves as a tracer of hydrothermal activity, we performed breakpoint analysis to examine the temporal variation in pH levels at the VN site (Fig. 6). Two breakpoints were identified, November 2020 and August 2021. Hence, the entire period was divided into two active periods, including the first before November 2020, the second beginning from November 2021, and a silent period spanning from February to August 2021.

Indicators and factors that influence the environment

PCA was used to determine spatio-temporal variations of water conditions (Fig. 7). PC1 accounted for 42.81% of the total variance, and the submarine conditions were positively and largely affected by sulfide and DIC (Fig. 7A). Based on the PC1 density distribution, water conditions varied across different sites, with the VN site showing the most distinct differences compared to the others during both the entire and active periods (Fig. 7B, C). However, such site-dependent variation was not observed during the silent period (Fig. 7D). According to PERMANOVA, the factor Site significantly explained the most (44.9%) of the PC1 variance (Table 1), suggesting the preponderance of hydrothermal activity contributing to the dissimilarity of different habitats. On the other hand, the interaction of Period and Site (23.2%; Table 1)

doi:10.6342/NTU202500809

reinforces the temporal trend of hydrothermal venting. PC2 merely accounted for 18.18% of the total variance on which temperature and SPLs at > 2 kHz of sound were positively influential (Fig. 7A). In PERMANOVA, MonthYear explained 66.0% of the PC2 variance (Table 1). The interaction between Site and MonthYear (12.1%) also contributed significantly.

Temporal shifts in physicochemical conditions and soundscape in Kueishan Island waters

According to the UMAP results, the physicochemical conditions at the VN, VF, and C sites showed a different pattern compared to those at the S, N, and T sites before February 2021 and after August 2021 (Fig. 8A).

Regarding the soundscape, before February 2021, the conditions of VN, VF, C, S, and N sites were similar, except for the T site. In February 2021, the soundscape of the N site shifted to resemble that of the T site, while the remaining sites were still influenced by hydrothermal activity (Fig. 8B). Subsequently, as winter ended in May 2021, the rise in water temperature affected the biological activities around Kueishan Island. During the warmer months of July and August 2021, both the N and S sites exhibited patterns similar to the T site.

doi:10.6342/NTU202500809

1.4 Discussion

Research on deep-sea and shallow-water HV systems has increasingly been treated as two independent fields in recent years. While studies of the deep-sea HVs have long fueled curiosity about the potential of marine life, shallow-water HVs have been receiving growing attention due to their proximity to human and atmospheric activities. The variability of shallow-water HV systems plays a crucial role in shaping biological and geological features. In the present study, we monitored the water quality and soundscape off Kueishan Island, a volcanic island surrounded by shallow-water HVs and corals, to explore the effects of hydrothermal activity on marine environments. During our two-year monitoring, two active venting periods were observed, separated by a silent period. Physicochemical conditions displayed a clear pattern of periodic transitions, while the soundscape exhibited greater complexity, likely influenced by seasonal biological activities.

Physicochemical indicators of hydrothermal activity

Previous studies have primarily identified pH as a tracer for HV fluids (Le Bris et al. 2001). Long-term observations at Kueishan Island suggest that DIC and sulfide, typically enriched in the fluid (Tivey, 2007), can also serve as indicators of hydrothermal activity. Higher levels of ambient DIC and pCO_2 indicated increased CO_2 emissions, which reduced water pH (Zeebe and Wolf-Gladrow, 2001). During active venting periods, as defined by pH levels, the vent site of Kueishan Island exhibits distinct environmental conditions compared to other habitats. However, these differences were not present during the silent period. This implies that the hydrothermal impacts on surrounding habitats are not constant, due to intermittent discharges of the

doi:10.6342/NTU202500809

vent fluid as well as the influence of tides and currents. Aperiodic venting has also been observed in another shallow-water HV system at Milos Island (Yucel et al., 2013).

Variability in hydrothermal vent chemistry

Moreover, the environmental conditions influenced by hydrothermal activity were not entirely identical. The highest recorded sulfide concentration in the first active period was higher than that in the second. Given the rapid oxidation of sulfide in natural environments (Houghton et al. 2019), this difference may also stem from the sampling timing. Even daily monitoring intervals have revealed significant fluctuations (Yücel et al. 2013). On the other hand, the minimum levels of DO, Alk, and pH were lower in the second active period compared to the first, while DIC concentration and pCO_2 were higher. These disparities between two active periods, or even individual sampling events, could be attributed to venting intensity, duration, fluid compositions, and surrounding environmental factors. Therefore, high-resolution temporal monitoring is essential for understanding the dynamics of these hydrothermal vents.

Hydrothermal influences on soundscape

Nevertheless, seasonal effects contributed to environmental variations in specific ways. Water temperature fluctuations are crucial for investigating the sound production of animals in subtropical coral reef ecosystems. The warmer breeding season led to increasing high-frequency pulse noises from snapping shrimps (> 2 kHz) and low-frequency fish sounds (0.2-2 kHz; Lin et al. 2023). These seasonal effects on the occurrence and activity of sound-producing organisms may influence the soundscape, as observed in coral reefs off Sesoko Island, Okinawa, Japan (Lin et al., 2021). During the warmer seasons (July and August 2021), all habitats, except for the VN site, shared

doi:10.6342/NTU202500809

soundscape similarities with the T site, which hosts coral ecosystems with high biodiversity. This may reflect contributions from fish assemblages (< 1 kHz) and mobile invertebrates such as sea urchins (< 2 kHz), snapping shrimps (> 2 kHz), and lobsters (> 10 kHz, Elise et al. 2019; Jezequel et al. 2020). The distribution and behavior of these organisms may change not only due to seasonal effects but also potentially in response to hydrothermal activity (Grassle 1985), leading to variations in the soundscape. Furthermore, peaks in SPLs < 200 Hz observed in the vent area during active periods were likely associated with venting events. Previous studies have shown that hydrothermal vents produce sounds at frequencies of 5–15 and 10–250 Hz (Crone et al. 2006). Bubbling activity at 100–2000 Hz may also contribute to the soundscape at the VN, VF, and C sites, where gas bubbles were observed (Longo et al. 2024). During the silent period, SPLs at 200–2000 Hz remained high at the C site, suggesting that the CO_2 vents there may not directly relate to hydrothermal activity at the VN site. Since soundscapes encompass all geophysical and biological factors in the environment, there could be phenomena involved that were not considered in this study, such as currents, monsoons, and typhoons (Liang et al. 2003; Lebrato et al. 2019).

Summary

Shallow-water HV systems provide an accessible and cost-effective proxy for studying hydrothermal activity and its effects on surrounding environments and vent-associated holobionts (Chiu et al. 2022; Chou et al. 2023). Meanwhile, they create a dynamic and unique marine environment throughout the entire ocean. However, their accessibility also exposes them to anthropogenic impacts. Polycyclic aromatic hydrocarbons, byproducts of incomplete combustion and pyrolysis of organic materials such as coals, fossil fuels, and oil spills, have been detected in the tissues of *X.*

doi:10.6342/NTU202500809

testudinatus inhabiting Kueishan Island (Lee et al. 2023). While shallow-water HVs have been used to simulate CO_2-induced ocean acidification (Dahms et al. 2018), these models easily overlooked potential influences of climatic and geographic factors. Given that shallow-water HV fields are inherently dynamic and concurrently subject to human activities, more frequent and comprehensive data collection is further required. Deploying underwater loggers for chlorophyll A, DO, temperature, pressure, conductivity, depth, turbidity, wave height, and tide to monitor on-site physicochemical conditions and implementing continuous soundscape recording to enable timely and integrated observations. These approaches will enhance our mastery of hydrothermal activity as a driver of environmental variability while providing extensive spatial and temporal coverage for future research.

doi:10.6342/NTU202500809

1.5 Tables and Figures

Chapter 1

Table 1; Figures 1-8

doi:10.6342/NTU202500809

Table 1. Permutational multivariate analysis of variance (PERMANOVA) results for PC1 and PC2 values. PC1 and PC2 values were derived from principal component analysis (PCA) of observed physicochemical and acoustic parameters. Df, degrees of freedom; SS, sum of squares; R^2, coefficient of determination; F, F value by permutation; *P*, *P*-value obtained by 9999 permutations (significance, $P < 0.05$). The factors Period (active vs. silent), Site (VN, VF, C, S, N, T), MonthYear, and their interactions were defined.

PC1

Factor	df	SS	R^2	*F*	*P*
Period	1	2.316	0.0732	321.263	< 0.001
Site	5	14.201	0.4490	393.944	< 0.001
MonthYear	9	2.926	0.0925	45.099	< 0.001
Period x Site	5	7.322	0.2315	203.113	< 0.001
Site x MonthYear	29	4.144	0.1310	19.818	< 0.001
Residual	100	0.721	0.0228		
Total	149	31.629	1		

PC2

Factor	df	SS	R^2	*F*	*P*
Period	1	0.683	0.0508	416.329	< 0.001
Site	5	1.803	0.1343	219.923	< 0.001
MonthYear	9	8.856	0.6595	600.016	< 0.001
Period x Site	5	0.297	0.0221	36.219	< 0.001
Site x MonthYear	29	1.626	0.1211	34.189	< 0.001
Residual	100	0.164	0.0122		
Total	149	13.429	1		

doi:10.6342/NTU202500809

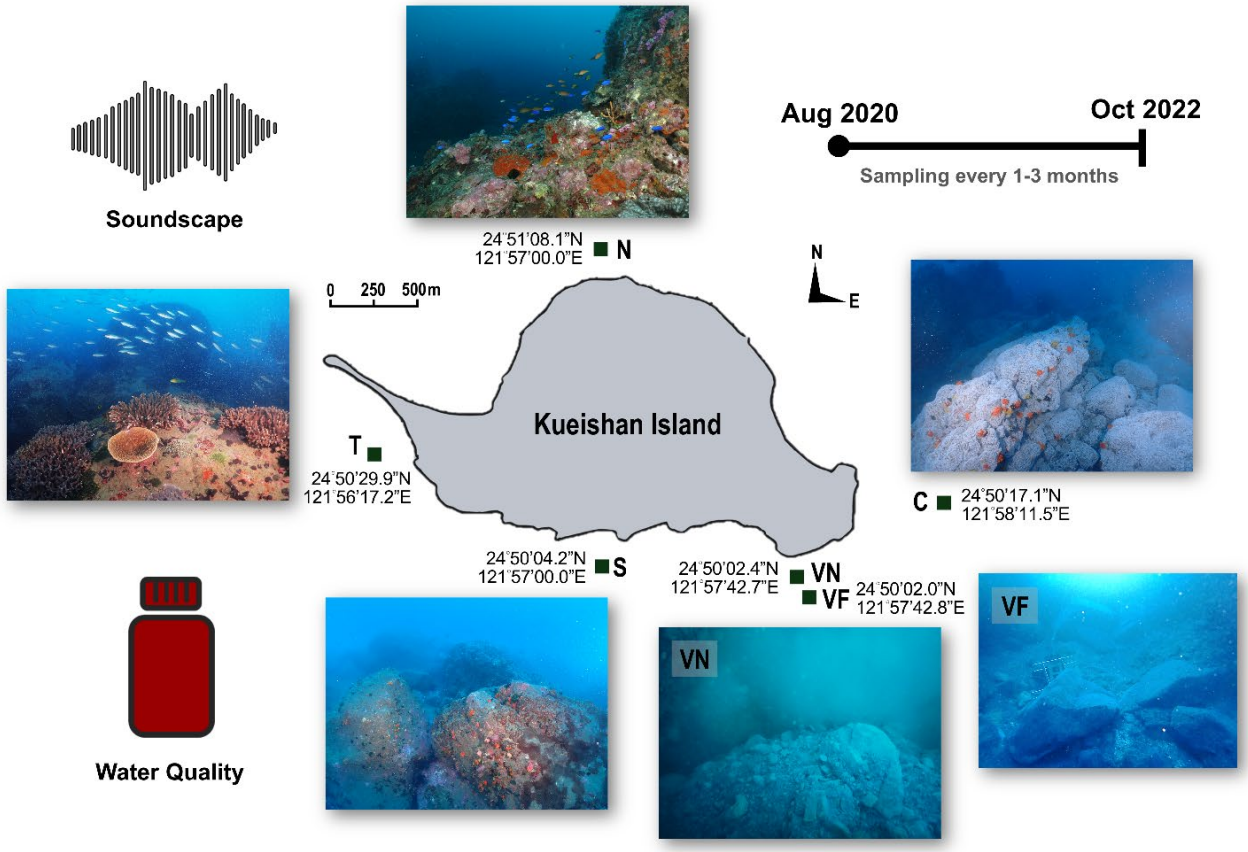

Figure 1. Water sampling and sound recording conducted around Kueishan Island. Sampling was conducted at six sites surrounding Kueishan Island from August 2020 to October 2022 at intervals of 1 to 3 months. VN, site near the vents, 15-17 m depth; VF, site far from the vents, 15-17 m depth; C, CO_2 vents without sulfide, 20-23 m depth; S, south site, 13-15 m depth; N, north site, 13-15 m depth; T, tail site, 8-10 m depth.

doi:10.6342/NTU202500809

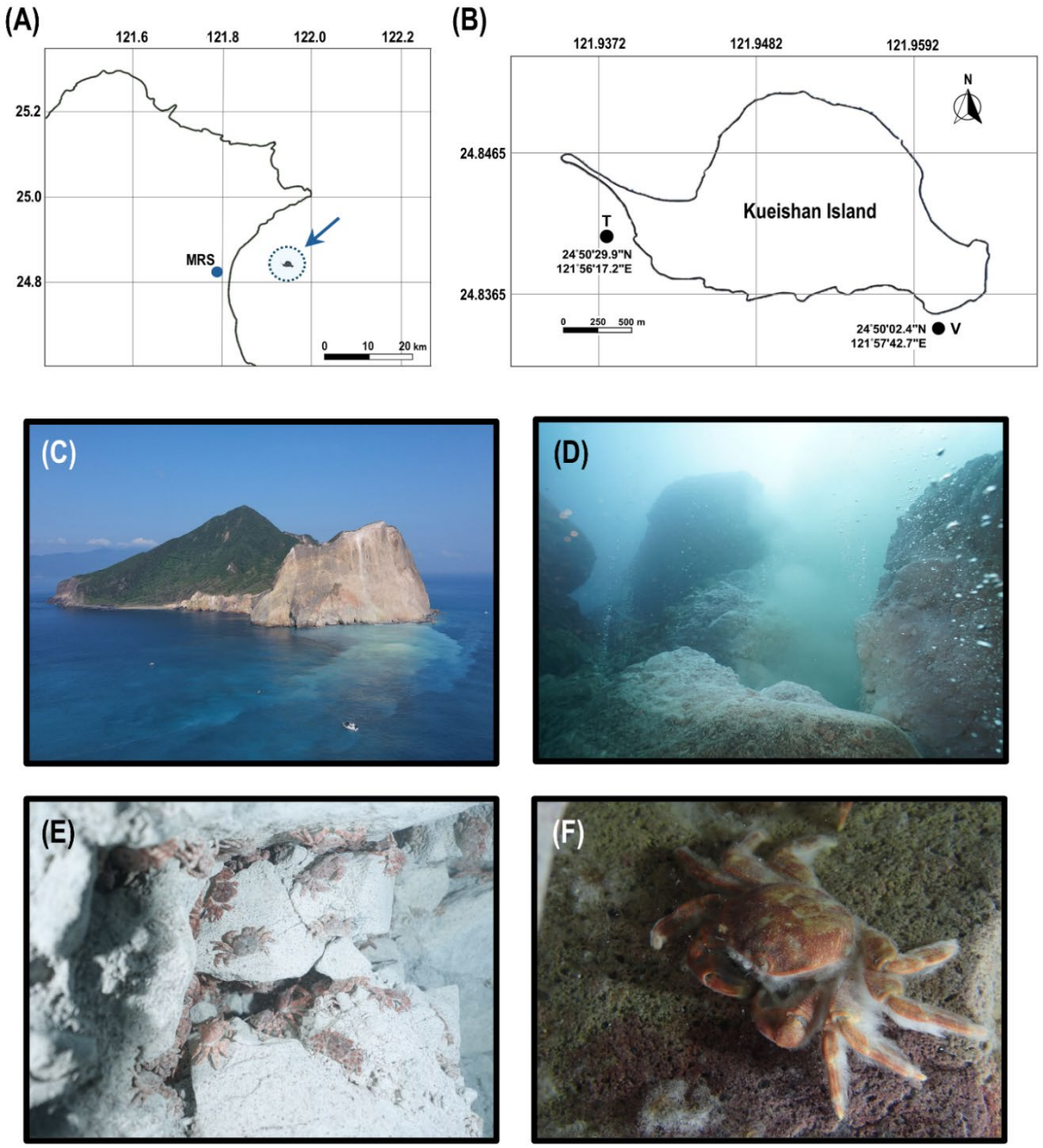

Figure 2. Kueishan Island with a shallow-water hydrothermal vent system. Maps show Kueishan Island located off the northeastern coast of Taiwan, indicated by an arrow (A). Relative positions, latitude and longitude coordinates of the sampling sites, the V site, and T site are presented (B). The photos show the southeastern tip of Kueishan Island, where white sulfur plumes are visible on the sea surface (C), which emanated from the subsurface hydrothermal vent system (D). A large number of hydrothermal vent crabs (*Xenograpsus testudinatus*) inhabit the area (E), and a white biofilm can be observed on the carapace surface of the crab (F). MRS, Marine Research Station, Institute of Cellular and Organismic Biology, Academia Sinica, Yilan, Taiwan; V, the vent site; T, the tail site.

doi:10.6342/NTU202500809

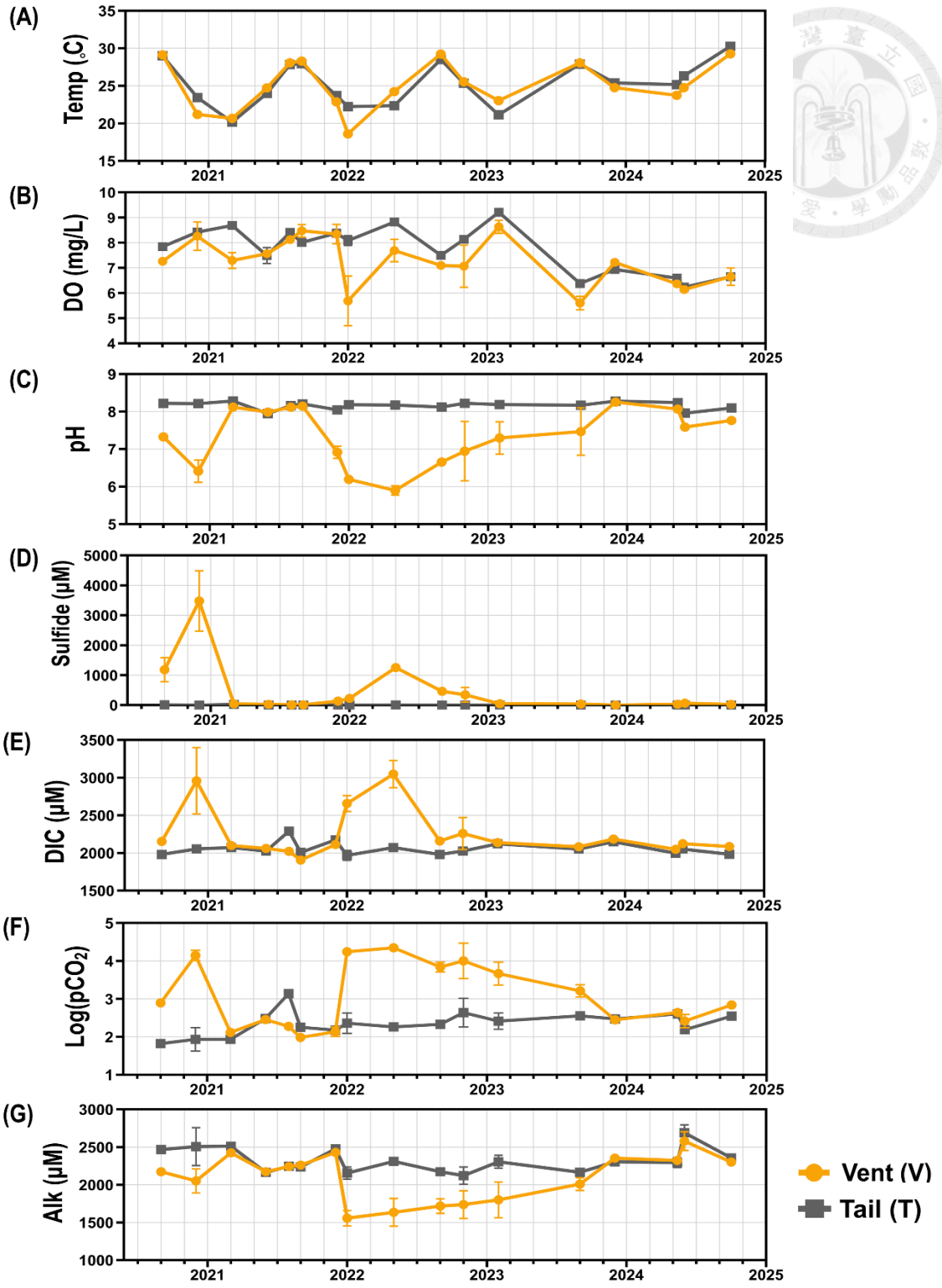

Figure 3. Physicochemical parameters of water quality at the vent and tail sites offshore Kueishan Island. Temp, temperature (A); DO, dissolved oxygen (B); pH (C); Sulfide (D); DIC, dissolved inorganic carbon (E); Log(pCO_2), base-10 logarithm of the partial pressure of carbon dioxide (CO_2) measured in μatm (F); Alk, alkalinity (G). Data are presented as mean ± standard deviation (SD), based on triplicate measurements.

doi:10.6342/NTU202500809

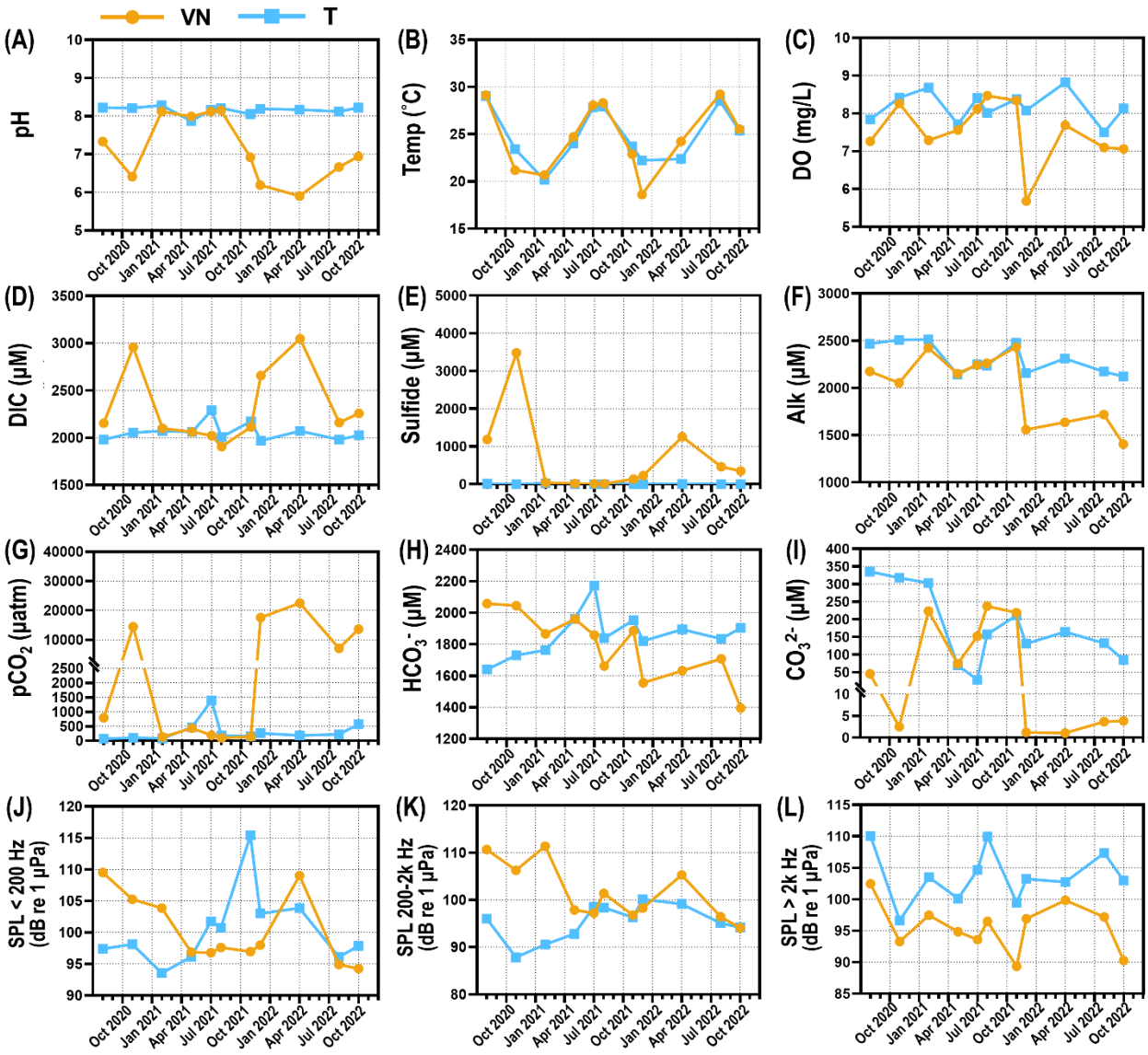

Figure 4. Parameters of water quality and soundscape at the VN and T sites. pH (A); Temp, temperature (B); DO, dissolved oxygen (C); DIC, dissolved oxygen (D); Sulfide (E); Alk, alkalinity (F); pCO_2, the partial pressure of CO_2 (G); HCO_3^{2-}, bicarbonate (H); CO_3^{2-}, carbonate (I); SPL < 200 Hz, sound pressure level (SPL) at frequencies of < 200 Hz (J); SPL at frequencies of 200-2k Hz (K); SPL at frequencies of > 2k Hz (L). VN, site near the vents; T, tail site. Data are presented as mean, based on triplicate measurements.

doi:10.6342/NTU202500809

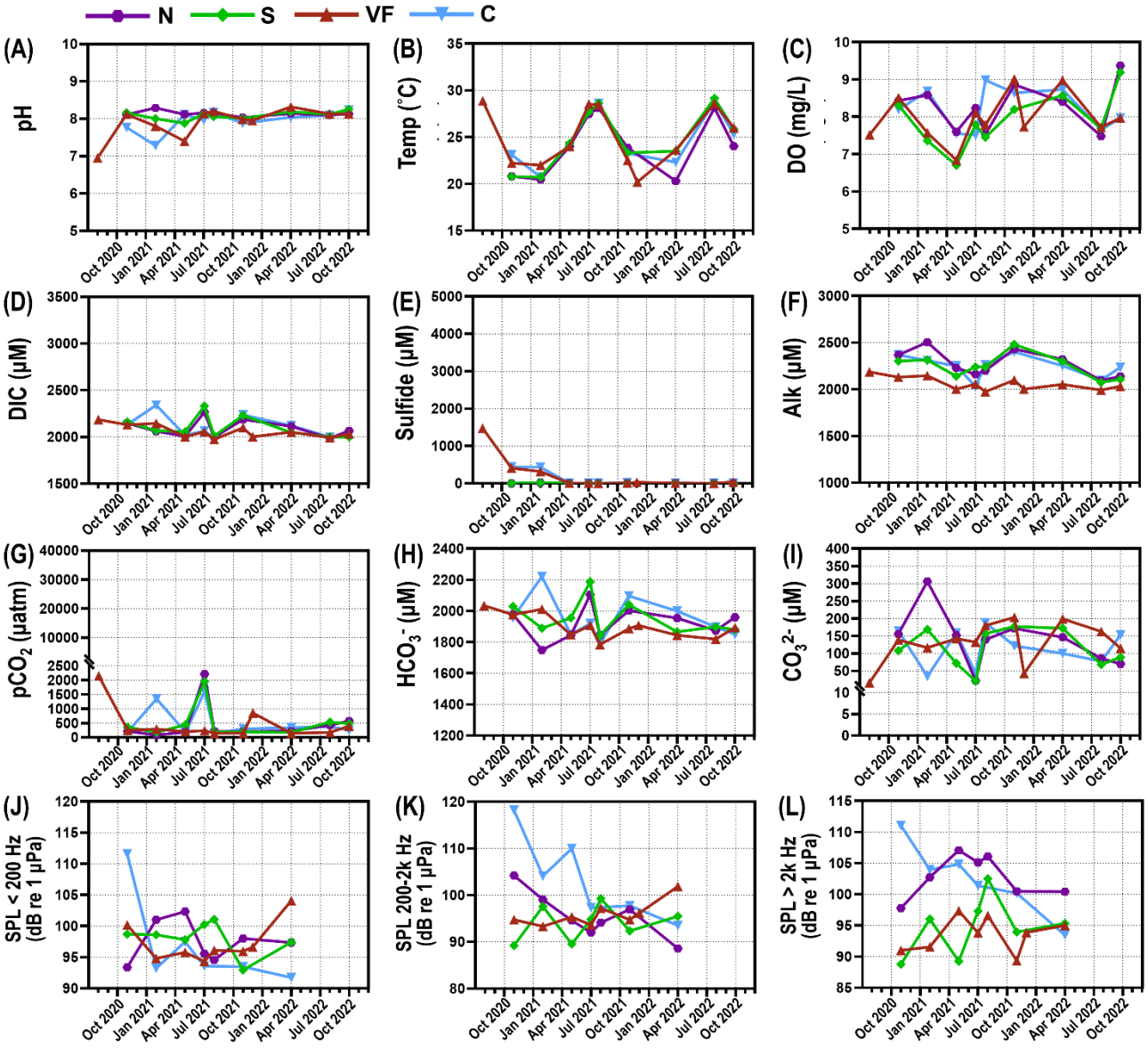

Figure 5. Parameters of water quality and soundscape at the other sites. pH (A); Temp, temperature (B); DO, dissolved oxygen (C); DIC, dissolved oxygen (D); Sulfide (E); Alk, alkalinity (F); pCO_2, the partial pressure of CO_2 (G); HCO_3^{2-}, bicarbonate (H); CO_3^{2-}, carbonate (I); SPL < 200 Hz, sound pressure level (SPL) at frequencies of < 200 Hz (J); SPL at frequencies of 200-2k Hz (K); SPL at frequencies of > 2k Hz (L). VF, site far from the vents; C, CO_2 vents without sulfide; S, south site; N, north site. Data are presented as mean, based on triplicate measurements.

doi:10.6342/NTU202500809

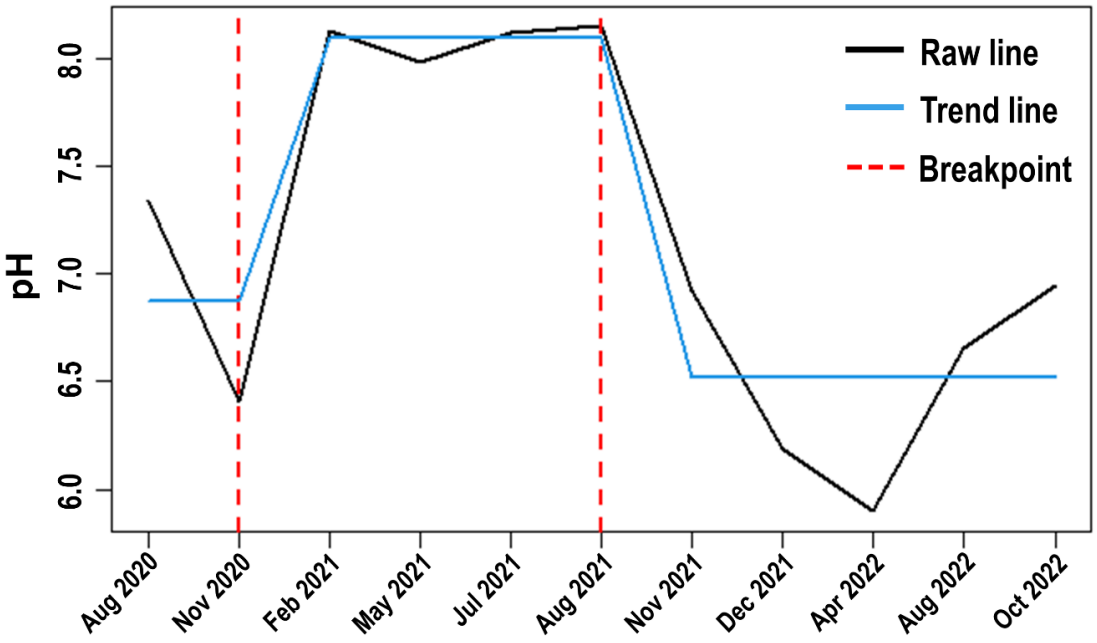

Figure 6. Structure change analysis of temporal variations in pH level at the VN site. The black solid line represents the raw data. The blue solid line represents the trend line estimated using Ordinary Least Squares (OLS), and the red dashed line represents the breakpoints.

doi:10.6342/NTU202500809

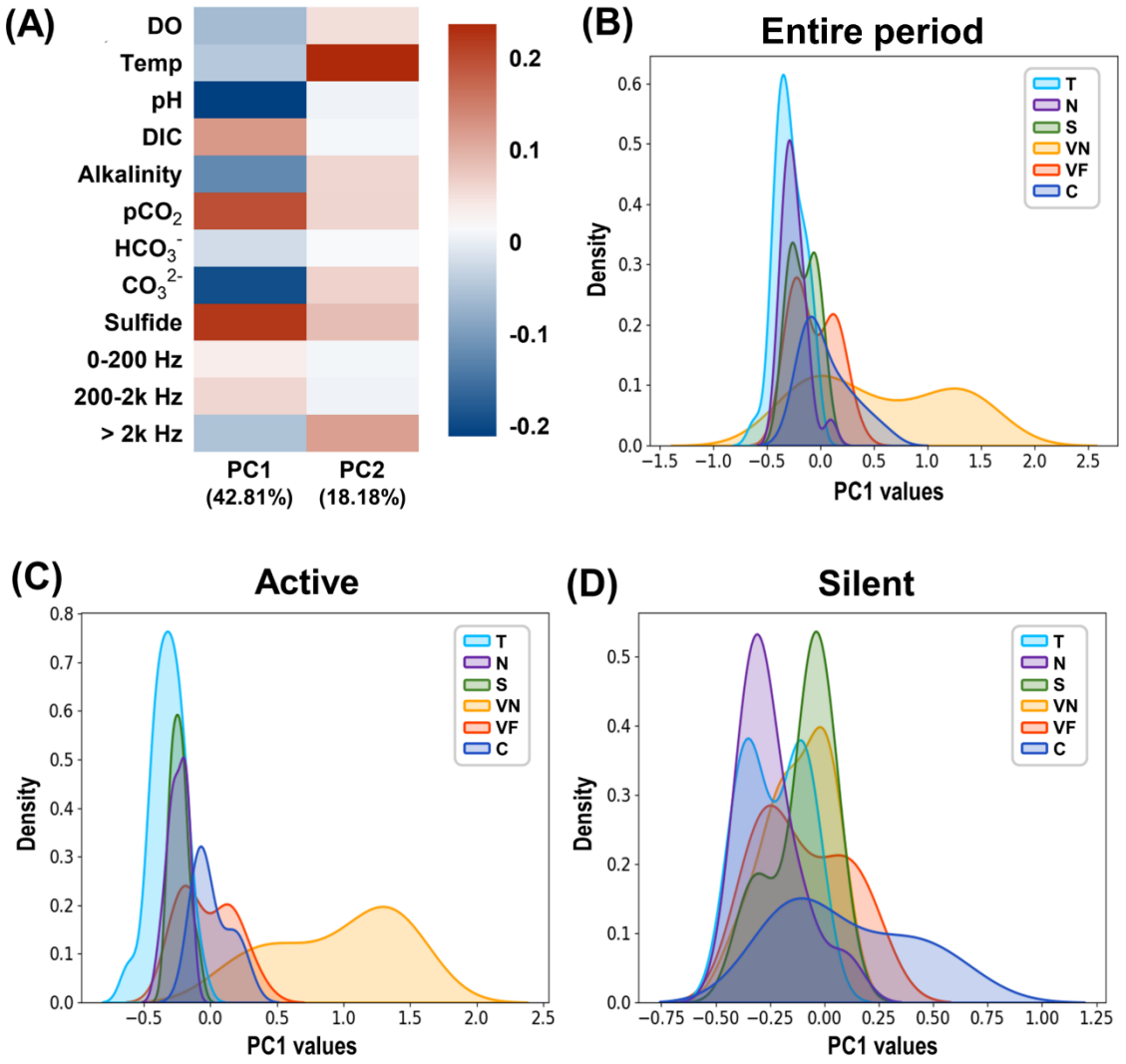

Figure 7. Principal component analysis (PCA) of the physicochemical and acoustic parameters. Contribution of PC1 and PC2 to the total variance and the correlation of each physicochemical and acoustic variable to PC1 and PC2 (A). The contribution coefficients for the variables are shown in the heatmap, where a diverging color scale from red to white to blue indicates values ranging from 0.237 to 0 to -0.211. Density distribution plots of PC1 values grouped by study sites for different periods, including the entire (B), active (C), and silent periods (D).

doi:10.6342/NTU202500809

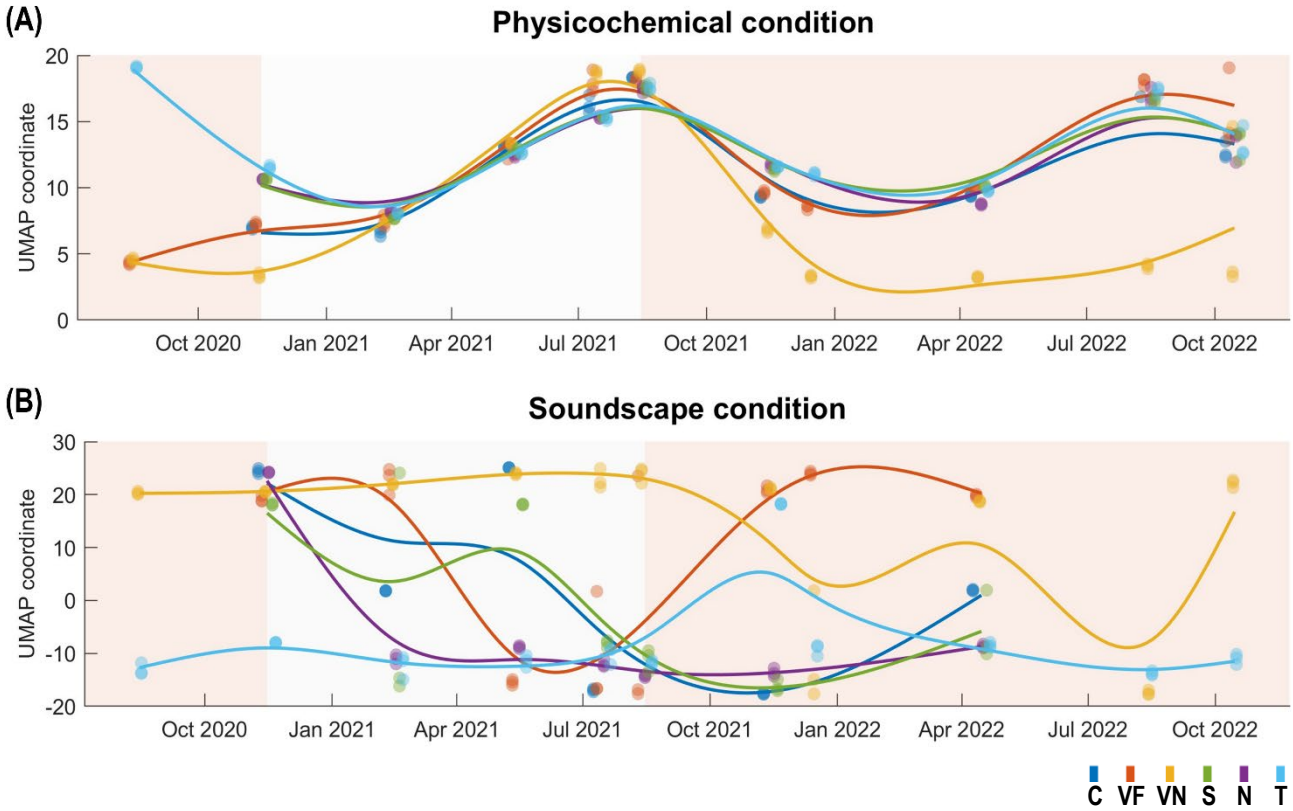

Figure 8. Temporal trends of the physicochemical and soundscape conditions derived from UMAP. Physicochemical (A) and acoustic conditions (B) were plotted using UMAP. The red and white background colors represent the active and silent periods, respectively, defined by breakpoints obtained from structure change analysis.

doi:10.6342/NTU202500809

Chapter 2

Bacterial Communities Dynamics at the Environment-Host Interface in the Hydrothermal Vent System

doi:10.6342/NTU202500809

2.1 Introduction

The extraordinary metabolic versatility of microorganisms drives biogeochemical cycles on a global scale, sustaining ecosystem functions across diverse habitats, including HV systems (Falkowski et al., 2008; Dick, 2019). HV fluids are typically enriched in dissolved metals, inorganic carbon, ammonium, nitrogen, methane, and hydrogen sulfide (Butterfield et al., 1990; Levin et al., 2016). High sulfide concentrations in the HV fluids are particularly significant, as microorganisms that can perform sulfur metabolism may utilize sulfide or sulfur derivatives accompanied by needed materials as energy sources (Tunnicliffe, 1991; Akerman et al., 2013). Several prominent sulfur-oxidizing bacteria (SOB) have been identified in shallow-water HV areas, including Vulcano, Eolian Islands, Italy (Maugeri et al., 2009), Milos Island, Greece (Giovannelli et al., 2013), Espalamaca, Faial, Azores (Rajasabapathy et al., 2014), and El Hierro, Canary Islands, Spain (Gonzalez et al., 2020). Advances in sampling and sequencing techniques have facilitated research on the spatial distribution of microbial communities in HV systems (Reveillaud et al., 2016; Trembath-Reichert et al., 2019), especially in shallow-water ones due to their accessibility (Arcadi et al., 2023; Barosa et al., 2023; Pérez-Barrancos et al., 2025). Despite growing research on HV-associated microbiomes, studies of their temporal dynamics remain limited, emphasizing the need for further investigation.

Microbiomes in HV ecosystems serve as an exceptional model for understanding fundamental ecological principles such as “functional redundancy” and “niche differentiation”. The presence of a variety of microbial taxa in these extreme environments indicates specialized ecological functions and metabolic partitioning of resources (Sievert and Vertriani, 2012; Dick, 2019). Functional redundancy, wherein multiple species perform similar ecological or metabolic functions, may enhance

doi:10.6342/NTU202500809

resilience to environmental variability (Galand et al., 2018; Louca et al., 2018). This is particularly pertinent in dynamic HV systems characterized by sporadic fluid discharge. Meanwhile, niche differentiation allows microorganisms with overlapping metabolic capabilities to partition resources, mitigating competition and facilitating cohabitation within an ecosystem (Macalady et al., 2008; Martens-Habbena et al., 2009). These mechanisms contribute to the stability and adaptability of microbial communities in hydrothermal fields, enabling them to withstand extreme and fluctuating environmental conditions.

Invertebrates are the metazoans dominant in HV ecosystems, which rely on the chemosynthesis of their bacterial symbionts for survival. Chemoautotrophic bacteria have been found in a variety of vent-endemic invertebrates, such as the vent shrimp *Rimicaris exoculate*, the yeti crab *Kiwa hirsute* (Goffredi et al., 2008; Zbinden et al., 2008), the galatheid crab *Shinkaia crosnieri* (Tsuchida et al., 2011), and gastropods *Alviniconcha* and *Ifremeria* (Breusing et al., 2022). These symbiotic bacteria are crucial in primary production and life-sustaining detoxification processes, especially within the gills of their hosts (Fialamedioni et al., 1986; Jouin and Gaill, 1990; Ponsard et al., 2013). However, the interactions between vent-endemic invertebrates and their symbiotic microbiome, particularly how these relationships react to environmental perturbations, have not been sufficiently investigated. There is a critical gap in our understanding of microbial communities in more variable shallow-water hydrothermal systems, as most studies have concentrated on either free-living microbial communities or stable symbiotic relationships in deep-sea HVs (Fortunato et al., 2018).

The vent crabs, *X. testudinatus*, which thrive in the Kueishan Island shallow-water HV system, have primarily been studied for their acid-base regulation. Functional ion channels, Na^+/K^+-ATPase (NKA) and V-type H^+ATPase (VHA) in the gills might

doi:10.6342/NTU202500809

play an important role in excess proton excretion and help the crabs cope with the acidic habitat (Hu et al., 2016). Another study demonstrated that *X. testudinatus* maintained homeostatic pH through HCO_3^-/Cl^- exchange and the retention of extracellular ammonia (Allen et al., 2020). However, acid-base homeostasis in such extreme environments represents just one component of numerous adaptive strategies. The interplay between host physiology and microbial symbionts likely forms an integrated system that enhances survival in hydrothermal environments. The gill structure of aquatic organisms features a large surface area and extensive vascularization, optimized for gas exchange and ion regulation (Henry and Wheatly, 1992; Evans et al., 2005), which may create an ideal habitat for specific microbial communities. In turn, the microenvironment in the gills may also provide a condition characterized by regulated pH, oxygen gradients, and a consistent nutrient supply for microbes. Previous studies have suggested that gill-associated microbes contribute to host physiological homeostasis by enhancing ion regulation capacity through microbial metabolites (Lai et al., 2022; François-Étienne et al., 2023). Additionally, sulfur-oxidizing bacteria may aid in acid-base regulation by consuming sulfide and producing energy-rich compounds advantageous to the host (Oeschger and Vetter, 1992; Goffredi et al., 2002). The abundance of NKA-rich cells in the gills may generate localized pH and ion concentration gradients, favoring the selection of bacterial taxa adapted to these conditions. While bidirectional interactions have been documented in other crustacean-microbe symbioses, they remain largely unexamined in HV crustaceans (Goffredi, 2010). Studies have identified symbiotic bacteria with varying compositions across different tissues of *X. testudinatus* (Ho et al., 2015; Yang et al., 2016). In the wild, a white hairy microbial mat is often observed on the carapace of *X. testudinatus*, (Wang et al., 2014; Fig. 2F). A previous study found that the microbial community on the

doi:10.6342/NTU202500809

carapace of fiddler crabs (*Uca panacea*) closely resembled that of the surrounding sediments (Cuellar-Gempeler and Leibold, 2019). The carapace-associated microbial communities of deep-sea squat lobsters (Munidopsis alvisca) were interpreted as a mutualistic adaptation for epibiotic habitation and sulfide detoxification (Leinberger et al., 2022). The adaptability of vent-endemic *X. testudinatus* holobiont may be further enhanced by the presence of diverse microbial communities, which provide ecological plasticity in response to environmental fluctuations through complementary metabolic processes.

In this chapter, we investigated the bacterial communities in the gills and carapace surface of *X. testudinatus*, as well as the surrounding water, to better understand the interactions between the HV environment and the crustacean host. To achieve an in-depth understanding of the bacterial composition associated with *X. testudinatus* holobiont, we used full-length 16S rRNA gene sequencing and performed functional annotation to predict the metabolic roles of dominant bacteria. Additionally, we analyzed water quality alongside microbiome data to explore how environmental changes influence microbial communities. Finally, we applied fluorescence *in situ* hybridization (FISH) to identify the localization of dominant gill-associated bacteria. Based on our knowledge of HV ecosystems and host-microbe interactions, we developed three testable hypotheses: (1) The bacterial communities in the surrounding water would directly respond to fluctuations in hydrothermal activity, with sulfur-metabolizing bacteria predominating during active venting periods; (2) The bacterial communities symbiotic with *X. testudinatus* would reflect their physiological functions and degree of environmental exposure, with gill-associated communities showing a stronger correlation with water chemistry than those on the carapace surface; and (3) The localization of dominant bacteria within gill tissues would correspond to areas most

doi:10.6342/NTU202500809

exposed to water flow, optimizing both sulfide access for bacteria and detoxification benefits for the host. These hypotheses provide a framework for comprehending the intricate interactions between the environment, microbiome, and host tissue in this extreme ecosystem.

doi:10.6342/NTU202500809

2.2 Materials and Methods

Sample collection

Water samples were collected every 1 to 3 months by SCUBA divers in the vent area (V site; 24°50′29.9″N, 121°56′17.2″E) and the non-vent area (T site; 24°50′02.4″N, 121°57′42.7″E) of Kueishan Island (Fig. 1B). Water quality data from each sampling time were averaged from triplicate samples. Then the water samples were filtered through 0.2 μm/47 mm membrane filters (mdi Membrane Technologies, NY, USA) using a 47 mm PES Filter Holder (ROCKER, Taiwan) to capture bacterial DNA in the environment. The filtered membranes were wrapped in aluminum foil, sealed in zip-lock bags, and frozen in liquid nitrogen. HV crabs *X. testudinatus* were collected from the V site. The 5th gills were excised, and the carapace surface was applied using sterile cotton swabs. Gill tissues and cotton swabs were placed into 1.5 mL and 5 mL tubes (Eppendorf, Hamburg, Germany), respectively, and frozen in liquid nitrogen aboard the fisheries craft. Upon arrival at the laboratory, all samples were stored at -80°C until DNA extraction.

Measurements of water quality

Water quality was assessed, including temperature (Temp), dissolved oxygen (DO), pH, sulfide concentration, dissolved inorganic carbon (DIC), pCO_2, and alkalinity (Alk). The temperature, DO, and pH levels were measured using a multiparameter portable meter (Multiline® Multi 3620 IDS, WTW, Weilheim, Germany) equipped with an IDS pH electrode (SenTix® 940, WTW) on the fisheries craft. Sulfide concentration was determined by a spectrophotometric method modified from (Cline, 1969), using a sulfide sulfur specific mixed diamine reagent containing N, N-Dimethyl-p-phenylenediamine sulfate and ferric chloride in 50% hydrochloric acid. The alkalinity

doi:10.6342/NTU202500809

was spectrophotometrically assayed following a previously published method (Sarazin et al., 1999). DIC contents were detected in triplicate using a DIC analyzer (AS-C3, Apollo SciTech, Newark, DE, USA) with nitrogen as an inert gas, followed by quantification via a nondispersive infra-red (NDIR) Li-7000 CO_2/HCO_3^- analyzer (LI-COR, Lincoln, NE, USA). pCO_2 was calculated based on temperature, pH, and DIC using the CO2SYS module in Microsoft Excel (Pierrot, 2006).

DNA extraction

DNA extraction was performed in a laminar flow hood to prevent contamination. All tools, including scissors, tweezers, pipettes, and tips, were soaked in 10% bleach for 10 minutes to eliminate residual DNA, followed by UV exposure for at least 30 minutes. The filter was cut into small pieces and placed into a 2 mL microcentrifuge tube (Eppendorf). Total DNA was extracted using the Wizard Genomic DNA Purification Kit (Promega, Madison, WI, USA) according to the manufacturer's protocol.

DNA from the crab gills was extracted using the Wizard Genomic DNA Purification Kit (Promega), and DNA from the carapace surface (cotton head) was extracted using the QIAamp DNA Microbiome Kit (QIAGEN, Hilden, Germany). Both extractions followed the manufacturers' instructions. The quantity and quality of extracted DNA were assessed using a NanoDrop 2000™ spectrophotometer (Thermo Fisher Scientific, Wilmington, DE, USA). DNA samples were then stored at -20°C until further use.

Full-length 16S rRNA gene sequencing

Bacterial full-length 16S rRNA amplicons were amplified using specific primers, 27F: AGRGTTYGATYMTGGCTCAGPCR and 1492R: RGYTACCTTGTTACGACTT

doi:10.6342/NTU202500809

with barcodes, referring to the guidelines for PacBio SMRT sequencing (PacBio, Menlo Park, CA, USA). PCR was performed with approximately 10 ng of DNA using 2X KAPA HiFi HotStart ReadyMix PCR Reagent (Kapa Biosystems, Woburn, MA, USA), containing 2.5 μM of both forward and reverse primers in a total volume of 25 μl. The amplification was conducted with an initial denaturation at 95°C for 3 min, followed by 30 cycles of 95°C for 30 sec, annealing at 57 °C for 30 sec, and elongation at 72 °C for 1 min, with a final extension at 72 °C for 1 min. PCR products were examined on 0.8% agarose gels and quantified using a Qubit 2.0 Fluorometer (Thermo Fisher Scientific). The qualified PCR products were mixed in equal amounts and purified using AMPure PB beads (PacBio). The pooled 16S amplicons (600 ng) were then used to prepare the library with the SMRTbell prep kit 3.0 (PacBio), according to the manufacturer's instructions. After damage repairing, end repairing, and A-tailing, the inserts were ligated to adapters. SMRT sequencing was performed on a SMRT 8M Cell (PacBio) using chemistry version 2 on PacBio Sequel IIe sequencer. A primary filtering analysis was achieved on the Sequel IIe System, followed by a secondary analysis using the SMRT analysis pipeline version 11.0.0.

Sequence processing and data analysis

Sequences were analyzed using CLC Genomic Workbench 24.0.1 (CLC Bio, QIAGEN, Aarhus, Denmark). Adapter sequences were trimmed and reads shorter than 1200 bp or longer than 1600 bp were removed. Amplicon Sequence Variants (ASVs) were obtained with a fixed read length of 1200 bp, a maximum expected error rate of 2.0 per read, and the removal of detected chimeric sequences. Taxonomic classification was assigned to ASVs using the SILVA SSU 138.1 database, applying a sequential similarity threshold of 97%, 90%, 85%, and 80%. Previously assigned taxonomies with

doi:10.6342/NTU202500809

a higher similarity were retained. Relative abundance was calculated as the number of reads assigned to each taxon divided by the total number of qualified reads in each sample. The number of bacterial samples varied at different time points based on sampling conditions and the results of sequence qualification (Table 2).

Alpha diversity was assessed using the observed taxa number (Observed), Chao 1 richness estimates (Chao 1), Simpson's index (Simpson), and Shannon entropy (Shannon) at the class and genus level, calculated within the CLC Genomic Workbench. Beta diversity was evaluated through principal coordinate analysis (PCoA) and permutational multivariate analysis of variance (PERMANOVA) based on Bray-Curtis distances, using the R packages *vegan* (Dixon, 2003) and *ade4* (Dray and Dufour, 2007) in RStudio (2024.04.1+748). The Bacterial relative abundances were depicted as bubble plots using the *ggplot2* (Valero-Mora, 2010) and *reshape2* (Wickham, 2020) packages. Pairwise Pearson's correlation analyses between water parameters and bacterial alpha diversity metrics were performed using the R package *psych* (Revelle and Revelle, 2015) and the resulting correlation matrix was visualized using the *corrplot* package (Wei et al., 2017). A Venn diagram was generated using the web-based tool InteractiVenn (Heberle et al., 2015) to illustrate the overlap between the top 20 genera identified in the water, gill and carapace samples.

To predict the potential functions of bacterial communities, the taxonomic abundance table was used to retrieve functional annotations of identified prokaryotic taxa (FAPROTAX 1.2.10). FAPROTAX provides an informative database that categorizes prokaryotic taxa (e.g., classes, genera, or species) into putative metabolic groups based on experimentally characterized representatives from culture-based studies (Louca et al., 2016). Visualization was performed using the R package *ggplot2*.

doi:10.6342/NTU202500809

Fluorescence *in situ* hybridization

Fluorescence *in situ* hybridization (FISH) was employed to detect bacteria in the gills of *X. testudinatus*. The gill tissue was fixed in 4% paraformaldehyde in phosphate-buffered saline (PBS) and temporarily stored on ice aboard the fishing craft. In the laboratory, the fixed gills were embedded in paraffin wax, sectioned at 8 μm, mounted on slides, and stored at 4°C. To perform FISH, paraffin sections were dewaxed using Histo-Clear (National Diagnostics, Atlanta, GA, USA) and Histo-Clear was removed through a graded ethanol series (100%, 75%, 50%, and 25%). The sections were then rehydrated in 20 mM Tris-HCl and treated with proteinase K (5 μg/mL) and lysozyme (5 mg/mL) to permeabilize bacterial cell walls. Hybridization was performed using the *Sulfurovum*-targeted probe EPI653, 5'-ATCTTCCCCTCCCASACTCT-3' (Watsuji et al., 2010), and the universal bacteria probe EUB338, 5'-GCTGCCTCCCGTAGGAGT-3' (Amann et al., 1990). Fluorescence signals were visualized using an Olympus FV3000 confocal laser scanning microscope (Olympus Corporation, Tokyo, Japan) at wavelengths of 488 and 640 nm.

doi:10.6342/NTU202500809

2.3 Results

Bacterial community dynamics in the water

Water quality parameters, including temperature, DO, pH, sulfide, DIC, pCO_2, and Alk, at the V and T sites were collated from February 2021 to April 2024 (Fig. 9). Troughs in DO, pH, and Alk were observed in December 2021 (Fig. 9B, C, G), and the peaks in DIC and pCO_2 were observed during the same period (Fig. 9E, F). Meanwhile, the highest sulfide concentration was recorded in August 2022 (Fig. 9D).

Alpha diversity results indicate that at the T site, peaks in observed taxa number (Observed) and Chao 1 richness estimates (Chao 1) at the class level occurred in December 2021 (Fig. 10A, B), and those at the genus level occurred in August 2022 (Fig. 10E, F). Simpson's index (Simpson) and Shannon entropy (Shannon) did not show clear peaks or troughs (Fig. 10C, D, G, H). At the V site, troughs in all four indices at both the class and genus levels were observed in December 2021. The correlogram (Fig. 11A) indicates that at the V site, all water parameters were significantly correlated with alpha diversity indices at the genus levels. Temperature, DO, pH, and Alk showed positive correlations, whereas sulfide, DIC, and pCO_2 were negatively correlated. At the T site, only pCO_2 was positively correlated with diversity indices, and meanwhile, sulfide and Alk showed negative correlations (Fig. 11B).

The bacterial compositions at class and genus levels are presented as bubble plots for the V site (Fig. 12) and the T site (Fig. 13). In V site water, Campylobacteria and Gammaproteobacteria were the two dominant bacterial classes, exhibiting opposite ebb and flow patterns over time (Fig. 12A). Within Campylobacteria, the most abundant genus was *Thioreductor*, primarily driving the temporal variations in the class. Relatively, *Thiomicrorhabdus* reflected the variations within Gammaproteobacteria (Fig. 12B). On the other hand, Alphaproteobacteria and Gammaproteobacteria were the

doi:10.6342/NTU202500809

two dominant classes in T site water, while other classes, such as Acidimicrobiia, Bacteroidia, Campylobacteria, and Cyanobacteriia, also showed observable variations over time (Fig. 13A). At the genus level, several genera belonged to Alphaproteobacteria, and *Thiomicrorhabdus* remained the most abundant genus within Gammaproteobacteria (Fig. 13B). Notably, *Thioreductor* and *Lebetimonas* were not detected within Campylobacteria here.

According to the functional analysis, nitrogen cycle (except for denitrification), sulfur respiration, and hydrogen oxidation were prominent between November 2021 and January 2023 (Fig. 14), a period with relatively low pH (< 7.5) and high sulfide concentrations (Fig. 9C, D). Subsequently, denitrification and sulfur oxidation were detected in small proportions. In contrast, phototrophic functions were observed at the T site but were either absent or present at very low levels at the V site (Fig. 14). Notably, sulfur- and nitrogen- related functions were observed once at the T site in August 2021

Bacterial compositions in the gills and on the carapace surface of *X. testudinatus*

Water quality data for the *X. testudinatus* microbiome are limited to the period from August 2020 to November 2021 at 3-month intervals, with data from only the V site presented (Fig. 15A-G). This limitation is due to sampling challenges, such as weather conditions and specimen preservation issues. During this period, troughs in pH and Alk were recorded in November 2020, alongside peaks in sulfide, DIC and pCO_2.

Alpha diversity results show that the bacterial diversity at both the class and genus levels on the carapace surface was generally higher than in the gills (Fig. 15H-O). Furthermore, all four indices at both taxonomic levels in the gills showed troughs in November 2020. The correlogram (Fig. 16) shows that, except for DO, water parameters were significantly correlated with alpha diversity indices in the gills at the genus level.

doi:10.6342/NTU202500809

Basically, temperature, pH and Alk had positive correlations, while sulfide, DIC, and pCO_2 had negative correlations with gill bacterial diversity. In contrast, only Simpson and Shannon indices on the carapace surface were correlated with water quality (Fig. 16). On the other hand, the patterns of correlation between water quality and bacterial diversity in the gills were opposite to those on the carapace surface.

The bacterial compositions at the class and genus levels are presented as bubble plots for the gills (Fig. 17) and the carapace surface (Fig. 18). In the gills, Campylobacteria was the dominant class, comprising around 70% of relative abundance across all time points, followed by Gammaproteobacteria and Bacteroidia (Fig. 17A). Within Campylobacteria, *Sulfurovum* was the most abundant genus and almost dominated the bacterial community in the gills (Fig. 17B). Also, Campylobacteria was the dominant class on the carapace surface (~50%; Fig. 18A), with Bacteroidia, Alphaproteobacteria, and Gammaproteobacteria being abundant as well. Similarly, at the genus level, *Sulfurovum* had the greatest abundance within Campylobacteria and even comprised nearly half of the bacterial community on the carapace surface across all time points (Fig. 18B).

The functional analysis shows that sulfur oxidation, denitrification and hydrogen oxidation had relatively high proportions both in the gills and on the carapace surface of *X. testudinatus* (Fig. 19). Throughout the entire period, these functions had the highest proportions in the gills in November 2020 (Fig. 19A). Additionally, the functional proportions on the carapace surface were generally lower than those in the gills, possibly reflecting a lower abundance of *Sulfurovum* (Fig. 19B).

The Venn diagram (Fig. 20) illustrates the top 20 bacterial genera across the gills, carapace surface, and surrounding water of *X. testudinatus*. The water contained 17 unique genera, represented by *Thioreductor* from Campylobacteria, one of the most

doi:10.6342/NTU202500809

abundant genera in the samples (Fig. 20A). The carapace surface harbored 12 unique genera and appeared to share none with the water, suggesting that the bacteria adhering to the carapace may not necessarily be the most abundant in the surrounding water. The gills contained 11 unique genera and shared one genus *Sulfurimonas* with the water and six genera with the carapace (Fig. 20B, C). Among the bacterial communities, two genera were shared across all three compartments, *Sulfurovum* from Campylobacteria and an uncultured genus from the family Rhodobacteraceae within the class Alphaproteobacteria (Fig. 20D). These two bacteria may play important roles in the *X. testudinatus* holobiont, linking the microbial communities at two key interfaces (the gills and carapace) that interact with the external environment.

The distribution of *Sulfurovum* in the gills of *X. testudinatus*

Using fluorescence *in situ* hybridization (FISH), the localization of bacterial communities in the gills of *X. testudinatus* was identified (Fig. 21; Fig. 22). The images clearly show the transverse section of the branchial structure, and the elongated structures on both sides are lamellae (L; Fig. 21). The universal bacteria probe EUB338 generated signals primarily distributed in the afferent vessel (AV; Fig. 21B). The signals from *Sulfurovum*-targeting probe EPI653 signals almost completely overlapped with those from EUB338, confirming that detected signals originated from bacteria and further supporting our finding that *Sulfurovum* is the dominant genus in the gill samples (Fig. 21D). Additionally, a few signals were also observed in the epithelial principal cells and pilaster cells of the lamella. The magnification images (Fig. 22D-F) reveal the subcellular localization within a single cell. The EUB338 signals occupied over half of the cell volume, while the EPI653 signals were more concentrated near the nucleus, possibly corresponding to the location of the endoplasmic reticulum.

doi:10.6342/NTU202500809

2.4 Discussion

Shallow-water HVs create dynamic ecosystems where primary production is sustained by both chemosynthesis and photosynthesis due to their epipelagic juncture. The hydrothermal activity at Kueishan Island exhibits temporal variability, driven by monsoons, typhoons, ocean currents (the Kuroshio), and seismic activity (Lebrato et al., 2019; Chiu et al., 2024). This dynamic system provides an ideal setting for investigating the temporal effects of hydrothermal venting on microbial communities, which act as a bridge between the environment and metazoans. In nature, microbes mediate energy flow, responding to environmental fluctuations and nutrient availability, especially essential in resource-limited extreme environments such as HV systems (Reysenbach and Shock, 2002). Unique HV microbial communities are potentially shaped by fluid chemistry (Barosa et al., 2023; Pérez-Barrancos et al., 2025). Using the *X. testudinatus* holobiont inhabiting the Kueishan Island HV system, we explored interactions between environmental factors, symbiotic bacteria, and crustacean host.

Bacterioplankton composition varies in response to hydrothermal activity

At the vent site, active venting periods between November 2021 and January 2023 during water bacterial sampling were indicated by drops in pH levels (< 7.5), coinciding with increases in sulfide content, DIC, and pCO_2. Although bacterial diversity was not consistently low, the lowest observations occurred within this period. Furthermore, correlations between physicochemical parameters and alpha diversity metrics suggest that temporal variations in water quality influence bacterial composition in the venting area. Hydrothermal fluids led to a decrease in bacterial diversity, with Campylobacteria (previously Epsilonproteobacteria) becoming dominant in the water, which is a class primarily associated with the utilization of sulfur compounds (oxidation and reduction)

doi:10.6342/NTU202500809

in HV environments (Takai et al., 2003; Campbell et al., 2006; Akerman et al., 2013). In the Panarea shallow-water HV system, Campylobacteria were also found in the surrounding water as well as the sediments (Maugeri et al., 2009). Within Campylobacteria, the four representative genera were all hydrogen-oxidizing, including *Sulfurimonas* and *Sulfurovum*, which are also sulfur-oxidizing (Wang et al., 2023); *Thioreductor*, a sulfur-reducing bacterium (Nakagawa et al., 2005); and *Lebetimonas*, which has been isolated from deep-sea HVs (Takai et al., 2005). Unlike *Thioreductor*, which became dominant with increasing sulfide levels, phylogenetic analysis revealed a large 16S rRNA sequence cluster related to *Sulfurovum* spp. in the sediments of shallow-water HV fields at Milos Island, Greece (Giovannelli et al., 2013).

During relatively silent venting periods (pH > 7.5), Gammaproteobacteria became abundant, which has also been reported to play important roles in some deep-sea HV fields, while utilizing sulfur-oxidizing pathways distinct from Campylobacteria (Yamamoto et al., 2011). The representative genus, *Thiomicrorhabdus*, is sulfur-oxidizing but basically not hydrogen-oxidizing (Liu et al., 2020). These observations suggest that bacterial cooperation in the ambient water involves not only sulfur oxidation but also sulfur reduction and hydrogen oxidation under sulfide (HS^-/S^{2-})-supplemented conditions. Despite the absence of hydrothermal venting, this habitat still retained sulfur compounds, such as elemental sulfur (S^0) or thiosulfate ($S_2O_3^{2-}$), which were available for sulfur oxidation by local bacterial communities. Although no temporal literature is available for comparison, a previous study indicated that sediments farther from the vents contained fewer Campylobacteria and were instead contributed by Gammaproteobacteria (Giovannelli et al., 2013). However, a relatively stable environment, such as the non-reefal coral ecosystem at the western tip of Kueishan Island (T site), may not support correlations similar to the hydrothermal

doi:10.6342/NTU202500809

habitat. Notably, a negative correlation between sulfide and bacterial diversity was still observed, likely due to east-to-west currents transporting hydrothermal fluids from the vents to the coral fields. In contrast, the correlations between bacterial diversity and both pCO_2 and alkalinity were opposite to those observed in the vent area. Higher pCO_2 and lower alkalinity corresponded to higher bacterial diversity. However, during our sampling, these two water parameters remained substantially consistent and were not correlated with ambient pH. The increase in pCO_2 here may not be sufficient to impact pH levels, but instead provides additional carbon sources for bacterioplankton, which in turn alters their metabolic potential and composition (James et al., 2019).

Accordingly, the functional analysis revealed temporal shifts in bacterial metabolic states. Active hydrogen oxidation and the reduction/respiration of nitrogen and sulfur compounds were concentrated between November 2021 and January 2023, reflecting the bacterial compositions. Subsequently, as previously discussed, residual substances or byproducts may drive bacterioplankton to adjust their metabolic strategies, involving denitrification, nitrogen respiration, sulfur and hydrogen oxidation, and other related processes. In contrast, higher bacterial diversity in the coral field resulted in a broader range of bacterial functions. Bacterioplankton in this non-vent habitat exhibited active photosynthesis-associated processes and chemoheterotrophy compared to those in the venting region.

Gill microbiome better reflects water quality compared to carapace surface

Similar to the bacterioplankton in the HV field during the active venting period, the dominant bacterial class in both the gills and carapace surface of *X. testudinatus* was Campylobacteria, which are known to be a major group of symbiotic bacteria in HV-endemic invertebrates, including yeti crabs *K. hirsute*, galatheid crabs *S. crosnieri*, and

doi:10.6342/NTU202500809

vent gastropods *Cyathermia naticoide* (Goffredi et al., 2008; Tsuchida et al., 2011; Zbinden et al., 2015). Unlike bacterioplankton, *Sulfurovum* was the dominant Campylobacteria associated with *X. testudinatus*. Our FISH results showed that *Sulfurovum* was abundantly labeled in the *X. testudinatus* gills. As a sulfur-oxidizing bacterium, *Sulfurovum* is capable of oxidizing reduced sulfur (S^{2-} or $S_2O_3^{2-}$) into less toxic forms (S^0, sulfite SO_3^{2-}, and SO_4^{2-}), mitigating the toxicity of hydrogen sulfide from HV fluids (Nelson et al., 1995; Akerman et al., 2013; Wang et al., 2023). On the other hand, bacterial diversity on the carapace surface was higher than that in the gills and appeared to be more stable over time. The bacterial diversity on the carapace was also more resembled to that of the bacterioplankton in the surrounding water. However, the gill-associated bacterial diversity showed a stronger correlation with physicochemical parameters compared to the carapace. Both the gills and carapace are in direct contact with the environment, implying that gills may have greater selectivity for symbiotic bacteria. Furthermore, considering that crabs are benthic organisms and *Sulfurovum* dominated the sediments rather than the water, the influence of water quality and bacterioplankton on gill microbiome may not be direct. It might first affect the sediments and then the gills.

Potential metabolic processes of symbiotic bacteria in *X. testudinatus*

The predominance of sulfur-oxidizing bacteria (SOB) in the *X. testudinatus* gills is reminiscent of findings in the gills of vesicomyid clams (Cruaud et al., 2019), mytilid mussels (Halary et al., 2008; Szafranski et al., 2015; Duperron et al., 2016), and bresiliid shrimps (Tokuda et al., 2008) from HV habitats. Serving as an interface between an aquatic animal's internal circulatory system and the external environment, the gills provide an enclave for SOB to carry out sulfide detoxification and organic production

doi:10.6342/NTU202500809

for the hosts (Felbeck and Somero, 1982). Compared to bacterioplankton, the symbiotic bacteria performed active denitrification and sulfur oxidation, with sustained nitrogen respiration and hydrogen oxidation, but weaker sulfur respiration. The high functional contribution of hydrogen oxidation was probably due to *Sulfurovum* spp., which possess hydrogenase enzymes (Nakagawa et al., 2007; Wang et al., 2023). Previous studies have shown that H_2 can serve as an energy source in HV systems, fueling chemosynthetic symbioses (Petersen et al., 2011). In the process of denitrification, *Sulfurovum* may utilize nitrate (NO_3^-) as an electron acceptor while oxidizing reduced sulfur compounds as electron donors (Cardoso et al., 2006). *Sulfurovum* spp. from HV habitats contain genes required for the complete denitrification pathway (Wang et al., 2023). Amino acid sequences of nitrate reductase (NapA) measured in HV fluids near the East Pacific Rise were primarily derived from *Sulfurovum* spp. (Smith et al., 2007; Vetriani et al., 2014). These findings suggest that sulfide or hydrogen oxidation-associated denitrification could also occur in the *X. testudinatus* holobiont (Huang et al., 2019; Wang et al., 2023).

The metabolic functions of *Sulfurovum* are likely essential for the physiological adaptations of *X. testudinatus* to hydrothermal environments. Previously documented acid-base regulatory ability through NKA, VHA, and HCO_3^-/Cl^- exchange could be reconsidered within the context of host-microbe interactions (Hu et al., 2016; Allen et al., 2020). The sulfide oxidation capacity of *Sulfurovum* helps detoxify sulfide from the hydrothermal fluids, which could otherwise inhibit cytochrome c oxidase (COX, complex IV) in the mitochondria, generating less toxic sulfur-oxidized derivatives such as thiosulfate (Chou et al., 2023; Wang et al., 2023). The acid generated through sulfide oxidation ($H_2S + 2O_2 \rightarrow 2H^+ + SO_4^{2-}$) and hydrogen oxidation ($H_2 \rightarrow 2H^+ + 2e^-$) could be buffered by strong acid-base regulatory mechanisms of *X. testudinatus*, indicating an evolved tolerance co-adapted with bacterial metabolism (Dick, 2019). The

doi:10.6342/NTU202500809

denitrification activities of *Sulfurovum* may supply nitrogen sources, complementing the ammonia excretion of *X. testudinatus*, which increased under acidified conditions (Allen et al., 2020). Furthermore, chemosynthetic products from *Sulfurovum*, including organic carbon compounds (McGonigle et al., 2020), may contribute to the host's energy budget during periods of limited food availability, as *X. testudinatus* experience episodic feeding opportunities (Jeng et al., 2004). This complex physiological integration suggests that host ion transport mechanisms have evolved not only to mitigate environmental acidity but also to exploit benefits for bacterial metabolism. Additionally, *Thiothrix*, identified within Gammaproteobacteria in the *X. tesdutinatus* gills, is also a well-documented sulfur oxidizer. These large filamentous bacteria are known to colonize rocks and sediments around hydrothermal vents, contributing to sulfur oxidation (Stein, 1984; Moyer et al., 1995). White filamentous microbial films observed in HV fields are often associated with *Thiothrix* spp. (Kalanetra et al., 2004), whereas they were not detected on the carapace of *X. testudinatus* as an abundant genus, despite the presence of a white hairy biofilm.

Overall, the carapace surface exhibited slightly higher functional proportions of fermentation and chemoheterotrophy compared to the gills, while chemoautotrophic processes such as sulfur and hydrogen oxidation were less prevalent. This suggests microniche differentiation occurring within the HV system, where nutrient availability shapes microbial interactions through cooperation or competition (Hoek et al., 2016). The distinct microbial communities in the gills and carapace likely reflect differences in the microenvironmental characteristics of these two interface tissues. The gills create a specialized microhabitat that facilitates gas exchange and water flow while being adjacent to the hemolymph, establishing oxygen and metabolites gradients (Farrelly and Greenaway, 1994). This continuous influx of seawater, enriched with dissolved

doi:10.6342/NTU202500809

inorganic compounds, provides an optimal environment for chemoautotrophic bacteria, which rely on reduced sulfur compounds and oxidants from hydrothermal fluids (Ponsard et al., 2013). The physical structure of the gills, including filaments, lamellae, and specialized epithelium, may serve as attachment sites or filters for the selective colonization of specific microbes (Silverman et al., 1996; Freitas et al., 2022; Fusi et al., 2023). In contrast, the carapace surface is directly exposed to ambient water but lacks the active water flow and gas exchange capacity found in the gills. The carapace microenvironment is characterized by ambient O_2 concentrations, pH levels, and nutrient compositions, likely favoring heterotrophy and fermentation rather than chemoautotrophy. Additionally, the carapace, composed primarily of chitin, may selectively promote the colonization of microorganisms capable of degrading chitin or its derivatives (Yurgel et al., 2022). This is supported by the presence of Bacteroidia, Clostridia, and Gammaproteobacteria, which possess chitin degradation genes (Shu et al., 2019). Bacterial communities within the gills and carapace demonstrated metabolic flexibility and unique adaptation mechanisms, allowing them to thrive in distinct host-associated niches. The persistent predominance of *Sulfurovum* in both tissues, with varying abundances correlated with physicochemical parameters, suggests its metabolic or physiological significance beyond sulfide detoxification, which reinforces its interdependence with the *X. testudinatus* host.

Evolutionary selection of environmental microorganisms on metazoan hosts

The substantial disparity in the relative abundance of *Sulfurovum* between ambient seawater, where it is not prominent, and the *X. testudinatus* gills, where it prevails, hints at the evolutionary pathways and ecological processes that drive microbial transitions from environmental to symbiotic states. This phenomenon extends

doi:10.6342/NTU202500809

beyond intuitive environmental acquisition, involving complex processes such as host filtering and microbial adaptation (Brooks et al., 2017). The habitat of *X. testudinatus* likely exerts considerable selective pressures favoring *Sulfurovum* over other sulfur-metabolizing bacteria through mechanisms such as specific recognition molecules, immune tolerance, or the establishment of specialized metabolic niches (Chaston and Goodrich-Blair, 2010). The presence of *Sulfurovum* across various host tissues and in the surrounding environment, albeit in lower abundance, indicates its adaptability to environmental conditions while benefiting from host association, suggesting a facultative rather than obligate symbiosis (Blow et al., 2020). This flexibility may represent an intermediate stage in the evolutionary transition from environmental microbes to specialized symbionts (Sachs et al., 2011). In extreme environments like HV system, selective pressures for these associations are significant, as both the symbiotic microbes and metazoan host derive adaptive benefits. The host gains detoxification capabilities and potential nutritional supplementation, while the microbes secure a stable habitat with reliable access to resources (Goffredi, 2010). The evolutionary processes likely originate from random environmental encounters, progressively developing into genomic crosstalk that enhances symbiotic competence and mutual fitness (Toft and Andersson, 2010). The hydrothermal environment at Kueishan Island, marked by intermittent venting, may impose selective pressures that promote flexible associations rather than strict obligate dependencies, allowing both partners to endure temporal environmental fluctuations. Future comparative genomic analyses of free-living and host-associated *Sulfurovum* species, or even strain-level comparison (Breusing et al., 2022), could reveal genomic signatures indicative of this evolutionary transition, which may encompass genes related to colonization, host

doi:10.6342/NTU202500809

interaction, or metabolic pathways that enhance symbiotic fitness (McCutcheon and Moran, 2007; Sach et al., 2011).

Summary

HV systems play a crucial role in oceanic biogeochemical processes and have been recognized as deep-sea oases of life, nourished by chemoautotrophs. (Tarasov et al., 2005). Kueishan Island, a geologically young volcanic island located in an earthquake-prone zone, experiences frequent volcanic and seismic activity, leading to intermittent hydrothermal venting in its HV field (Konstantinou et al., 2013; Deffontaines et al., 2022; Chiu et al., 2024). The episodic release of vent fluids alters the surrounding water chemistry, contributing toward the dynamics of microplankton and the symbiotic microbiota of resident holobionts. While most research on sulfur detoxification mechanisms in marine organisms has focused on deep-sea HV systems along mid-ocean ridges (Zierenberg et al., 2000; Zhang et al., 2017), shallow-water HV systems are increasingly used as accessible and cost-effective proxies (Chiu et al., 2022; Chen et al., 2023; Chou et al., 2023). The Kueishan Island HV system enables long-term and continuous observations of hydrothermal microbial community fluctuations. Our study reveals correlations between water quality and both bacterioplankton and the gill-associated bacteria of *X. testudinatus* holobiont. Moreover, bacterial metabolic functions, from ambient water to the carapace surface and gills, suggest biochemical interactions with environmental materials. The symbiotic bacterial community is dominated by the chemolithotrophic SOB *Sulfurovum* (Campylobacteria), which performs sulfur and hydrogen oxidation and likely drives denitrification, while *Thioreductor* dominates the bacterioplankton, engaging in sulfur reduction/respiration.

doi:10.6342/NTU202500809

Although taxonomically sound, the 16S rRNA gene sequencing approach cannot conclusively determine metabolic capacity, phylogenetic assumptions and reference database constraints limit functional predictions (Langille et al., 2013; Louca et al., 2016). Future studies should incorporate advanced techniques to further investigate hydrothermal holobiont interactions. Metagenomic and metatranscriptomic analyses could identify genetic potential and active microbial pathways (Aguiar-Pulido et al., 2016), and metabolomic profiling could clarify host-microbe chemical interactions (Phelan et al., 2012). Comparative genomics may uncover symbiotic adaptations between free-living and host-associated *Sulfurovum* spp. or other related microbes. Additionally, stable isotope probing could provide evidence of metabolic activities at the tropical level within specific microenvironments of the host tissues (Kleiner et al., 2018). While further research is needed to fully elucidate these associations, this chapter offers profound insights into the adaptation of HV-endemic holobionts, highlighting the role of microbes in shaping inter-domain co-evolution in extreme and dynamic ecosystems.

doi:10.6342/NTU202500809

2.5 Tables and Figures

Chapter 2

Table 2; Figures 9-22

doi:10.6342/NTU202500809

Table 2. The sample size of bacterial samples. The sample sizes of bacterial samples collected from the water, gills and carapace are listed along with the corresponding dates. Due to variations in sampling conditions and sequence quality, the sample numbers varied across dates.

Water	Date	Number
Vent	2021 Feb	2
	2021 Aug	1
	2021 Nov	1
	2021 Dec	3
	2022 Aug	3
	2022 Oct	3
	2023 Jan	3
	2023 Oct	3
	2024 Apr 11	3
	2024 Apr 30	3
Tail	2021 Feb	2
	2021 Aug	1
	2021 Nov	1
	2021 Dec	2
	2022 Aug	3
	2022 Oct	3
	2023 Jan	2
	2023 Oct	3
	2024 Apr 11	3
	2024 Apr 30	3

Tissue	Date	Number
Gills	2020 Aug	9
	2020 Nov	4
	2021 Feb	11
	2021 May	16
	2021 Aug	15
	2021 Nov	16
Carapace	2020 Aug	9
	2020 Nov	12
	2021 Feb	14
	2021 May	12
	2021 Aug	11
	2021 Nov	13

doi:10.6342/NTU202500809

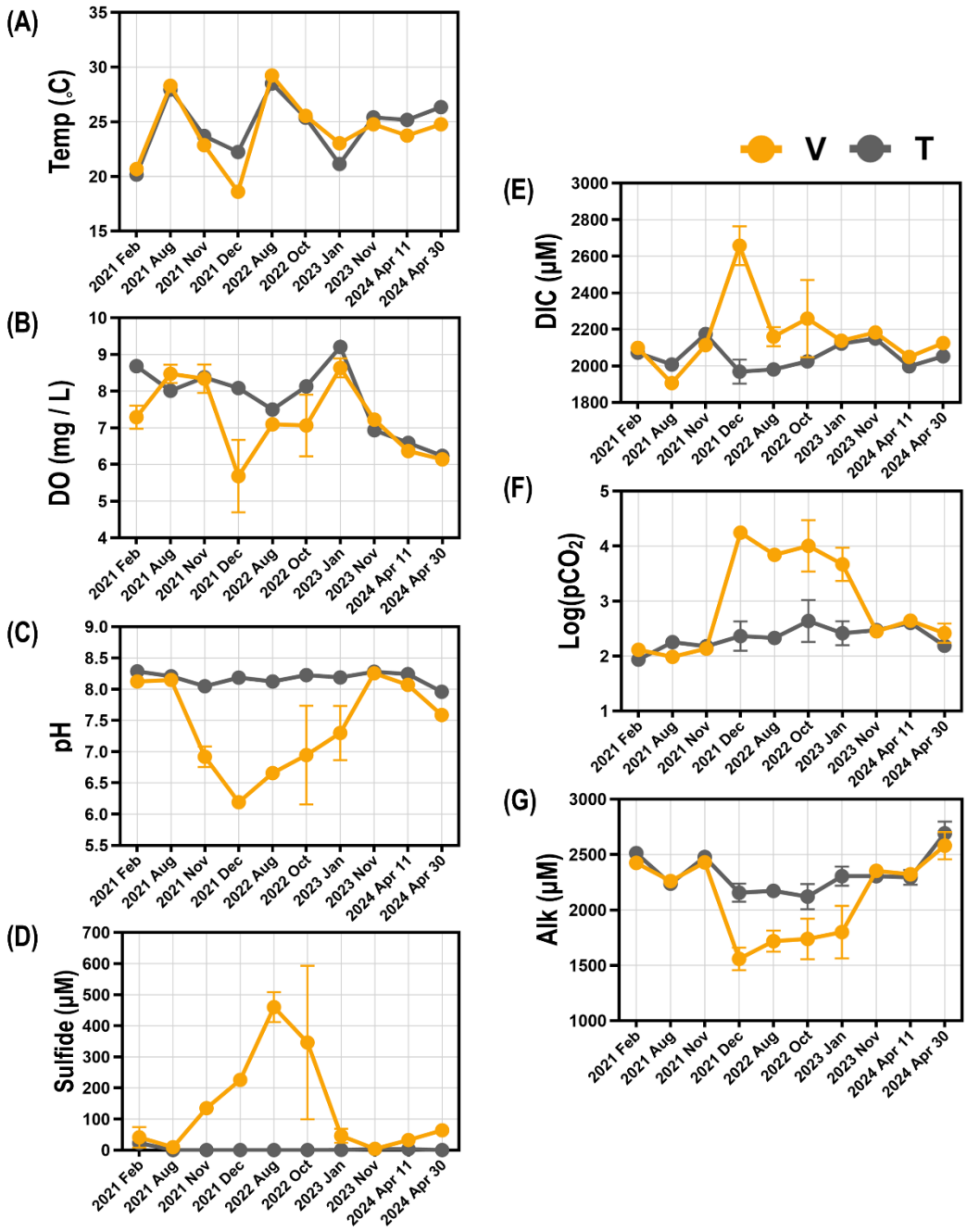

Figure 9. Water quality of the V and T sites based on the bacterial community in the water. Temp, temperature (A); DO, dissolved oxygen (B); pH (C); sulfide (D); DIC, dissolved inorganic carbon (E); Log(pCO_2), base-10 logarithm of the partial pressure of carbon dioxide (CO_2) measured in μatm (F); Alk, alkalinity (G). V, site near the vents; T, tail site. Data are presented as mean ± standard deviation (SD), based on triplicate measurements

doi:10.6342/NTU202500809

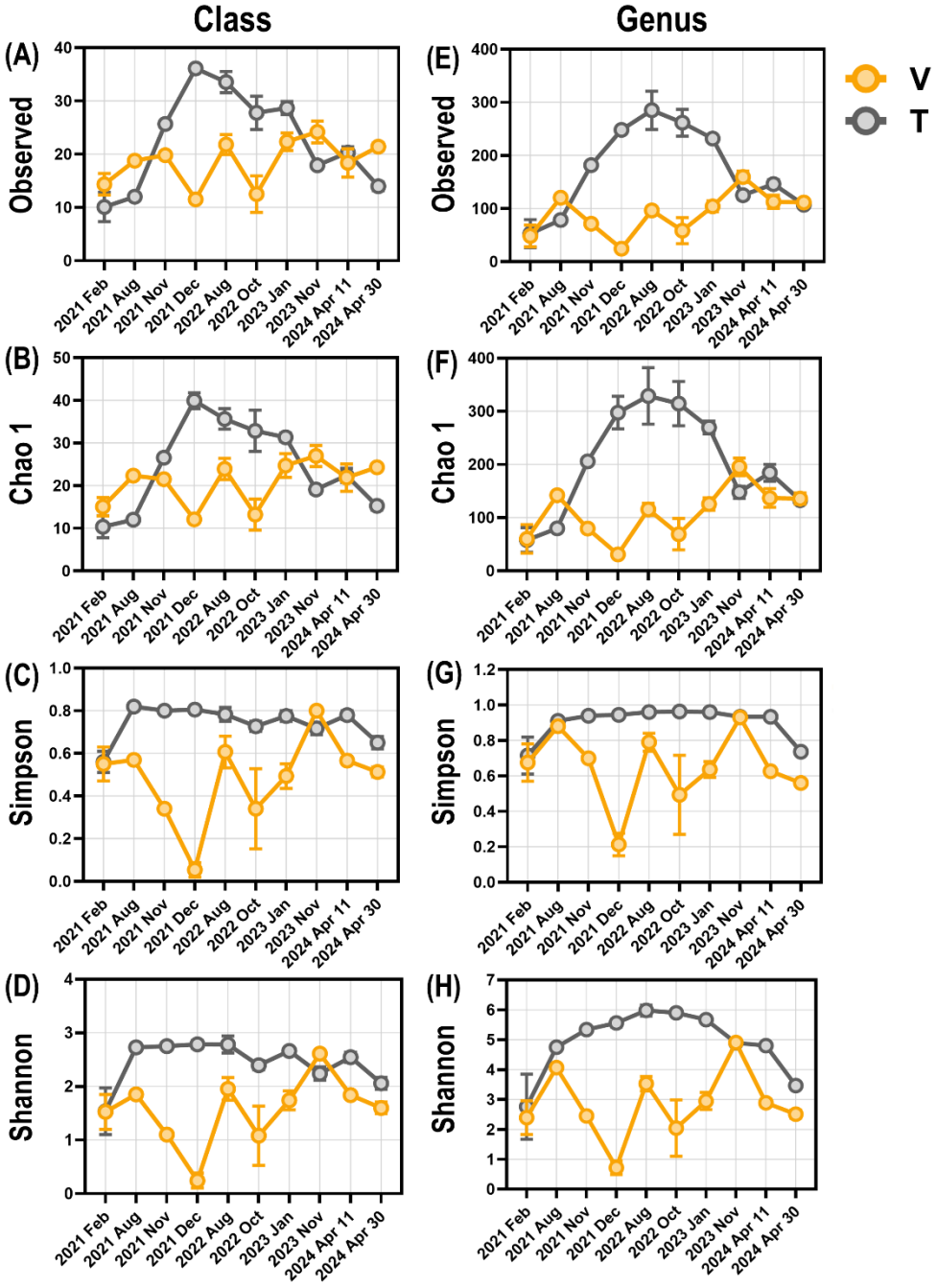

Figure 10. Temporal dynamics of bacterial alpha diversity in the water. Temporal dynamics in alpha diversity indices for water bacterial communities at the vent (V) and tail (T) sites are presented. The indices presented include observed taxa number, Chao1 richness estimates, Simpson's index, and Shannon entropy, all calculated at both the class (A-D) and genus (E-H) taxonomic levels. V, site near the vents; T, tail site.

doi:10.6342/NTU202500809

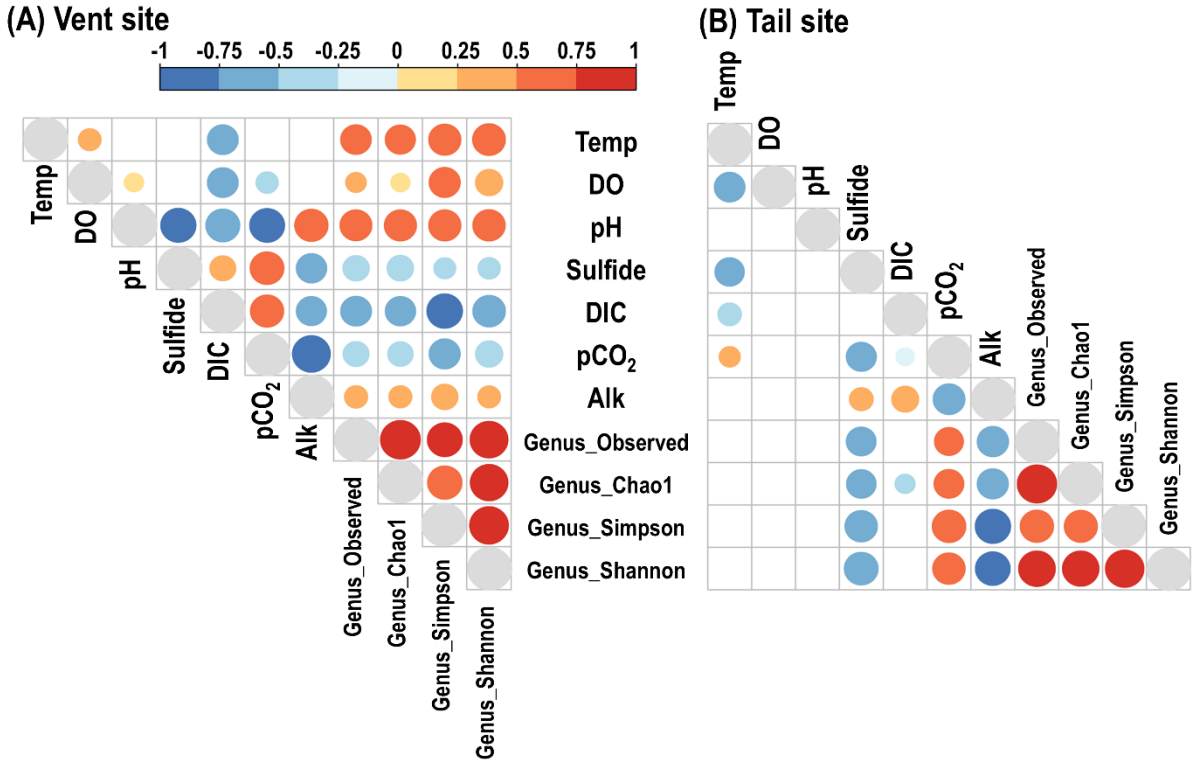

Figure 11. Correlations between water parameters and bacterial diversity in the water. The correlations at the vent site (A) and tail site (B) are shown. Circle size and color scale indicate correlation coefficients ranging from -1 (blue) to 1 (red), with weak or negligible correlations in shades of blue and yellow. Only significant correlations are shown (Pearson's correlation, followed by Bonferroni correction, $p < 0.05$). Temp, temperature; DO, dissolved oxygen; DIC, dissolved inorganic carbon; pCO_2, base-10 logarithm of the partial pressure of carbon dioxide measured in μatm; Alk, alkalinity.

doi:10.6342/NTU202500809

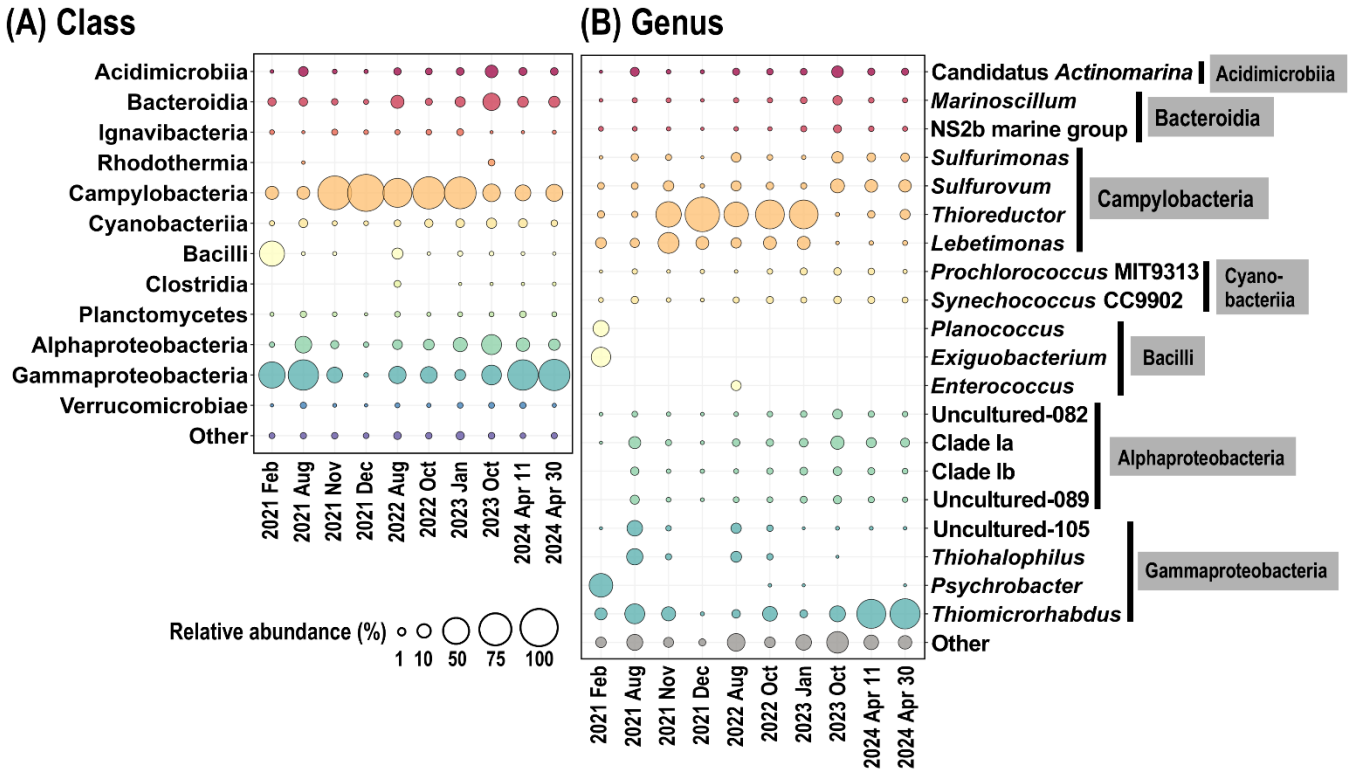

Figure 12. Bacterial composition of the water at the vent site. Bubble plots show vent site bacterial composition at the class (A) and genus (B) levels. Circle size represents the relative abundance (%) of taxa at each time point.

doi:10.6342/NTU202500809

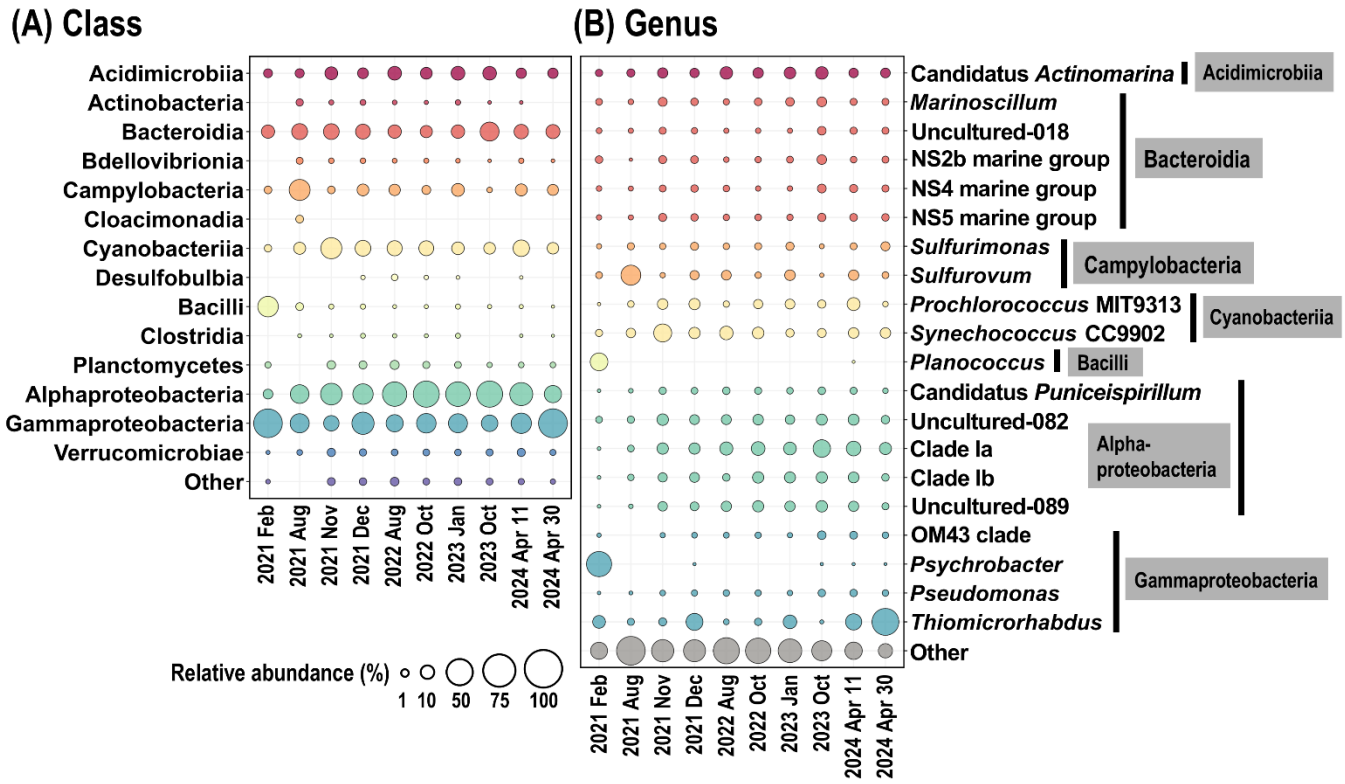

Figure 13. Bacterial composition of the water at the tail site. Bubble plots show tail site bacterial composition at the class (A) and genus (B) levels. Circle size represents the relative abundance (%) of taxa at each time point.

doi:10.6342/NTU202500809

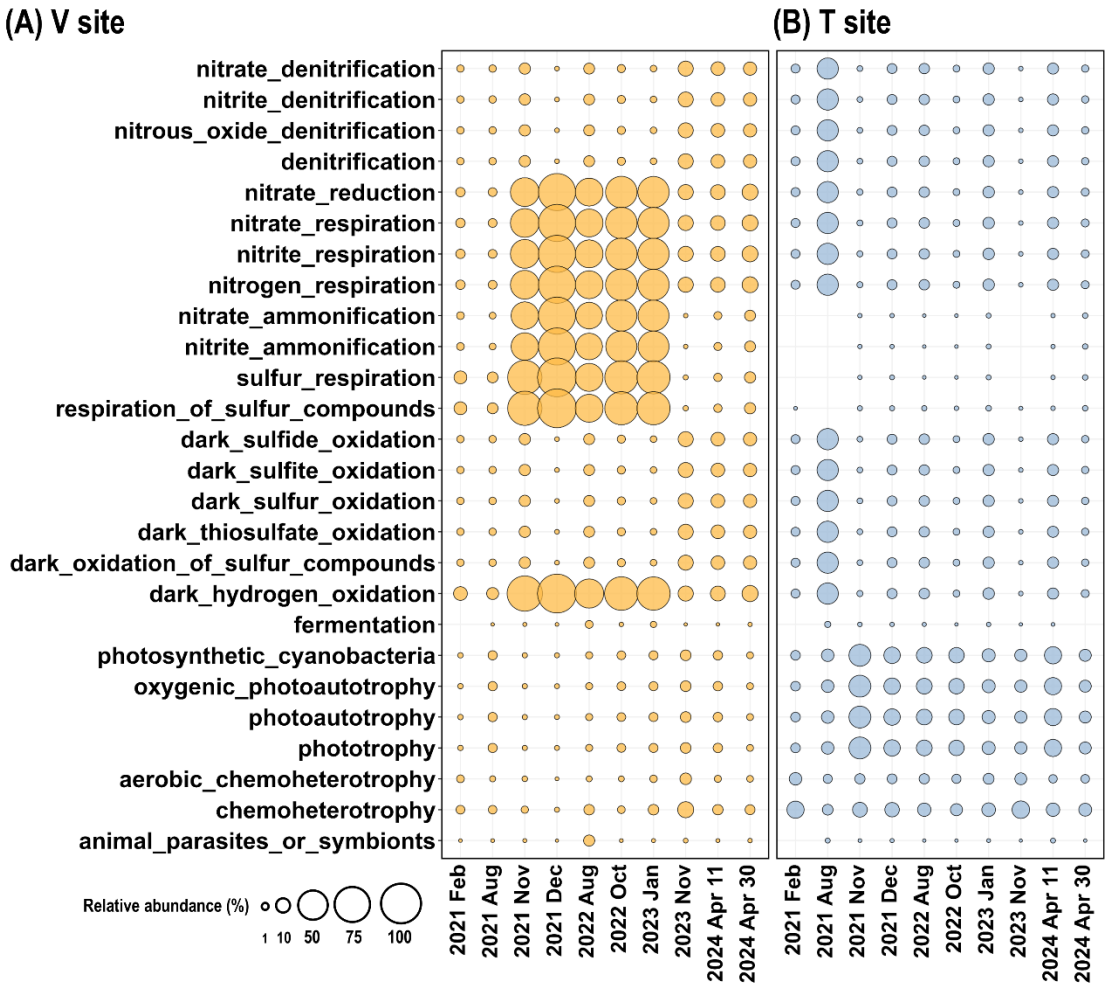

Figure 14. FAPROTAX functional analysis of the water bacterial community. Temporal dynamics of potential functions of the water bacterial communities at the V site (A) and T site (B). Circle size represents the functional proportion (%) at each time point. V, site near the vents; T, tail site.

doi:10.6342/NTU202500809

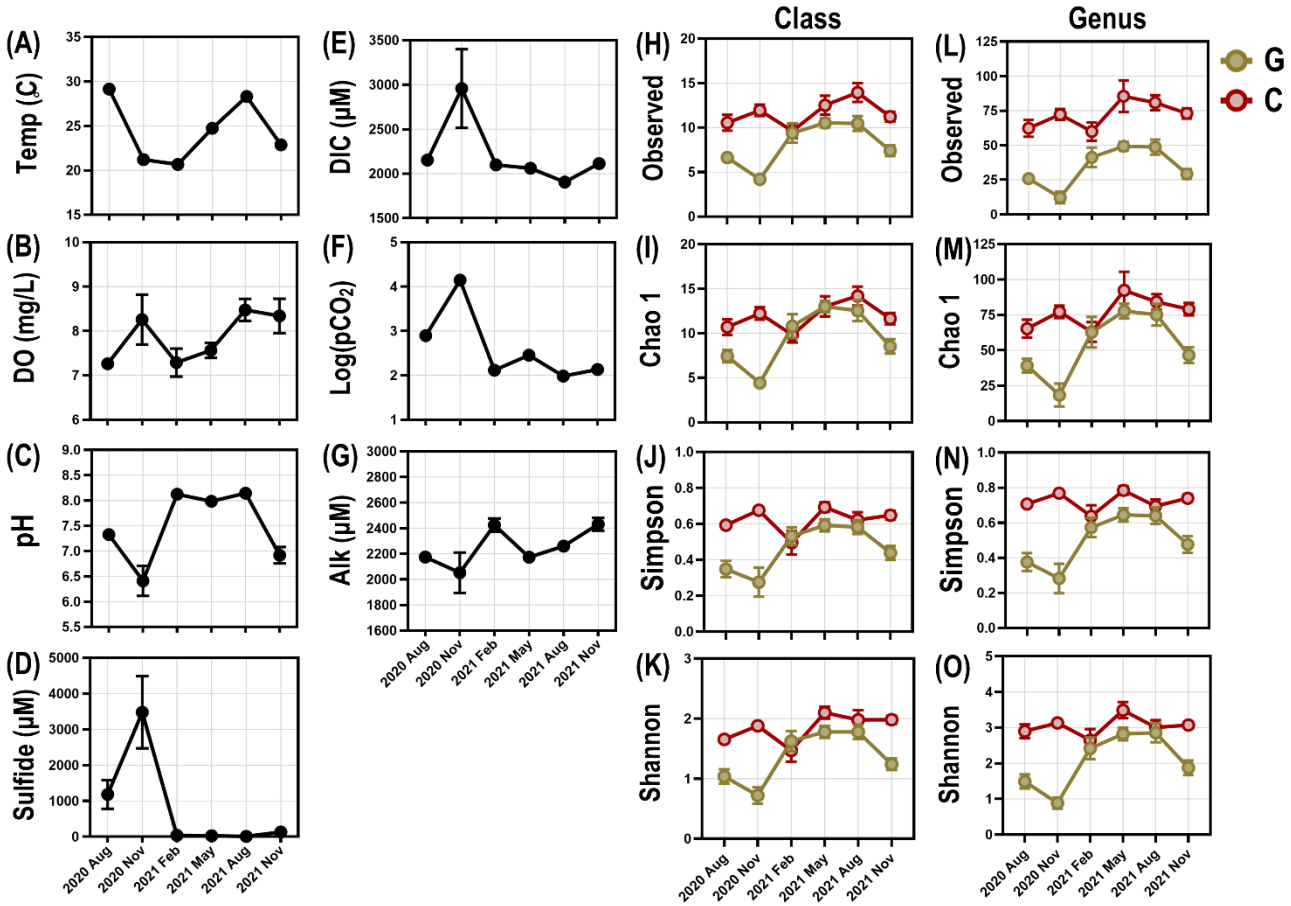

Figure 15. Water quality and bacterial alpha diversity of the gills and carapace surface. Water parameters, including temperature (Temp; A), dissolved oxygen (DO; B), pH (C), sulfide (D), dissolved inorganic carbon (DIC; E), Log(pCO_2) (F), and alkalinity (Alk; G), are shown. Bacterial alpha diversity indices, including observed taxa number (Observed), Chao 1 richness estimates (Chao 1), Simpson's index (Simpson), and Shannon entropy (Shannon), are presented at the class level (H-K) and genus level (L-O). G, gills; C, carapace surface. Data are presented as mean ± SD, based on triplicate measurements.

doi:10.6342/NTU202500809

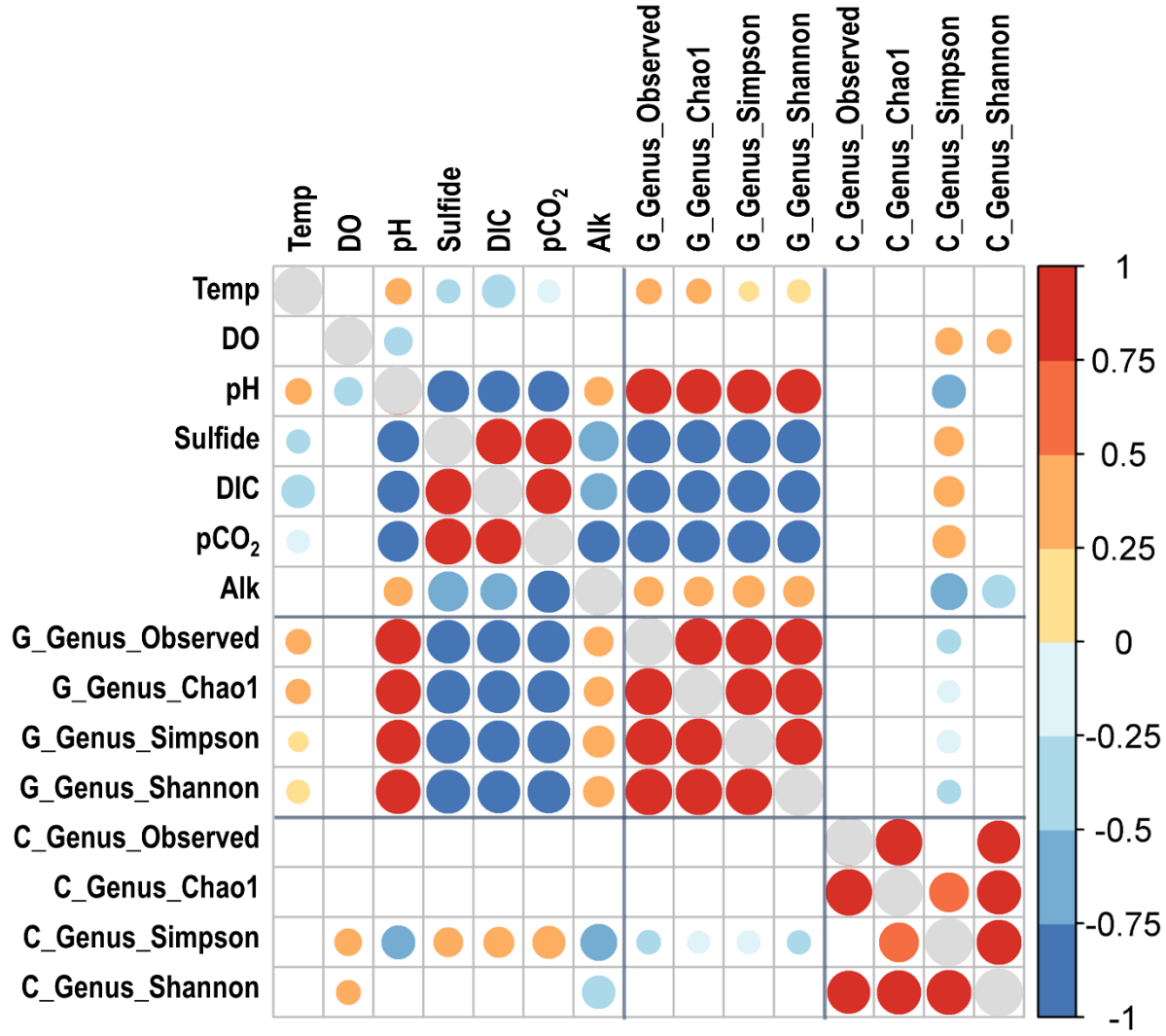

Figure 16. Correlation between water parameters and bacterial diversity of the gills and carapace surface. Circle size and color scale indicate correlation coefficients ranging from -1 (blue) to 1 (red), with weak or negligible correlations in shades of blue and yellow. Only significant correlations are shown (Pearson's correlation, followed by Bonferroni correction, $p < 0.05$). G, gills; C, carapace surface. Temp, temperature; DO, dissolved oxygen; DIC, dissolved inorganic carbon; pCO_2, base-10 logarithm of the partial pressure of carbon dioxide measured in μatm; Alk, alkalinity.

doi:10.6342/NTU202500809

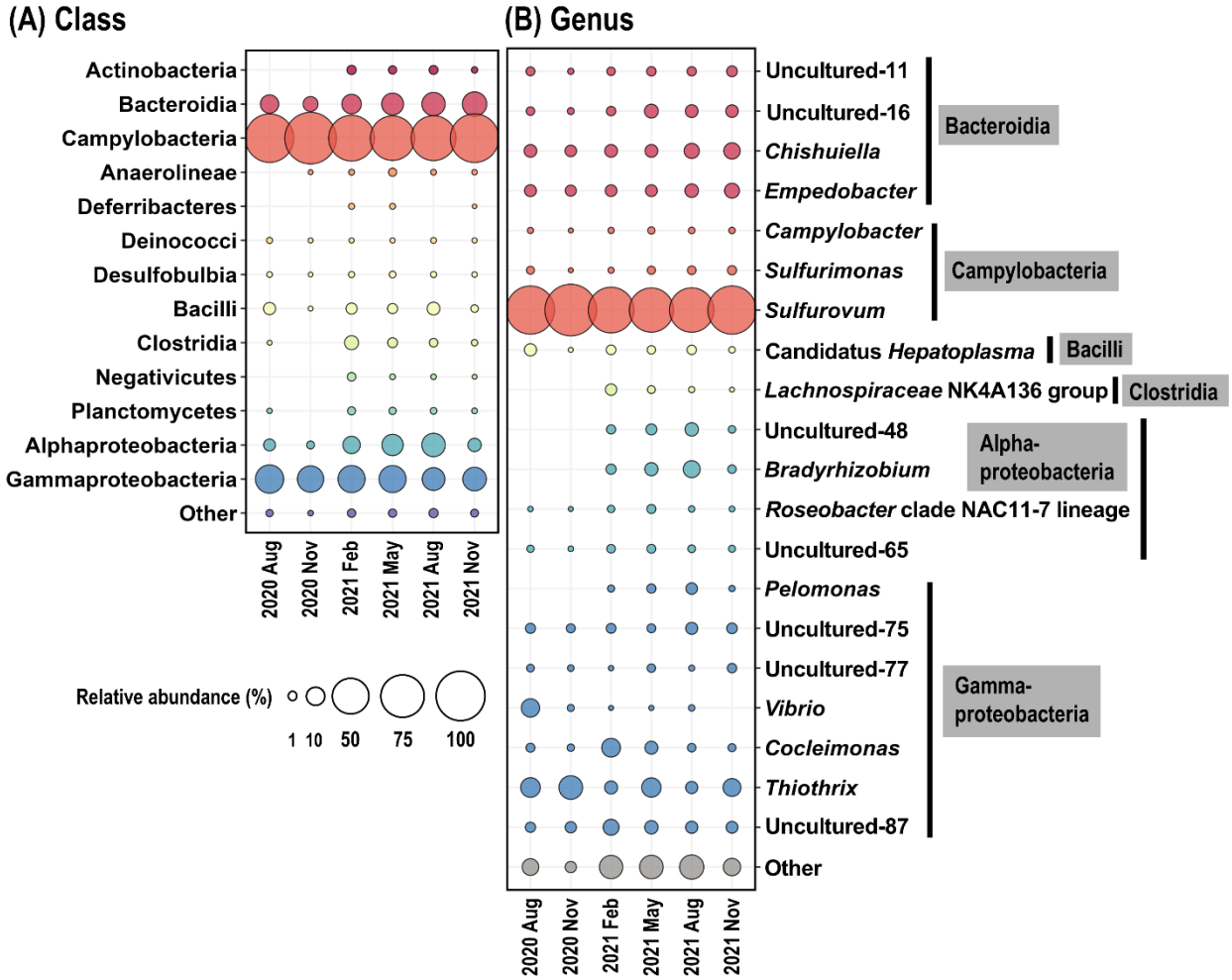

Figure 17. Dynamics of bacterial composition in the gills. Bubble plots show gill bacterial composition at the class (A) and genus (B) levels. Circle size represents the relative abundance (%) of taxa at each time point.

doi:10.6342/NTU202500809

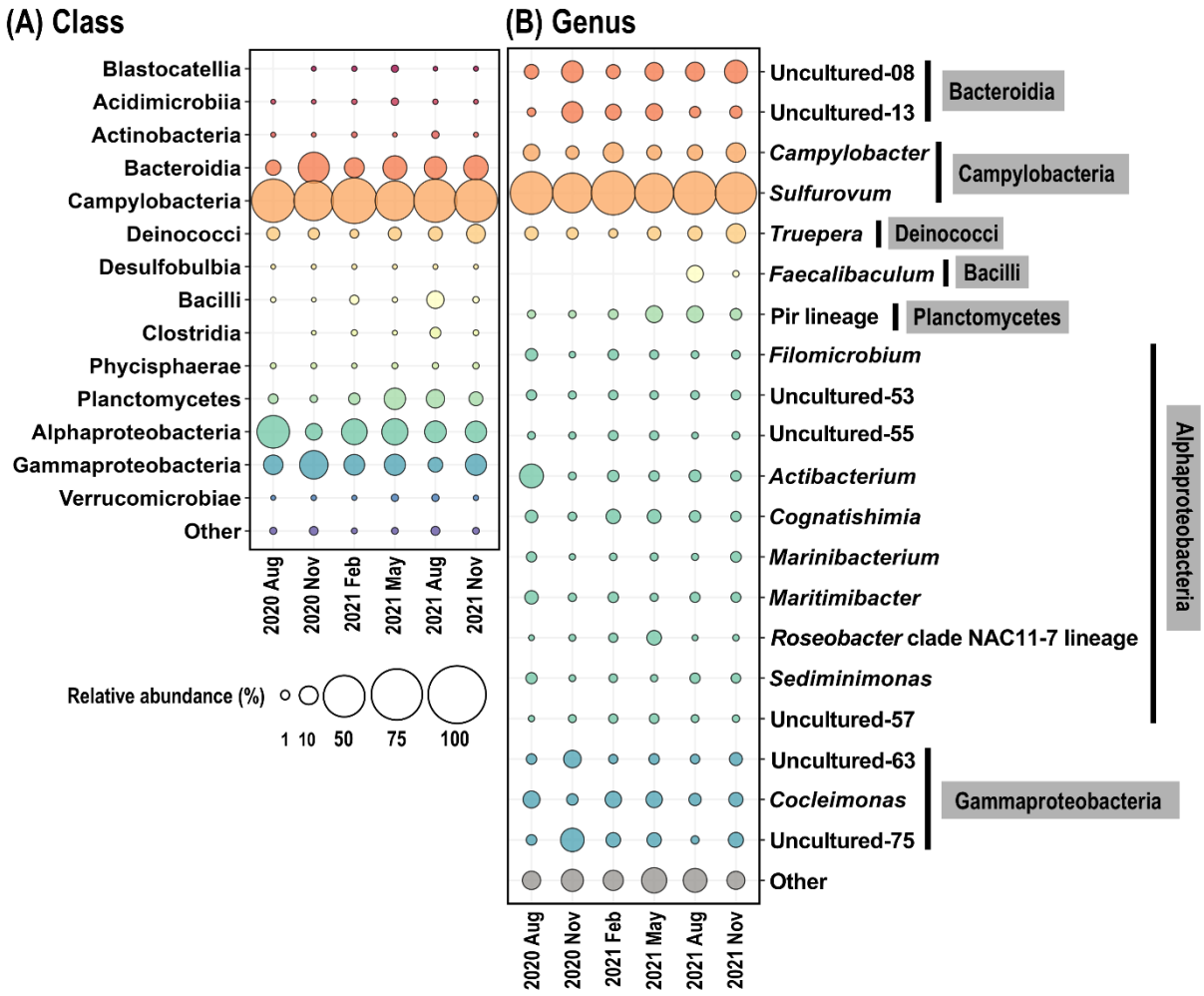

Figure 18. Dynamics of bacterial composition on the carapace surface. Bubble plots show carapace bacterial composition at the class (A) and genus (B) levels. Circle size represents the relative abundance (%) of taxa at each time point.

doi:10.6342/NTU202500809

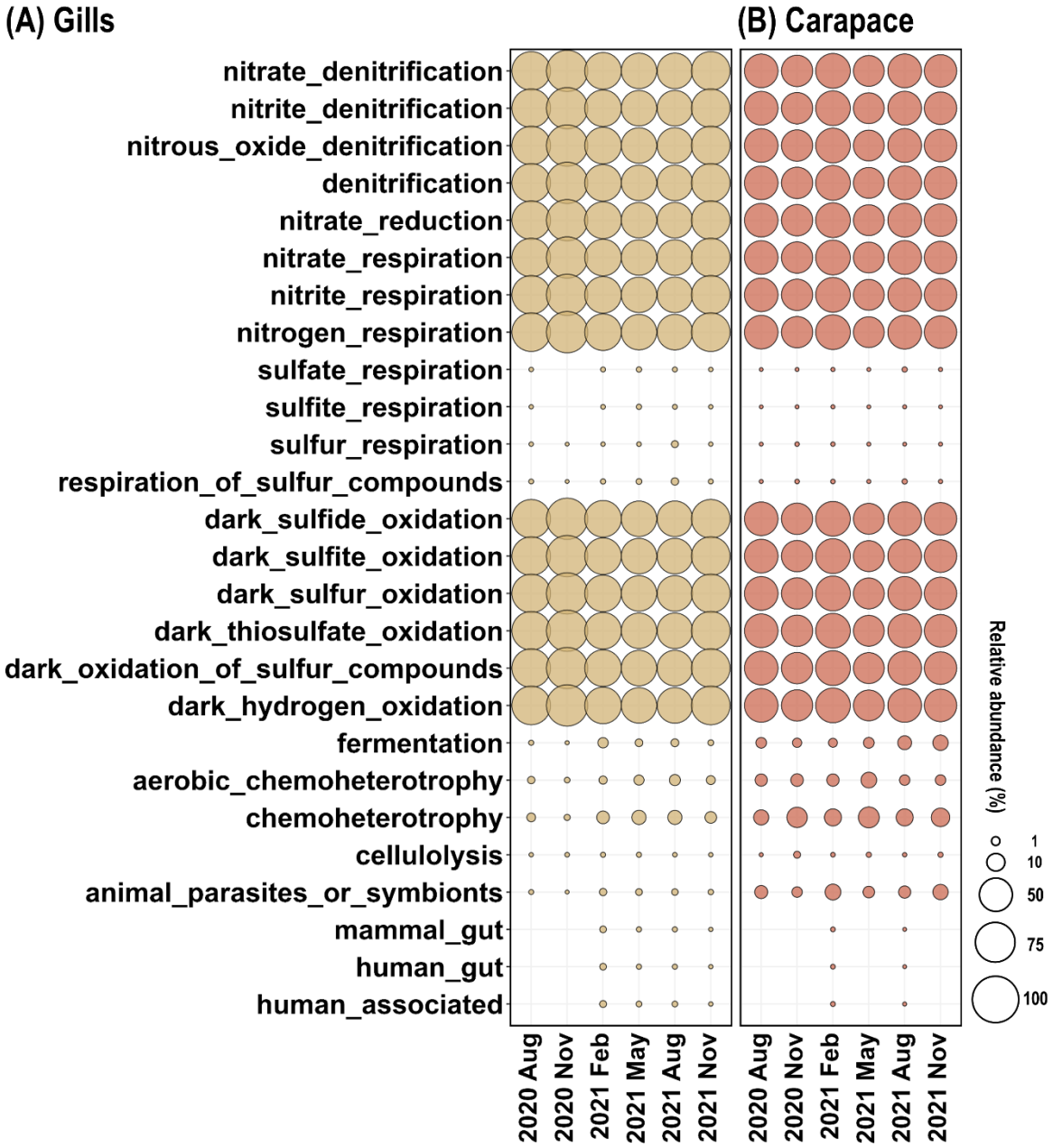

Figure 19. FAPROTAX functional analysis of the bacterial community in the gills and on the carapace surface. Temporal dynamics of potential functions of the bacterial communities at in the gills (A) and on the carapace surface (B). Circle size represents the functional proportion (%) at each time point.

doi:10.6342/NTU202500809

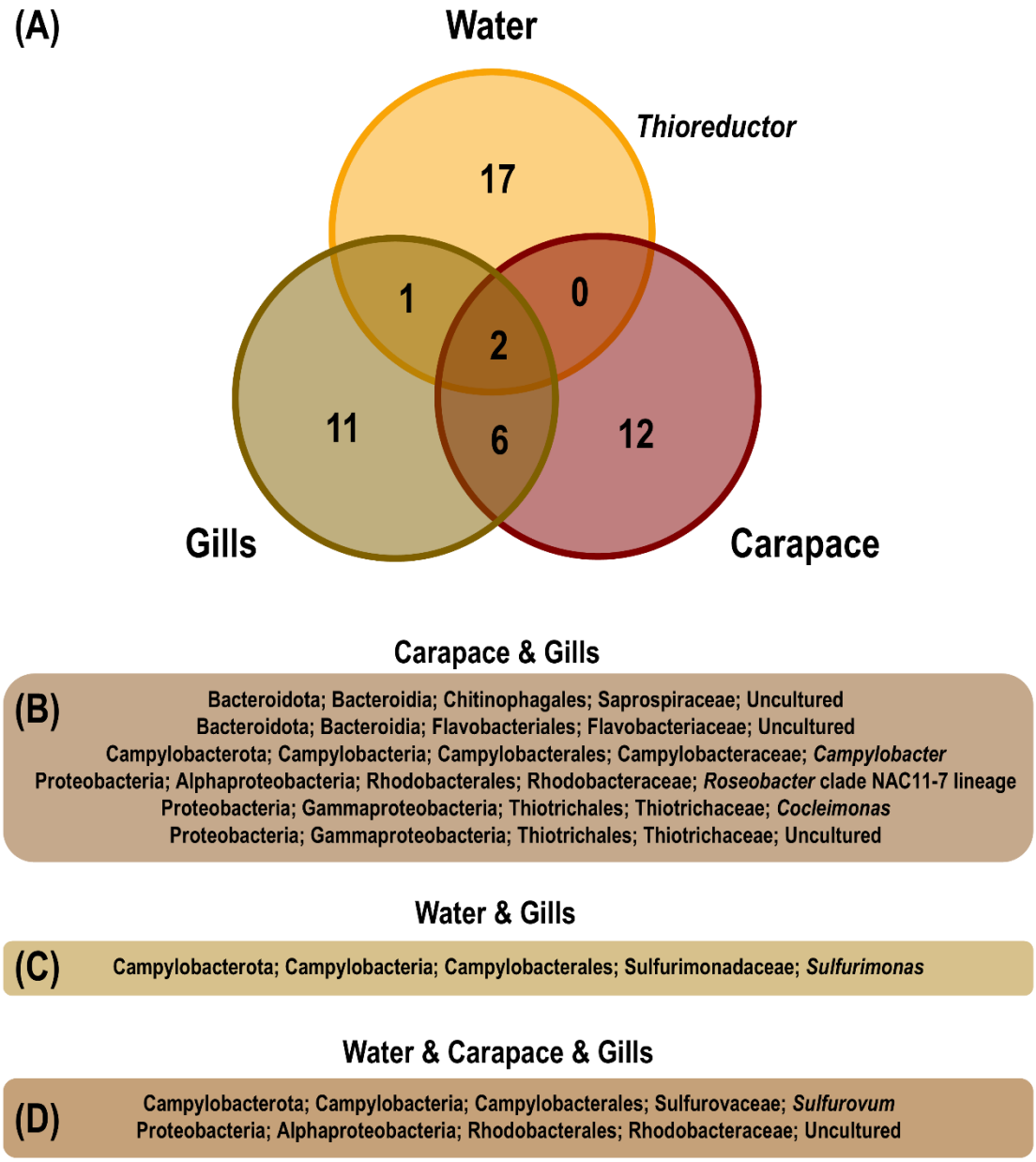

Figure 20. Venn diagram showing the Top20 genera in the gills, carapace, and the surrounding water. The Venn diagram shows the numbers of shared and unique genera among gills, carapace, and surrounding water (A). The bacterial genera common to both the carapace and gills are highlighted (B). The bacterial genera common to both the water and gills are highlighted (C). The core genera shared across the water, carapace, and gills are highlighted (D).

doi:10.6342/NTU202500809

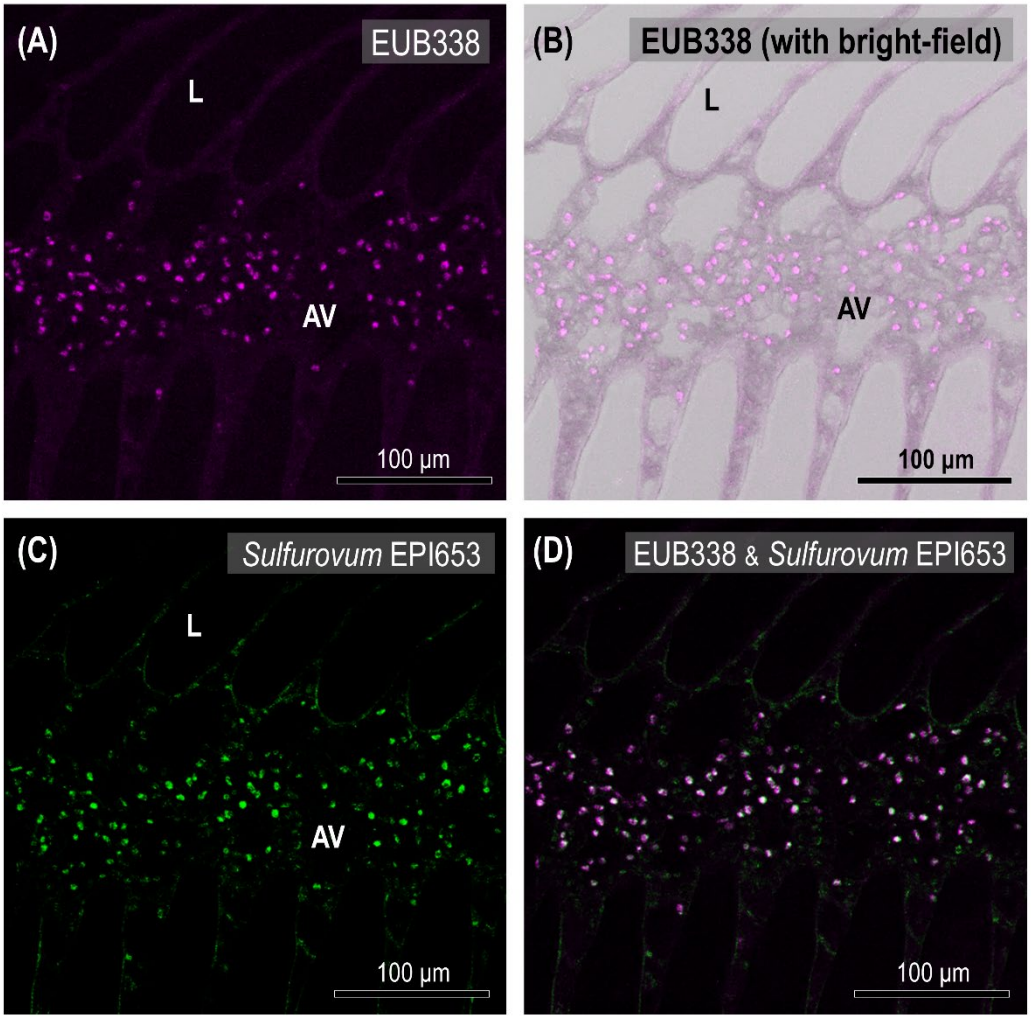

Figure 21. Fluorescence in situ hybridization (FISH) of the transverse section of gill filaments. The fluorescence images show representative Cy5 signals (far-red, universal bacteria probe EUB338) and Alexa 488 signals (green, genus *Sulfurovum*-targeted probe EPI653) on the transverse section of gill filaments. The universal EUB338 signal showed the distribution of bacteria within the gills (A), which overlaps on a bright-field image, revealing the anatomical distribution primarily around the afferent vessel (B). The genus-targeted EPI653 signal (green) showed the distribution of *Sulfurovum* (C). The co-localization of EUB338 and EPI653 signals were presented (D). Scale bars = 100 µm. L, lamella; AV, afferent vessel.

doi:10.6342/NTU202500809

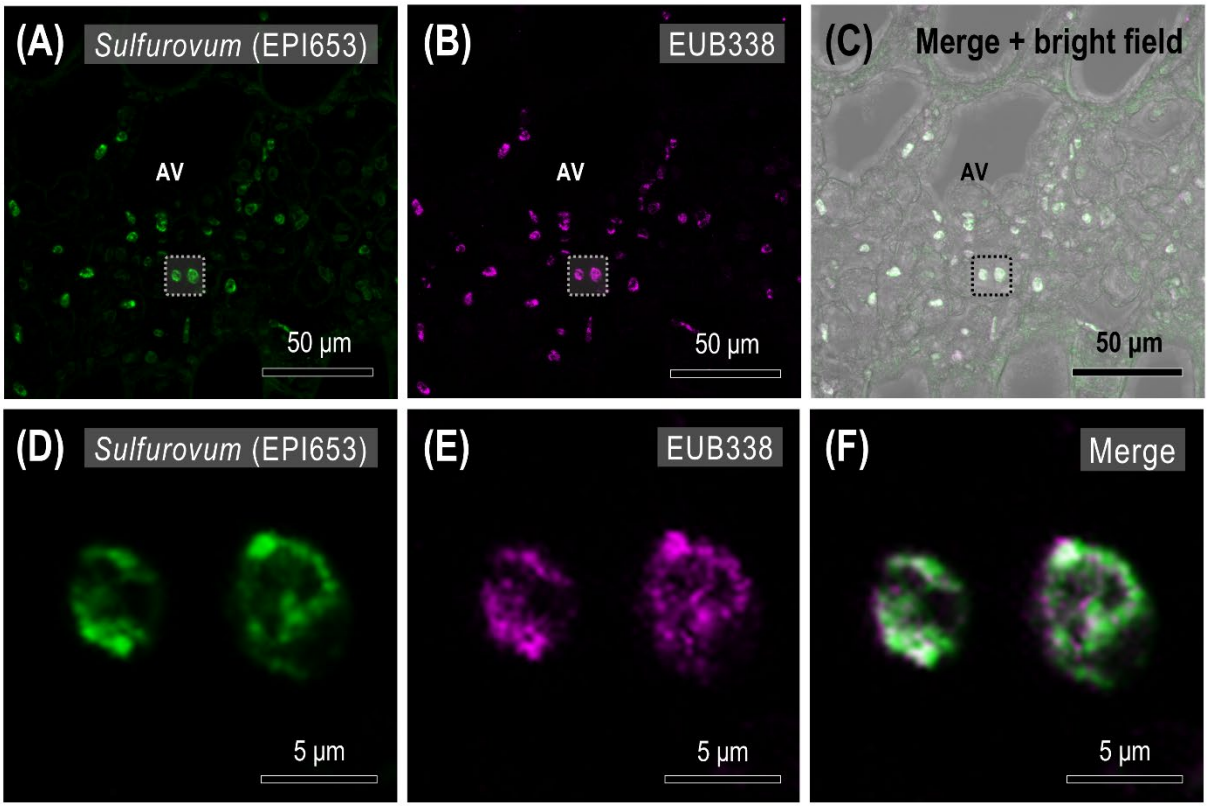

Figure 22. Fluorescence in situ hybridization (FISH) magnification images. Representative Alexa 488 signals (green, *Sulfurovum* probe EPI653) and Cy5 signals (far-red, universal bacteria probe) in the transverse sections of gill filaments. The *Sulfurovum*-targeted EPI653 signal (green, A) and universal EUB338 signal (far-red, B) showed the distribution of bacteria within the gills The signals of *Sulfurovum* and universal bacteria overlap on a bright-field image (C). The magnification of EPI653, EUB338, and merged images were presented (D-F). Scale bars = 50 μm (A-C) and 5 μm (D–F), respectively. AV, afferent vessel.

doi:10.6342/NTU202500809

Chapter 3

Sequential Strategy Underlies *Xenograpsus testudinatus* Holobiont Resilience in Extreme Hydrothermal Environments

doi:10.6342/NTU202500809

3.1 Introduction

Life relies on the production of chemical compounds for metabolic processes, enzymes to catalyze biochemical reactions, biological membranes to compartmentalize cell structure, and energy sources essential for these properties. Several theories have been proposed to explain the origin of life, including the “primeval soup” hypothesis, in which basic organic compounds formed from inorganic precursors such as CO_2 and ammonia, with lightning providing the necessary energy (Wills and Bada, 2001). Another hypothesis assumes that amino acids could have been synthesized in the atmosphere via long- wavelength UV radiation (Miller, 1953), while others proposed that organic compounds were delivered by carbonaceous meteorites and cosmic dust (Miller and Urey, 1959). However, HV systems appear to be the only environment capable of providing a constant and substantial energy source to sustain life and drive evolution. Smokers release reduced compounds such as hydrogen sulfide (H_2S), hydrogen (H_2), and ferrous iron (Fe^{2+}), which could have fueled the earliest metabolic pathways, while CO_2 served as the backbone for biomolecules (Olson, 2019). Furthermore, the “iron-sulfur world” hypothesis suggests that the formation and derivation of iron sulfide (FeS) from hydrothermal fluids may have supported a chemoautotrophic origin of life under the restrictive conditions of early Earth (Wächtershäuser, 1998).

To this day, hydrothermal vent systems continue to supply chemicals that sustain life and shape ocean chemistry. However, these environments also impose considerable physiological stress on organisms and thus serve as natural laboratories for exploring fundamental evolutionary principles governing adaptation to extreme environments, particularly the interplay between ecological succession, microbial symbiosis, and organismal responses. Understanding how organisms have adapted to survive under

doi:10.6342/NTU202500809

such extreme and dynamic conditions remains a compelling scientific issue. In their daily life, environmental stressors affect energy balance due to the additional demands required to maintain homeostasis. Maximizing energy efficiency is crucial for survival in resource-limited environments and is considered a key factor in the evolutionary interactions between organisms and their habitats (Parsons, 2005). Energy availability, transformation, and storage are fundamental to the fitness of an organism (Sokolova et al., 2012). Consequently, energy utilization plays a vital role in physiological adaptation and stress tolerance in response to environmental fluctuations. The hydrothermal vents offshore the northeast coast of Kueishan Island create an extreme and stressful environment that hosts unique inhabitants, including the dominant metazoan *X. testudinatus* (Jeng et al., 2004). The strong ion and acid-base regulatory mechanisms of *X. testudinatus* have been demonstrated, which enable its physiological adaptation to acidic conditions (Hu et al., 2016; Allen et al., 2020). In terms of nutrient utilization, a study reported high proteolytic enzyme activity and significant lipid storage in the midgut gland of *X. testudinatus*, with some unsaturated fatty acids possibly derived from microbial contributions (Hu et al., 2012). These traits may relate to irregular food availability (zooplankton debris), exposure to toxic compounds such as hydrogen sulfide (H_2S/S^{2-}), and inhabitation of an environment where the survival and function of metazoans closely rely on microorganisms (Bang et al., 2018).

Previous studies have shown that survival in fluctuating marine environments relies on holobiont systems, which are integrated host-microbe relationships with collective adaptive capabilities (Webster and Taylor, 2012; Bordenstein and Theis, 2015). Chemosynthetic symbiosis has been widely documented in various vent-endemic organisms. For example, the giant tubeworm *Riftia pachyptila* depends entirely on endosymbiotic sulfur-oxidizing bacteria within a specialized organ called the

doi:10.6342/NTU202500809

trophosome for its nutritional needs (Hinzke et al., 2019). Deep-sea hydrothermal vent mussels (*Bathymodiolus* spp.) host methanotrophic and thiotrophic bacterial symbionts in their gills, enabling them to metabolize methane and H_2S (Ikuta et al., 2016). The vent shrimp *Rimicaris exoculata* harbors filamentous episymbionts within its gill chamber, which contribute to sulfide detoxification and carbon source supplements (Ponsard et al., 2013). Beyond nutrition, symbiotic relationships play crucial roles in detoxifying hazardous compounds (Chou et al., 2023), enhancing host physiological mechanisms (Kleiner et al., 2012), and influencing gene expression through metabolite signaling, which can affect environmental adaptation pathways (Shi et al., 2023). Moreover, studies on eukaryotic responses to H_2S have uncovered intriguing metabolic remodeling involving electron transport chain plasticity (Olson, 2021). The competition between sulfide oxidation and Complex IV activity induces mitochondrial reductive stress, triggering metabolic shifts such as accelerated aerobic glycolysis, glutamine-dependent reductive carboxylation, and lipogenesis (Hanna et al., 2023). The bacterial communities identified in the gills and the white biofilm on the carapace provide preliminary evidence of potential symbiotic associations between *X. testudinatus* and microorganisms (Yang et al., 2016; Chiu et al., 2022). While previous studies suggest the presence of symbiosis in hydrothermal vent ecosystems, the specific physiological mechanisms, functional significance, and potential host-microbe interactions remain unclear. This points out the necessity for a thorough examination of microbial community dynamics, host transcriptional regulation, and metabolic adjustments in response to hydrothermal environments to better understand these intricate adaptive pathways.

In this chapter, we investigated the physiological and microbial responses of *X. testudinatus* to hydrothermal vent exposure. Individuals collected from the Kueishan

doi:10.6342/NTU202500809

Island vent field were acclimated to normal seawater in the laboratory and subsequently reintroduced to their natural habitat in a time-course experiment (0, 1, 2, and 4 hours). Based on existing evidence of host physiological regulation and symbiotic bacterial communities in *X. testudinatus*, three primary research aims are established: (1) Characterize time-dependent changes in gill-associated bacterial communities during re-exposure to hydrothermal conditions; (2) Identify key transcriptional pathways activated in response to environmental shifts, particularly those involved in sulfide metabolism and cellular homeostasis; and (3) Explore metabolic adjustments underlying amino acid and fatty acid profiles, that may reflect regulatory requirements against hydrothermal stress. We anticipated that *X. testudinatus* would exhibit a phased strategy that ranges from rapid shifts in bacterial community composition favoring sulfide-oxidizing taxa, to enhancements in host detoxification and stress response pathways, culminating in the reprogramming of metabolic networks to sustain survival in this dynamic environment. The integration of microbiota, transcriptome, and metabolome (including amino acid and fatty acid profiles) will provide valuable insights into the perennial adaptation of the *X. testudinatus* holobiont to hydrothermal vent ecosystems, a co-evolution process that has likely occurred over thousands of years (Chen et al., 2001).

doi:10.6342/NTU202500809

3.2 Materials and Methods

Habitat reintroduction experiments

The vent crabs *X. testudinatus* were collected from the hydrothermal venting area at Kueishan Island and reared in a transparent tank with a flow-through system filtered fresh seawater under 12 hours:12 hours light-dark cycle at the Marine Research Station, Institute of Cellular and Organismic Biology, Academia Sinica. After a two-month acclimation, the crabs were immersed in aerated seawater and transferred back to their original habitats at Kueishan Island using nets for positioning. For time-course observations, crabs were re-collected at 1, 2 and 4 hours (H) post-reintroduction, while lab-acclimated crabs were sampled as controls (0H). The 5th and 6th pairs of gills were sampled and stored at -80˚C for molecular and metabolomic analyses.

Bacterial full-length 16S rRNA gene sequencing and analysis

The 6th pair of gills (n = 8) on one side was used for DNA extraction using the Wizard Genomic DNA Purification Kit (Promega) according to the manufacturers' instructions. The quantity and quality of extracted DNA were assessed using a NanoDrop 2000™ spectrophotometer (Thermo Fisher Scientific). DNA samples were then stored at -20°C until further use.

Bacterial full-length 16S rRNA amplicons were amplified using specific primers, 27F: AGRGTTYGATYMTGGCTCAGPCR and 1492R: RGYTACCTTGTTACGACTT with barcodes, referring to the guidelines for PacBio SMRT sequencing (PacBio, Menlo Park, CA, USA). PCR was performed with approximately 10 ng of DNA using 2X KAPA HiFi HotStart ReadyMix PCR Reagent (Kapa Biosystems, Woburn, MA, USA), containing 2.5 μM of both forward and reverse primers in a total volume of 25 μL. The amplification was conducted with an initial denaturation at 95°C for 3 min, followed by

doi:10.6342/NTU202500809

30 cycles of 95°C for 30 sec, annealing at 57 °C for 30 sec, and elongation at 72 °C for 1 min, with a final extension at 72 °C for 1 min. PCR products were examined on 0.8% agarose gels and quantified using a Qubit 2.0 Fluorometer (Thermo Fisher Scientific). The qualified PCR products were mixed in equal amounts and purified using AMPure PB beads (PacBio). The pooled 16S amplicons (600 ng) were then used to prepare the library with the SMRTbell prep kit 3.0 (PacBio), according to the manufacturer's instructions. After damage repairing, end repairing, and A-tailing, the inserts were ligated to adapters. Sequencing was performed on a SMRT 8M Cell (PacBio) using chemistry version 2 on the PacBio Sequel IIe sequencer. A primary filtering analysis was achieved on the Sequel IIe System, followed by a secondary analysis using the SMRT analysis pipeline version 11.0.0.

Sequences were processed using CLC Genomic Workbench 24.0.1 (CLC Bio). Adapter sequences were trimmed and reads shorter than 1200 bp or longer than 1600 bp were removed. ASVs were obtained with a fixed read length of 1200 bp, a maximum expected error rate of 2.0 per read, and the removal of detected chimeric sequences. Taxonomic classification was assigned to ASVs using the SILVA SSU 138.1 database, applying a sequential similarity threshold of 97%, 90%, 85%, and 80%. Previously assigned taxonomies with higher similarity scores were retained. Relative abundance was calculated as the number of reads assigned to each taxon divided by the total number of qualified reads in each sample.

Alpha diversity was assessed using the observed taxa number (Observed), Chao 1 richness estimates (Chao 1), Simpson's index (Simpson), and Shannon entropy (Shannon) at the class and genus level, calculated within the CLC Genomic Workbench. Beta diversity was evaluated through principal coordinate analysis (PCoA) and permutational multivariate analysis of variance (PERMANOVA) based on Bray-Curtis

doi:10.6342/NTU202500809

distances, using the R packages *vegan* (Dixon, 2003) and *ade4* (Dray and Dufour, 2007) in RStudio (2024.04.1+748). Bacterial relative abundances at the class and genus levels were depicted as bubble plots using the *ggplot2* and *reshape2* packages (Valero-Mora, 2010; Wickham, 2020). FAPROTAX (database version 1.2.10) was used to predict the potential functions of bacterial communities (Louca et al., 2016). Visualization was performed using the R package *ggplot2* (Valero-Mora, 2010).

RNA-seq transcriptome analysis

The 6th pair of gills on one side (n = 6) was prepared for total RNA extraction using RNeasy Plus Universal Kit (QIAGEN, Germany). The extracted RNA was treated with DNase I (Promega, WI, USA) to remove genomic DNA. Directional cDNA libraries were constructed for 2x150 paired-end sequencing using an Illumina NovaSeq 6000 platform (San Diego, CA, USA), and 6-Gb data was acquired for each sample. Raw sequences were demultiplexed and trimmed to remove non-target and low-quality reads using the CLC Genomics Workbench 22.0.1. The remaining sequences were subsequently utilized for de-novo assembly of transcripts. The quality of all the obtained pair-end reads was estimated by fastQC (v0.12.1). Based on the fastQC reports, the first and last bases, the adaptors, and reads with quality lower than Q30 were removed by fastp (v0.12.1). Sequences not belonging to invertebrates were removed by Kraken2 (v2.1.3). The RNA de novo assembly was performed by Trinity (v2.15.1) with default setting. The output assembled transcripts were then clustered and filtered by EvidentialGene (v2020.02.25) to remove redundancy. The filtered transcripts were also translated to amino acid sequences by EvidentialGene as well. For functional annotation of assembled transcripts, the transcripts and amino acid sequences from EvidentialGene were searched by blastx and blastp against UniProt

doi:10.6342/NTU202500809

databases, respectively. The ontology was predicted by EggNog-mapper (v2.1.12) against the database of bilateria taxa. The output results of blast and eggnog were integrated and a database was generated by the AnnotationForge package in Rstudio (Carlson and Pagès, 2024). The differential expression of transcripts was performed by the R package *DESeq2* (v1.44.0; Love et al., 2014). Transcripts with expression counts less than 10 and appeared in fewer than 3 samples were excluded from the downstream analysis. The batch effect between sample batches was estimated and corrected by the *sva* package (v3.52; Leek et al., 2012). The corrected log fold change of the differentially expressed gene (DEG) shrunk using the apeglm shrinkage estimator by the R package *clusterProfiler* (v4.12; Yu et al., 2012) was then utilized for Gene Set Enrichment Analysis (GSEA; Subramanian et al., 2005). The sequence read count was used to calculate transcripts per million (TPM). Z-scores for each gene were calculated by subtracting the mean TPM value across all individuals and dividing by the standard deviation. PCoA of TPM, followed by PERMANOVA, were performed based on Bray-Curtis distances, using the R packages *vegan* (Dixon, 2003) and *ade4* (Dray and Dufour, 2007) in RStudio.

Free amino acid derivatization and determination

The 6th pair of gills on one side (n = 8) was homogenized in 4 mL 100% ethanol with 10.6 μL 12.5 mM norvaline (served as an internal standard). The homogenate was centrifuged at 4300 x g for 10 min, and 1.5 mL supernatant was transferred into a new tube for vacuum drying. The dried samples were dissolved with 100 μL of 8 mM HCl and extruded through a 0.2-μm syringe filter (Millipore Syringe Filters, Millipore Millex, MA, USA). Following the manufacturer's method, 10 μL of the filtrate was derivatized with AccQ Tag Ultra Derivatization Kit (Waters, MA,

doi:10.6342/NTU202500809

USA). Determination of free amino acids (FAAs) was conducted using ultra-performance liquid chromatography (UPLC; ACQUITY UPLC H-Class System, Waters) via an ACCQ-TAG ULTRA C18 column equipped with a TUV detector and a FLR detector. Amino acid profiles were identified and quantified by comparing peaks with the retention times and peak areas of standards (WAT088122, Waters). PCoA of amino acid profiles, followed by PERMANOVA, were performed based on Bray-Curtis distances, using the R packages *vegan* and *ade4* in RStudio. The amino acid content was normalized by gill wet weight as pmol/g and presented in bar charts using GraphPad Prism 10 (GraphPad Software, San Diego, CA, USA). The fold change of the 1H, 2H, and 4H groups was calculated relative to the 0H control group and visualized using GraphPad Prism 10.

Fatty acid extraction and measurement

The 6th pair of gills on one side (n = 7 or 8) was homogenized with 0.1% tricosanoic acid (C23:0; Sigma-Aldrich) in chloroform and 0.25 M methanolic trimethylsulfonium hydroxide solution (TMSH; Sigma-Aldrich). Tricosanoic acid was used as an internal standard for further quantification. The homogenate was sonicated for 30 min at room temperature, then mixed with n-Hexane (EBR12R, Hettich, Germany). The mixture was centrifuged at 3000 ×g for 3 min at room temperature, and the supernatant was collected as the measured sample. Measurement of fatty acids (FAs) was performed using an Agilent 7890A-5975 GC/MS system (Agilent Technologies, CA, USA) equipped with a DB-5MS column (30 m x 0.250 mm, 0.25 μm film thickness, J & W Scientific). Helium served as a carrier gas with a 50 mL/min flow rate. The GC settings were programmed as follows: 70 °C for 2 min, then rise to 240 °C at a rate of 20 °C/min, and finally to 270 °C. The temperature of the injector was 250 °C in a

doi:10.6342/NTU202500809

splitless mode, and the mass range was 50550 amu. FAs were identified and quantified by comparing peaks with the retention times and peak areas of internal standards. PCoA of fatty acid profiles, followed by PERMANOVA, were performed based on Bray-Curtis distances, using the R packages *vegan* and *ade4* in RStudio. The fatty acid content (relative to C23:0) was normalized by gill wet weight (g) and presented in bar charts using GraphPad Prism 10 (GraphPad Software, San Diego, CA, USA). The fold change of the 1H, 2H, and 4H groups was calculated relative to the 0H control group and visualized using GraphPad Prism 10.

doi:10.6342/NTU202500809

3.3 Results

The hydrothermal vent crabs *X. testudinatus* collected from the venting area were acclimated to normal seawater in the laboratory before being reintroduced (0, 1, 2, 4H) to their original habitats. Symbiotic bacteria, transcriptome, free amino acid profile, and fatty acid composition were analyzed in the gills.

Changes in microbiome of the *X. testudinatus* gills

PCoA revealed dissimilarity in bacterial composition across time points (0, 1, 2, and 4H) following a perturbation at different levels. At the ASV level (Fig. 23A), significance was observed between time points (PERMANOVA, $F = 2.4087$, $R^2 = 0.2051$, $p = 0.0001$). Pairwise comparisons show that 2H significantly differed from 0H ($p = 0.0021$), 1H ($p = 0.0062$), and 4H ($p = 0.0021$). At the class level (Fig. 23B), a significance was also detected (PERMANOVA, $F = 2.3284$, $R^2 = 0.1997$, $p = 0.0064$), with 0H differing from 1H ($p = 0.0408$) and 4H ($p = 0.0480$), while 1H differed from 4H ($p = 0.0102$). At the genus level (Fig. 23C), a significance was also observed (PERMANOVA, $F = 2.5270$, $R^2 = 0.2131$, $p = 0.0001$), with significant differences detected between all the time points. These results indicate a temporal shift in bacterial composition, with the most pronounced variations at the genus level. However, except for the observed taxa number and Chao 1 estimates at the genus level between 0H and 2H (one-way ANOVA followed by Bonferroni post hoc analysis $p < 0.05$; Fig. 24E, F), alpha diversity did not show significant differences between time points at either the class or genus levels (Fig. 24).

Bacterial compositions at the class and genus levels are presented as bubble plots (Fig. 25). Bacteroidia, Alphaproteobacteria, and Gammaproteobacteria were the three dominant classes, with Campylobacteria showing a higher abundance at 1H compared

doi:10.6342/NTU202500809

to other time points (Fig. 25A). At the genus level, *Ruegeria* and *Sulfitobacter* from Alphaproteobacteria, along with *Halioglobus* from Gammaproteobacteria, were the most abundant genera (Fig. 25B). Notably, *Sulfurovum* from Campylobacteria, the dominant genus in wild *X. testudinatus* gills, was also among the top 20 genera during reintroduction, showing the highest abundance at 1H. According to the functional analysis (Fig. 26), chemoheterotrophy had the highest proportions in the gills, with a decrease at 1H, coinciding with an increase in sulfur oxidation and denitrification/nitrogen respiration.

Changes in transcriptomic profiling of the *X. testudinatus* gills

The PCoA (Fig. 27A) indicates that transcriptomic profiles (TPM) varied across time points (PERMANOVA, $F = 4.4771$, $R^2 = 0.3242$, $p = 0.0001$), with significant differences detected between all the time point groups. Differentially expressed genes (DEGs) were analyzed at 1, 2, and 4H compared to 0H (Fig. 27B-D). At 1H, more genes were significantly upregulated, while at 4H, more significantly downregulated genes were detected. At 2H, gene regulation was generally balanced.

Gene set enrichment analysis (GSEA) based on DEG results revealed several upregulated and downregulated pathways. At 1H, pathways related to GTPase activity and actin cytoskeleton were predominantly upregulated (Fig. 28A), while chitin-related pathways were downregulated (Fig. 28B). At 2H, pathways related to chitin/cuticle constitution, actin cytoskeleton, oxidoreduction, and GTPase activity were upregulated (Fig. 29A), while those related to epigenetic and transcriptional regulations were downregulated (Fig. 29B). At 4H, pathways related to chitin/cuticle formation and oxidoreduction were upregulated (Fig. 30A), while pathways related to symbiotic interactions, cell growth/differentiation, gene regulation, and cellular metabolism were downregulated (Fig. 30B).

doi:10.6342/NTU202500809

Therefore, some of the pathways mentioned above and genes of interest were organized into heatmaps to analyze changes across the different time point groups. For genes involved in GTPase activity (Fig. 31), many expressed a basal level at 0H. Over time, reintroduction to the hydrothermal habitat appeared to induce several genes encoding Rho GTPase-activating protein at 1H and 2H, which were subsequently downregulated at 4H. In contrast, other genes encoding Rab-related proteins and guanine nucleotide exchange factors were gradually downregulated at 1H and 2H, with some upregulating again at 4H.

Regarding genes involved in actin cytoskeleton (Fig. 32), those encoding actin-related proteins and dynactin subunits were gradually downregulated at 1H and 2H compared to 0H and were subsequently induced at 4H. In contrast, genes encoding LIM domain-containing proteins were upregulated at 1H but downregulated thereafter. Meanwhile, genes encoding actin were upregulated at later time points, 2H and 4H.

Given that GSEA indicated differential regulation of pathways related to chitin and cuticle formation across time points, the relevant genes are presented (Fig. 33). However, individual genes did not exhibit a clear trend of change. Only genes encoding chitinase 6A and certain chitin-binding type-2 domain-containing proteins were upregulated at 4H.

For genes involved in sulfide metabolism (Fig. 34), several fundamental sulfur metabolism-related genes were expressed under normal seawater conditions (0H). At 1H, all genes were downregulated except for the one encoding Glutathione S-transferase 11. Later, at 2H and 4H, genes encoding sulfide quinone oxidoreductase 2, glutathione peroxidase, glutathione S-transferase, and glutathione transferase were gradually upregulated.

doi:10.6342/NTU202500809

Lastly, considering the transfer from normal seawater to extreme hydrothermal conditions, genes encoding stress response and apoptosis were addressed (Fig. 35). In the first hour (1H) after reintroduction to the habitat, substantially all relevant genes were downregulated. This persisted until 4H, when a few genes encoding heat shock proteins 60/70/90 and caspase 8 were upregulated.

Changes in the free amino acid profile of the *X. testudinatus* gills

The PCoA (Fig. 36A) indicates that free amino acid (FAA) profiles varied across time points (PERMANOVA, F = 2.5359, R^2 = 0.2137, p = 0.0079). Pairwise comparisons revealed no significant difference between 0H and 1H, while 0H vs. 4H (p = 0.0341) and 1H vs. 2H (p = 0.0151) showed significant differences. Other comparisons, 0H vs. 2H, 1H vs. 4H, and 2H vs. 4H had p-values approaching significance ($p < 0.07$). Based on PCoA, the contribution of each amino acids to the first (PCoA1) and second (PCoA2) principal coordinates were analyzed (Fig. 36B). Serine (Ser) and arginine (Arg) had strong positive contribution (> 0.05) to PCoA1, while glutamate (Glu), glycine (Gly), alanine (Ala), proline (Pro), and taurine (Tau) contributed negatively. On the other hand, phenylalanine (Phe), histidine (His), arginine (Arg), serine (Ser), valine (Val), leucine (Leu), and isoleucine (Ile) showed negative contribution to PCoA2.

The bar charts presenting the original values of individual free amino acids (Fig. 37) indicate significant differences (one way-ANOVA, Bonferroni post hoc test) across reintroduction time points for the aromatic amino acids Phe and His; the charged amino acids Asp, Glu, and Arg; the polar amino acids Gln; as well as alpha-aminobutyric acids AABA and taurine (Tau). The fold change (FC) analysis (Fig. 38A) reveals that certain amino acids, such as Arg, hydroxylysine (HyLys), Ser, and Ala, tend to increase over

doi:10.6342/NTU202500809

time. Meanwhile, His, Gln, Pro, and methionine (Met) accumulated at 4H. However, the levels of other FAAs generally decreased during the reintroduction. The heatmap for genes involved in amino acid metabolism (Fig. 38B) shows that most related genes were downregulated at 1H, except for cysteine dioxygenase. Subsequently, genes encoding glutaminase and histidine ammonia-lyase were upregulated at 2H compared to 1H, while the former remained expressed until 4H and the latter was downregulated. At 4H, genes encoding cystathionine gamma-lyase and alanine transaminase were upregulated.

Changes in the fatty acid composition of the *X. testudinatus* gills

The PCoA (Fig. 39A) indicates that fatty acid (FA) compositions did not vary across time points (PERMANOVA, F = 1.3851, R^2 = 0.1334, p = 0.2029), and no significant differences were observed in pairwise comparisons. The contribution analysis (Fig. 39B) reveals strong positive contributions of unsaturated FAs to PCoA1. In contrast, unsaturated FAs showed slight or negative contributions to PCoA2, while saturated FAs 16:00 and 18:00 positively contributed to PCoA2.

The bar charts presenting the original values of individual FAs show no significant differences between time points, as determined by one way-ANOVA and Bonferroni post hoc test (Fig. 40). Nevertheless, trends in FA changes could still be observed through FC analysis (Fig. 41). During the reintroduction, saturated FAs (16:0 and 18:0) appeared to remain stable. Hypogenic acid (16:1n-9) levels increased at 1H, followed by a slight gradual decrease at subsequent time points. In contrast, the levels of vaccenic acid (18:1n-11), arachidonic acid (20:4n-6), and eicosapentaenoic acid (EPA, 20:5n-3) tended to increase over time, while linoleic

doi:10.6342/NTU202500809

acid (18:2n-6), oleic acid (18:1n-9), and docosahexaenoic acid (DHA, 22:6n-3) initially decreased at 1H before gradually accumulating at 2H and 4H.

doi:10.6342/NTU202500809

3.4 Discussion

Hydrothermal fluids are toxic and stressful for most organisms (Dahms et al., 2017), shaping their distribution, diversity, and activity (Tarasov et al., 2005; Mantha et al., 2013). Ven-endemic organisms must have evolved effective strategies to survive these extreme and dynamic environments. At Kueishan Island, vent fluids contain high concentrations of sulfide, reduced gases, and metal ions (Peng et al., 2011; Chan et al., 2016), creating a chemically challenging habitat. An *in situ* observational study reported increased activity of the vent crabs *X. testudinatus* under low-pH conditions, suggesting behavior adaptation to venting events (Chan et al., 2024). The intermittent nature of fluid discharge exposes *X. testudinatus* to repeated transitions between normal seawater and hydrothermal conditions, requiring continual physiological and microbial adjustments. The crustacean host and symbiotic microbes would coordinate to cope with environmental perturbations, where *X. testudinatus* can prioritize essential rapid-response mechanisms derived from extremophiles to tolerate acute stress before reaching their homeostatic threshold. Through time-course reintroduction experiments, progressive responses of the *X. testudinatus* holobiont to such environmental perturbations were explored.

Rapid shifts in the bacterial community in response to hydrothermal conditions

Bacterial analyses revealed that even in the absence of hydrothermal fluids, *X. testudinatus* still retained a subset of hydrothermal-associated bacteria in their gills. Upon re-exposure to hydrothermal conditions, *Sulfurovum* emerged as an early bacterial responder within Campylobacteria, the dominant symbiotic bacterial class in wild vent crabs. The abundance of *Sulfurovum* peaked at 1H post-reintroduction and then declined over the next 3 hours. Similar transient trends were observed in *Ruegeria*

doi:10.6342/NTU202500809

(Alphaproteobacteria) and *Halioglobus* (Gammaproteobacteria). *Ruegeria* has been identified in corals inhabiting Kueishan Island HV systems (Girija et al., 2024) and potentially involved in sulfur and nitrogen cycling within coral hosts (Doering et al., 2023). *Halioglobus,* recognized as an environmentally relevant bacterium, includes species previously isolated from seawater (Park et al., 2012) and costal sediments (Han et al., 2019). Our initial hypothesis proposed a continuous accumulation of the dominant genus *Sulfurovum* in *X. testudinatus* gills over time, but this was not observed. Instead, we interpret these findings as potential evidence of a "bet-hedging" strategy employed by the symbiotic bacteria. In a complex and erratic environment, such a strategy may minimize the risk of drastic shifts in microbial community composition during the critical establishment of symbiosis with the host (Cao and Goodrich-Blair, 2017). Furthermore, functional analysis revealed an initial decrease followed by an increase in the proportion of chemoheterotrophy. The early contribution of *Sulfurovum* and associated metabolic processes, such as denitrification, nitrogen respiration, and sulfide/hydrogen oxidation, may indicate a period of hydrothermal input and chemical fluxes favoring chemoautotrophy. As the interaction between the environment and *X. testudinatus* symbiosis progressed, the decline in *Sulfurovum* abundance, along with the resurgence of chemoheterotrophs such as *Maribacter*, *Chishuiella*, *Blastopirellula*, *Amylibacter*, *Roseovarius*, *Ruegeria*, *Sulfitobacter,* and *Halioglobus*, may reflect organic matter accumulation or the availability of electron acceptors in the gills, probably derived from the prior activity of chemolithoautotrophic *Sulfurovum* (Burgin et al., 2011; Wang et al., 2023). Additionally, the diminished phototrophic functions suggest that phototrophy may not be essential as an immediate response in vent-endemic holobiont encountering hydrothermal conditions. These processes demonstrate

doi:10.6342/NTU202500809

the delicate regulation of microbial functional groups in response to environmental fluctuations within hydrothermal vent ecosystems.

Cytoskeleton stabilization as an initial response to hydrothermal exposure

Actin polymerization and reorganization are critical for early cellular responses to extracellular stimuli, with Rho GTPases playing a key role in modulating actin filament dynamics (Papakonstanti and Stournaras, 2008; Bement et al., 2024). Transcriptomic analysis revealed the activation of pathways related to actin cytoskeleton remodeling and GTPase functions in *X. testudinatus* gills at 1H post-reintroduction. Several genes encoding Rho GTPase-activating proteins were upregulated, while those encoding actin and actin-related proteins remained unchanged or even downregulated. However, genes encoding actin-binding LIM proteins and LIM-domain containing proteins were upregulated, which may contribute to cytoskeleton stabilization by inhibiting actin depolymerization to reduce the formation of branched cytoskeleton filaments (Khurana et al., 2002). This suggests that, during early exposure to vent fluids, branchial cells prioritize the construction of a rigid and stable cytoskeleton framework, potentially limiting cell motility to mitigate stress from large amounts of chemicals. As LIM-related gene expression declined at 2H, actin gene expression was upregulated, likely preparing for subsequent cytoskeleton remodeling. By 4H post-reintroduction, upregulation was observed in genes encoding Ras GTPase-activating proteins, Ras-related proteins, actin-related proteins, and dynactin subunits. Their interactions may enhance intracellular transport of substances, while facilitating the reestablishment of regular cell division and differentiation (Wittinghofer et al., 1997; Urnavicius et al., 2015). These processes suggest that after prolonged exposure to the hydrothermal environment, intracellular activity in *X. testudinatus* gills gradually returned to a functional state, whereas the

doi:10.6342/NTU202500809

initial response primarily involves cytoskeletal stabilization to withstand abrupt environmental challenges. The stabilization of the host cytoskeleton, along with the rapid recruitment of sulfide-oxidizing bacteria, may indicate a coordinated mechanism that provides immediate protection against toxic substances.

Consistent with the observations in actin cytoskeleton regulation, chitin formation and chaperon functioning appeared to be suppressed during the early response. It was not until 4H post-reintroduction that genes encoding chitinase 6A, chitin-binding type-2 domain-containing proteins, and heat shock proteins (HSPs) were upregulated. Chitinases hydrolyze chitin, a major component of the crustacean exoskeleton, tissue cuticle, and fungal cell walls, as well as peptidoglycan, which constitute bacterial cell walls (Arakane and Muthukrishnan, 2010; Dworkin, 2018). Therefore, crustacean chitinases are believed to be involved in development, growth, and pathogen defense (Nikapitiya et al., 2015). It suggests that at this time point, *X. testudinatus* may begin preparing for molting or remodeling the gill structure while simultaneously strengthening pathogen defense, and these processes could play a crucial role in symbiont selection. Furthermore, chitin synthase expression remained unchanged, which may indicate its involvement in new epidermis synthesis at a later stage (Rocha et al., 2012). During this critical period of poised cellular activity and protein functioning, the chaperone function of heat shock proteins became significant (Becker and Craig, 1994; Feder and Hofmann, 1999), reflecting the upregulation of multiple HSP genes. While all act as molecular chaperones, HSP60 primarily aids mitochondrial protein folding, HSP70 assists in nascent protein folding and prevents aggregation (Jebara et al., 2017), and HSP90 maintains the stability of signaling proteins in the cytoplasm (Prodromou, 2016). The protective role of HSPs against environmental stress has also been documented in marine organisms, including mussels (Hamer et al., 2004),

doi:10.6342/NTU202500809

ascidians (Pineda et al., 2012), fish (Deane et al., 2002), and shrimps (Giffard-Mena et al., 2024). Notably, a previous study reported delayed upregulation of HSP70/90 expression between 3-6 hours in the gills of milkfish exposed to hypotonic stress (Umam et al., 2020), which supports the transcriptomic response of HSPs observed in *X. testudinatus* reintroduced to the hydrothermal habitat.

Essential mechanisms against sulfur toxicity and oxidative stress

The minimal changes observed in genes associated with mitochondrial sulfur oxidation may indicate the fundamental importance of these functions. Key enzymes, including sulfide: quinone oxidoreductase (Sqr), rhodanese (Rhod), persulfide dioxygenase (Pdo), and sulfite oxidase (So), catalyze a series of sulfide oxidation reactions, converting sulfide (HS^-/S^{2-}) to glutathione persulfide (GSSH), then to thiosulfate ($S_2O_3^{2-}$), or alternatively, the oxidation of sulfite (SO_3^{2-}) to sulfate (SO_4^{2-}; Hildebrandt and Grieshaber, 2008; Libiad et al., 2014). Despite a brief downregulation, genes encoding glutathione peroxidases, glutathione S-transferases, and glutathione synthetase were upregulated at 4H post-reintroduction. In hydrothermal fields, sulfide is a prevalent compound capable of generating reactive oxygen species (ROS) that snatch electrons from cellular molecules, which mostly exist in the reduced state, thus causing oxidative stress (Joyner-Matos et al., 2010). The upregulation of glutathione peroxidase genes suggested an enhanced capacity to neutralize ROS by catalyzing their reduction using glutathione, protecting cellular components from oxidative damage (Hayes and McLellan, 1999). In addition, the increased expression of glutathione S-transferases indicated an elevated ability to conjugate glutathione with electrophilic compounds, such as metal ions, ROS, nitrate, and sulfide-derived metabolites, facilitating their detoxification and excretion (Salinas and Wong, 1999). Simultaneously, glutathione

doi:10.6342/NTU202500809

synthetase may replenish depleted glutathione storage, ensuring sustained antioxidant processes (Lu, 2001). These enzymes collectively contribute to cellular defense against sulfur toxicity and oxidative stress, highlighting the adaptation of *X. testudinatus* to sporadic venting activity in hydrothermal environments. Similar oxidative stress compensatory mechanisms have been reported in other organisms, including polar and temperate fish and invertebrates, and species inhabiting environments with fluctuating pH and salinity, where enhanced antioxidant defenses serve as a primary adaptive strategy (Abele and Puntarulo, 2004; Tomanek, 2015). These pre-existing detoxification systems can be further co-opted and enhanced to cope with emerging ecological pressures (Tüzün et al., 2020). Additionally, a previous study has shown that the hydrothermal vent mussel *Bathymodiolus azoricus* retained the capacity for regulating genes critical for physiological adaptation to their natural habitats even after months of laboratory acclimation (Bettencourt et al., 2011), suggesting an inherent preparedness for extreme conditions. Such adaptive strategies may also be modulated by microbial symbionts, which contribute to host resilience through metabolic and nutritional interactions (Sun et al., 2023).

Potential metabolic reestablishment triggered by ETC inhibition

On the other hand, mitochondrial sulfide oxidation potentially induces atypical metabolic processes for nutrient utilization. The inhibition of complex IV by sulfide oxidation may reduce ATP production and cause a reductive shift in NADH/NAD^+ pool (Libiad et al., 2019). An increased NADH/NAD^+ ratio can drive NADPH generation through nicotinamide nucleotide transhydrogenase (NNT; Vitvitsky et al., 2021). NADPH, in turn, may facilitate the reductive direction of the TCA cycle, where isocitrate dehydrogenase 2 (IDH2) catalyzes the conversion of α-ketoglutarate (α-KG)

doi:10.6342/NTU202500809

to citrate, supplying substrates for fatty acid synthesis/lipogenesis (Carballal et al., 2021). Additionally, glutaminolysis might be stimulated to provide the final product α-KG due to its increased usage (Yoo et al., 2008). During the reintroduction, most genes related to nutrient metabolism were suppressed at 1H, consistent with the observations above, except for cysteine dioxygenase, probably due to its activity of converting cysteine into cysteine sulfonate, an essential intermediate for sulfide detoxification (Nagasaki et al., 2015). Also, the sustained expression of cystathionine gamma-lyase may reduce free S^{2-} by generating cysteine persulfide (Cys-SSH) from cysteine (Araki et al., 2023). While the NNT gene was upregulated at 2H, isocitrate dehydrogenase 2 (Idh2) gene remained unchanged, and the fatty acid synthase gene, which encodes a key enzyme in lipogenesis, was downregulated. This suggests that NADPH was not utilized to support Idh2 activity here but was instead preferentially directed towards mitigating acute oxidative stress via the glutathione- or thioredoxin-dependent redox buffering systems (Marty et al., 2009; Scherschel et al., 2024). However, certain shifts in amino acid and fatty acid profiles still reflect the gene regulation of metabolic enzymes.

Possible metabolic adjustments associated with free amino acids

Downregulation of the glutamate synthase gene could result in continuous glutamate consumption and the accumulation of glutamine (Van den Heuvel et al., 2004), potentially stimulating the glutaminase gene to degrade glutamine for ammoniagenesis as a mechanism of acid elimination in response to acidic stress (Chuang et al., 2023). Serving as crucial precursors for glutathione synthesis, the fluctuations in glutamine and glutamate levels are also linked to oxidative stress (Amores-Sánchez and Medina, 1999). Furthermore, as major amino acids in ammonia metabolism, their interactions m could regulate the related metabolic pathways

doi:10.6342/NTU202500809

(Newsholme et al., 2003). Excessive aspartate depletion may drive the downregulation of the aspartate aminotransferase gene, while the decreased expression of arginase gene may indicate urea cycle inhibition, leading to a gradual accumulation of arginine (Morris Jr, 2002). Histidine metabolism also exhibited dynamic regulation, with an initial histidine degradation, supported by upregulation of histidine ammonia-lyase gene at 1H and 2H, followed by a downregulation at 4H, resulting in histidine accumulation (Brosnan and Brosnan, 2020). Given that histidine cannot be synthesized by most animals, this accumulation was likely derived from bacterial biosynthesis (Bender, 2012). In contrast, the gradual accumulation of alanine may contribute to the upregulation of the alanine transaminase gene at 4H, potentially reactivating the stalled urea cycle, and the produced pyruvate could then be utilized for gluconeogenesis (Katunuma et al., 1966). Under sulfidic conditions, the metabolism of cysteine, a sulfur-containing amino acid crucial for cellular redox balance through the cysteine sulfinate (CSA) pathway, was likely regulated by both cystathionine gamma-lyase and cysteine dioxygenase (Koito et al., 2018). Cystathionine gamma-lyase upregulation and cysteine dioxygenase downregulation at 4H after utilization of cysteine, suggests a metabolic shift toward cysteine synthesis to maintain its homeostasis. Additionally, the initial increase in taurine levels may also indicate the activity of the CSA pathway, where taurine is one of the terminate products (Kohl et al., 2019), while the subsequent consumption may reflect the utilization of taurine as a free radical scavenger to mitigate ROS-induced damage (Zhang et al., 2014). The CSA pathway has been identified in the gills of hydrothermal-endemic mussels *Bathymodiolus septemdierum* (Nagasaki et al., 2015) as well as the human gut, where it facilitates crosstalk between the host epithelium and the symbiotic microbiome for systemic sulfur metabolism (Hansen and Venkatachalam, 2023).

doi:10.6342/NTU202500809

Possible metabolic adjustments related to fatty acids

Fatty acid composition reflects the biological state of marine organisms, and the nutrients obtained from various sources, including internal biosynthesis, algae, and bacteria (Monroig et al., 2013). Although lipogenesis may not have been stimulated, shifts in saturated and unsaturated fatty acid profiles were observed. Palmitic acid (16:0), the initial product of fatty acid synthesis and the precursor of all other fatty acids, exhibited minor fluctuations during reintroduction, with an initial slight decrease, followed by an increase, and then another decrease. An initial elevation in stearic acid (18:0) levels was probably associated with elongation of very long chain fatty acid protein (Elovl), which utilizes palmitic acid as a substrate. The subsequent depletion of both 16:0 and 18:0 may indicate increased activity of stearoyl-CoA desaturase 1 (Scd1) and fatty acid desaturases. The sustained expression of Scd1 gene, which catalyzes the desaturation of saturated fatty acids into monounsaturated fatty acids (MUFA), could have led to the progressive accumulation of oleic acid (18:1n-9) and vaccenic acid (18:1n-11). The consumption of oleic acid at 1H for cell membrane phospholipid biosynthesis suggests an immediate demand for maintaining cellular structural integrity (Kurniawan et al., 2017), potentially reflecting the actin cytoskeleton stabilization, as previously discussed. Additionally, the production of hypogeic acid (16:1n-9) via the beta-oxidation of oleic acid provides a plausible explanation for the observed initial elevation in hypogenic acid abundance (Bermúdez et al., 2022). Nevertheless, analytical methods may confuse palmitoleic acids (16:1n-7) and hypogeic acids due to their similar structures. Palmitoleic acid, an isomer of hypogeic acid primarily derived from bacterial sources, was found to accumulate in the midgut of *X. testudinatus* during starvation, serving as an energy reserve (Hu et al., 2012). Vaccenic acid, which is also a

doi:10.6342/NTU202500809

component of cell membranes, has been suggested to function as a potential immunomodulatory trans fatty acid through the attenuation of inflammatory responses (Blewett et al., 2009). Polyunsaturated fatty acids (PUFAs), synthesized by fatty acid desaturases that introduce multiple double bonds into fatty acid chains (Lee et al., 2016), also exhibited dynamic changes during reintroduction. Linoleic acid (18:2n-6) was initially consumed at 1H, followed by continuous accumulation. The utilization of linoleic acid as a substrate for (Z, Z)-6,9-heptacosadiene synthesis was reported in cockroaches for protection against environmental chemicals (Jurenka et al., 1987). While linoleic acid is generally considered to be synthesized by bacteria, protozoa, and plants, some studies suggest that certain invertebrates, including crustaceans, nematodes, and mites, may possess endogenous linoleic acid synthesis mechanisms (Malcicka et al., 2018). Arachidonic acid, conferred by its cis double bonds, is essential for cell membrane dynamics, and its reactivity with oxygen drives both oxidative stress and the production of bioactive eicosanoids, which play a role in innate immune responses (Brash, 2001). The observed accumulation of arachidonic acid could potentially be attributed to the cellular response to NADPH production by NNT, wherein arachidonic acid functions to activate NADPH oxidase, thereby mitigating the surplus of NADPH and restoring redox equilibrium (Dana et al., 1998).

Regarding PUFAs, eicosapentaenoic acid (EPA, 20:5n-3) and docosahexaenoic acid (DHA, 22:6n-3) are two long-chain n-3 fatty acids abundant in most marine organisms. They are widely recognized for their anti-inflammatory properties in animals, contributing to cardiovascular and neurological health (Gorjão et al., 2009). Due to their inherent physical characteristics, EPA and DHA have the highest capacity among all PUFAs to modulate phospholipid membrane structure (Onuki et al., 2006). The initial decrease in DHA levels at 1H post-reintroduction may serve as a mechanism

doi:10.6342/NTU202500809

to prevent excessive membrane fluidity and instability, contributing to the stabilization of cell structure. In *X. testudinatus* gills, DHA was less abundant than EPA, which has also been observed in deep-sea hydrothermal polychaetes (Phleger et al., 2005). While EPA and DHA can be synthesized by certain marine bacteria (DeLong and Yayanos, 1986; Moi et al., 2018), they are also recognized for their potential antimicrobial effects (Clare et al., 2024). The dual roles of PUFAs as nutrients and as modulators of the microbiome illustrate a host-symbiont interaction. Specific fatty acids like PUFAs were identified as biochemical signals, potentially facilitating recognition between hosts and symbionts in chemosynthetic environments (Fujita et al., 2007; Zhukova, 2019). Specialized membrane lipid compositions selectively facilitate colonization by beneficial symbionts and deter potential pathogens (Jiang et al., 2017; Adigun et al., 2021). The initial depletion and the following accumulation of DHA may play a role in modulating the symbiotic microbiome, particularly affecting bacteria with heightened responsiveness. This could explain the biphasic pattern observed in *Sulfurovum*, with an initial increase in abundance followed by a subsequent decline. Furthermore, despite the molecular machinery remaining unclear, EPA and DHA have been found to have greater resistance to ROS-induced peroxidation in aqueous biological systems compared to other fatty acids, suggesting that their incorporation into phospholipid membranes with proper amounts may enhance oxidative stability (Araseki et al., 2002). These traits may reinforce the significance of EPA and DHA in holobiont inhabiting hydrothermal environments characterized by oxidative stress.

Summary

The multidisciplinary responses in *X. testudinatus* provide important insights into the inter-kingdom evolutionary mechanisms that enable metazoan survival in extreme

doi:10.6342/NTU202500809

environments. The coordination of bacterial communities, host gene expression, and metabolic pathways exemplifies the concept of "hologenomic evolution" (Bordenstein and Theis, 2015; Brooks et al., 2017), acting on the integrated host-symbiont interactions rather than individual components. The phased adaptation process, which commences with rapid ecological and genetic modulation of the microbiome, followed by molecular and metabolic regulation of the host, may have evolved in various metaorganisms, including mycorrhiza in soils, corals in oligotrophic sea areas, and invertebrates in intertidal zones and hydrothermal fields (Bang et al., 2018).

The *X. testudinatus* holobiont exhibits an early stress response to chemically extreme conditions driven by hydrothermal venting through a tolerance strategy, stabilizing cellular structures while suppressing metabolic and physiological processes to minimize environmental perturbations. Nevertheless, the potential influx of sulfide, various reduced chemical species, and bacteria like *Sulfurovum* necessitated sustained engagement of sulfide detoxification and oxidative stress defense within the gill tissues. Given the essential role of metabolic crosstalk in holobiont adaptation (Garg, 2021), metabolites involved in cellular maintenance, sulfide oxidation, and ROS detoxification revealed coordinated regulation, leveraging their intrinsic physicochemical properties to facilitate resilience in this extreme habitat. The observed temporal dynamics indicate distinct response phases, an initial stabilization focused on structural integrity, succeeded by metabolic reprogramming, and ultimately leading to homeostatic restoration. The final chapter suggests the evolutionary success of the *X. testudinatus* holobiont and its specialized adaptive strategies for coping with the inherent variability of hydrothermal habitats, which have been primarily attributed to the complex interactions of this metaorganism with one of Earth's most challenging ecosystems.

doi:10.6342/NTU202500809

3.5 Figures

Chapter 3

Figures 23-41

doi:10.6342/NTU202500809

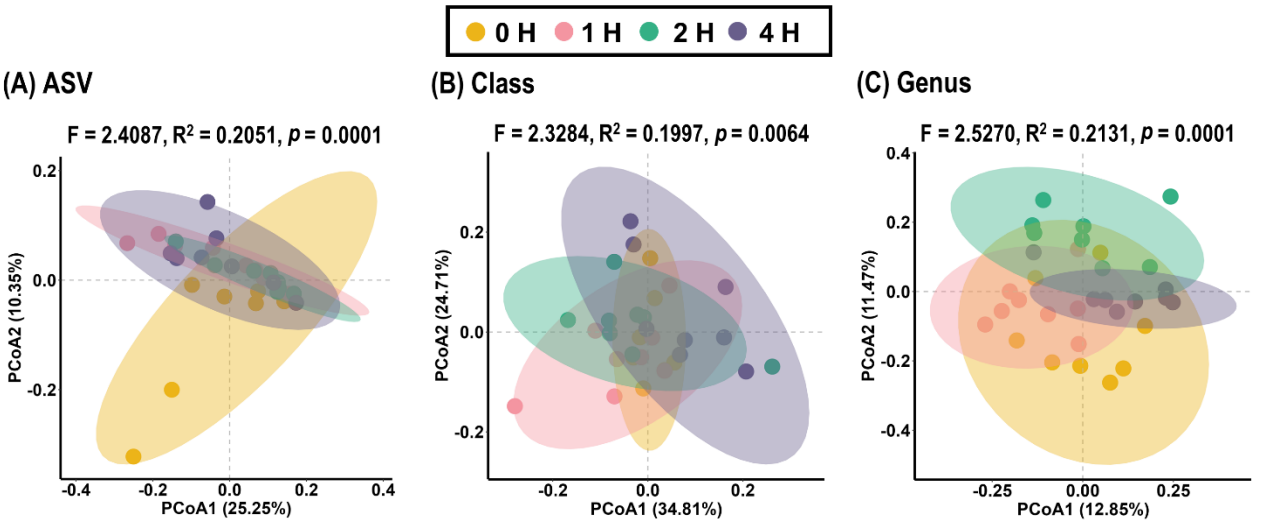

Pairs	R^2	*p*-value
0 H vs 1 H	0.1039	0.1094
0 H vs 2 H	0.1920	**0.0021**
0 H vs 4 H	0.0927	0.1118
1 H vs 2 H	0.2109	**0.0062**
1 H vs 4 H	0.0892	0.1430
2 H vs 4 H	0.2252	**0.0021**

Pairs	R^2	*p*-value
0 H vs 1 H	0.1497	**0.0408**
0 H vs 2 H	0.0795	0.2820
0 H vs 4 H	0.1708	**0.0480**
1 H vs 2 H	0.0871	0.2820
1 H vs 4 H	0.2302	**0.0102**
2 H vs 4 H	0.1096	0.2325

Pairs	R^2	*p*-value
0 H vs 1 H	0.1565	**0.0012**
0 H vs 2 H	0.1695	**0.0003**
0 H vs 4 H	0.1143	**0.0063**
1 H vs 2 H	0.1784	**0.0003**
1 H vs 4 H	0.1624	**0.0010**
2 H vs 4 H	0.1401	**0.0052**

Figure 23. PCoA for the bacterial composition in the gills of *X. testudinatus* reintroduced from the lab to the original habitat. PCoA was conducted at the ASV, class, and genus levels. Time points 0H (lab-acclimated), 1H, 2H, and 4H post transfer are represented by yellow, pink, green, and purple dots, respectively.

doi:10.6342/NTU202500809

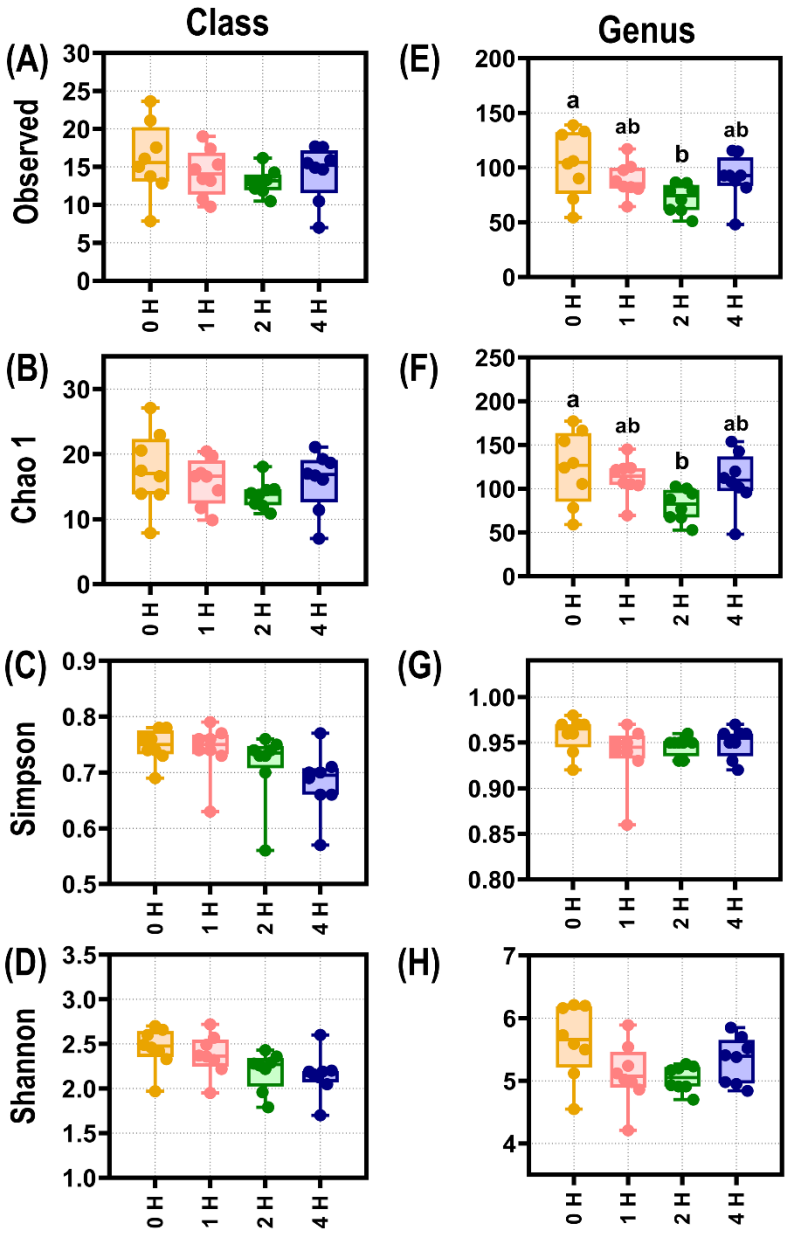

Figure 24. Comparison of bacterial alpha diversity in the gills of *X. testudinatus* reintroduced from the lab to the original habitat. Alpha diversity indices presented include observed taxa number (Observed), Chao1 richness estimates (Chao 1), Simpson's index (Simpson), and Shannon entropy (Shannon), all calculated at both the class (A-D) and genus (E-H) taxonomic levels. Time points 0H (lab-acclimated), 1H, 2H, and 4H post transfer are represented by yellow, pink, green, and purple dots, respectively. Statistical significance was determined using one-way ANOVA followed by Bonferroni post hoc analysis ($p < 0.05$).

doi:10.6342/NTU202500809

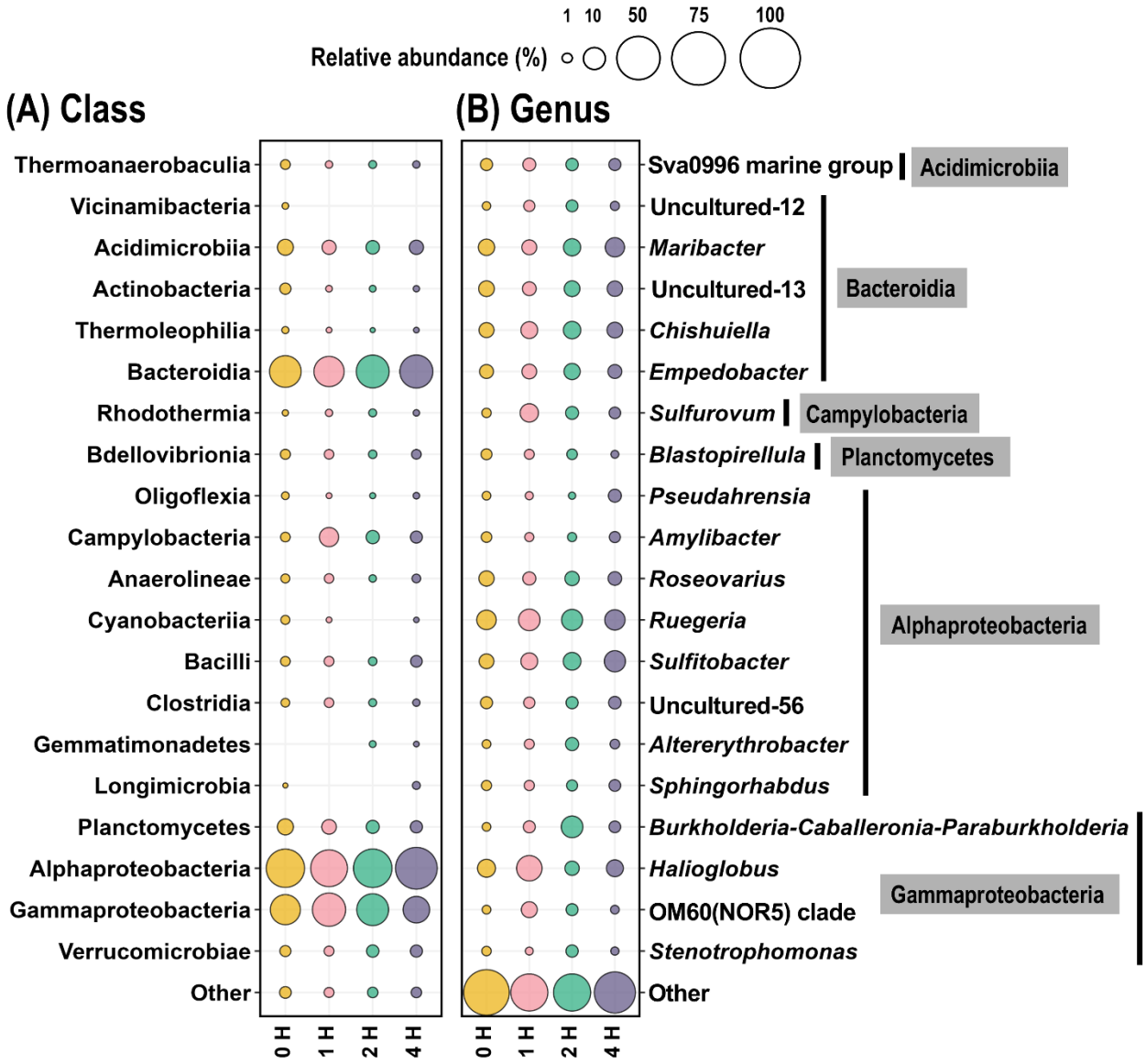

Figure 25. Bacterial composition in the gills of *X. testudinatus* after lab-to-habitat reintroduction. The relative abundance (%) is represented by the size of circles, shown at the Class (A) and Genus (B) levels (Top 20 genera represented).

doi:10.6342/NTU202500809

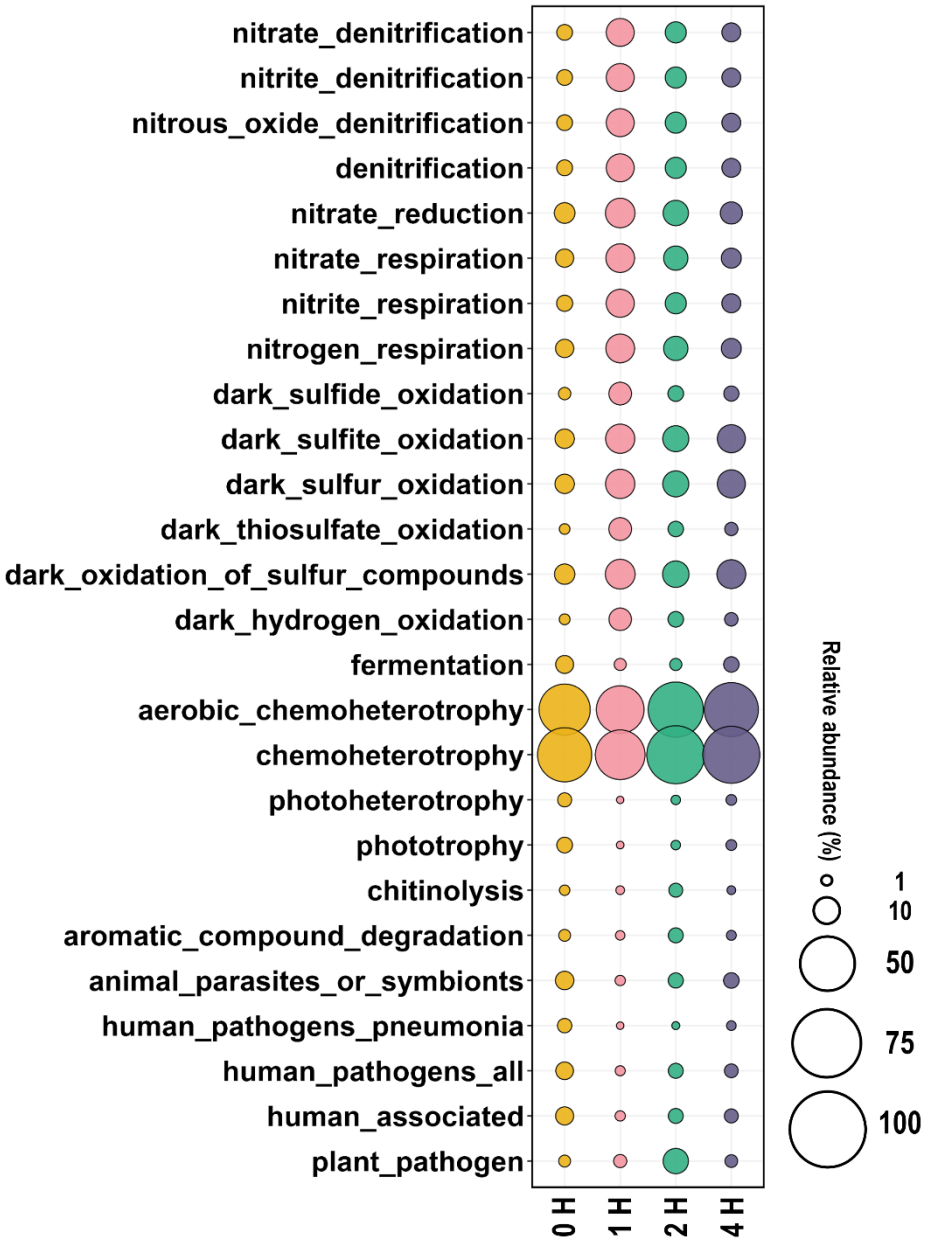

Figure 26. FAPROTAX functional analysis for the bacterial community in *X. testudinatus* gills after reintroduction. The functional proportions are shown as percentages and represented on a color scale from black (0%) to purple to yellow (100%). The x-axis represents time points 0H, 1H, 2H, and 4H, while the y-axis lists bacterial functions.

doi:10.6342/NTU202500809

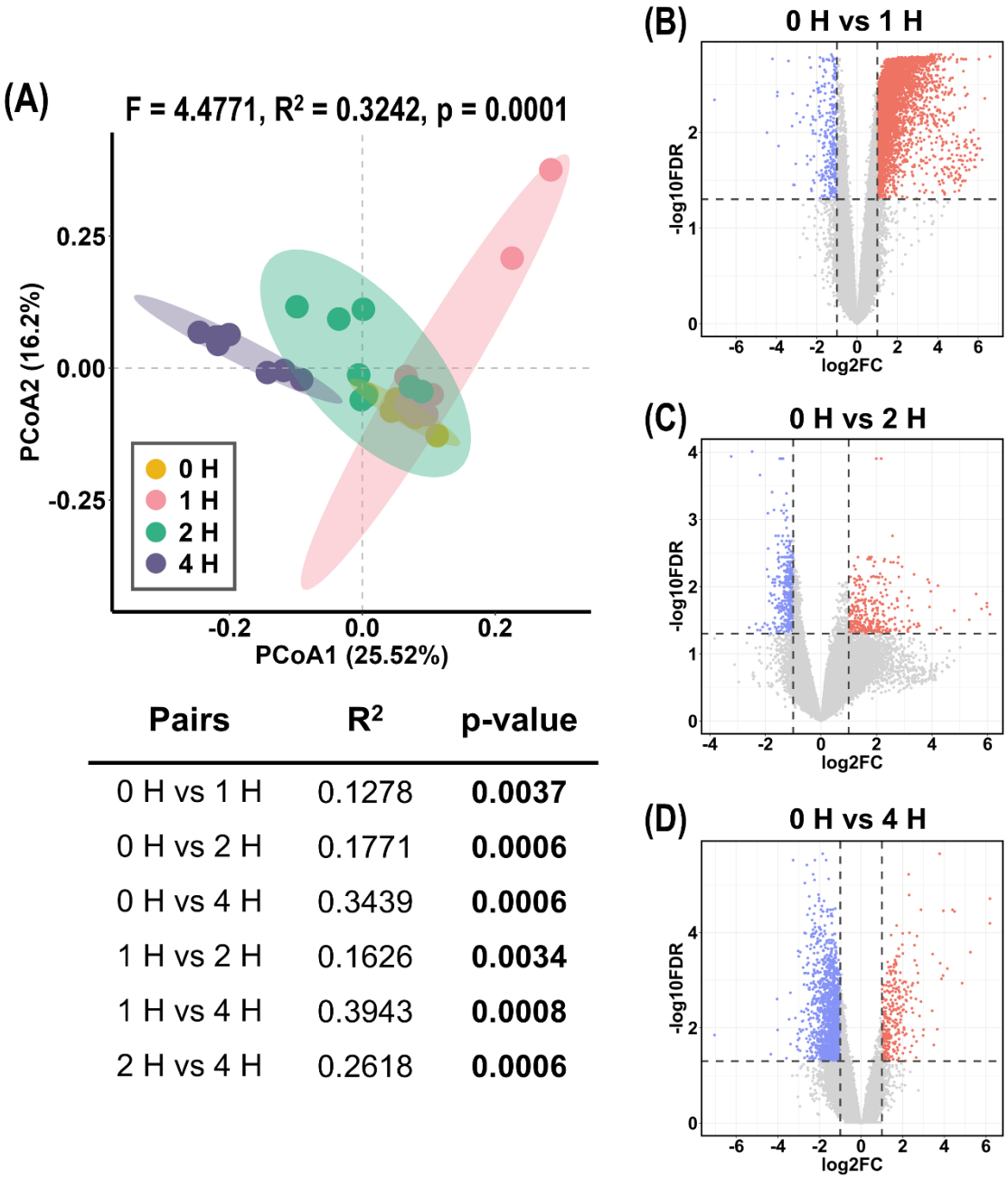

Pairs	R^2	p-value
0 H vs 1 H	0.1278	**0.0037**
0 H vs 2 H	0.1771	**0.0006**
0 H vs 4 H	0.3439	**0.0006**
1 H vs 2 H	0.1626	**0.0034**
1 H vs 4 H	0.3943	**0.0008**
2 H vs 4 H	0.2618	**0.0006**

Figure 27. PCoA for RNA-seq TPM in the gills of *X. testudinatus* after reintroduction. PCoA and PERMANOVA was performed by 9999 permutations, and the pairwise comparison table is included (A). Differentially Expressed Gene (DEG) analysis was conducted for 1H (B), 2H (C), 4H (D) relative to 0H, with the results visualized as volcano plots. Dots are colored based on significance and expression fold change (FC): red for upregulated genes, blue for downregulated genes, and gray for non-significant genes. Significance thresholds were set at a false discovery rate (FDR) of 0.05, corresponding to $-\log_{10}p = 1.30$ and a $\log_2FC$ greater than 1 or less than -1.

doi:10.6342/NTU202500809

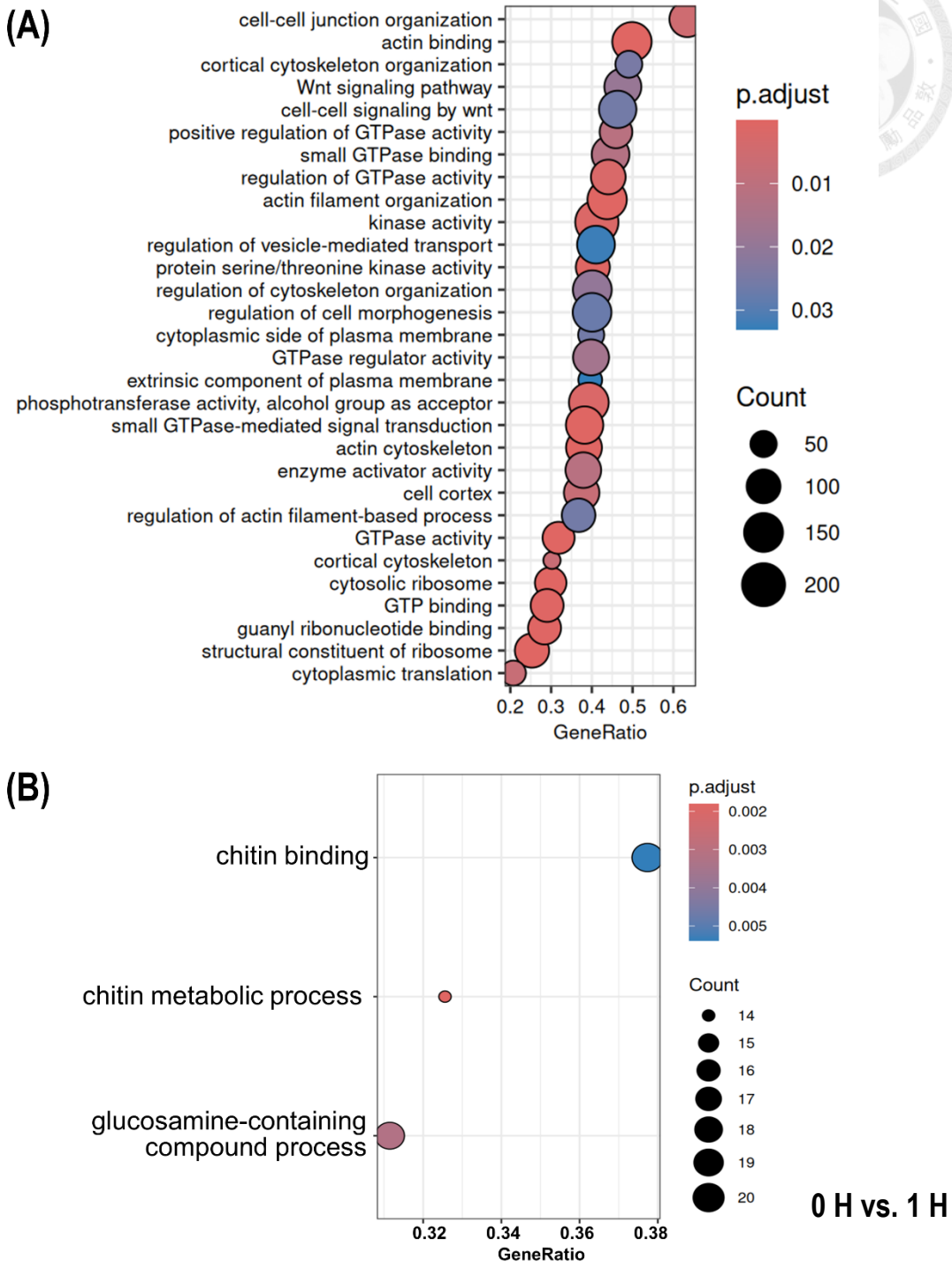

Figure 28. Gene set enrichment analysis (GSEA) based on DEG results between the 0H and 1H groups. Enriched upregulated (A) and downregulated (B) pathways, with dot size representing the number of genes associated with each pathway and color indicating the adjusted *p*-value (p.adjust). The GeneRatio represents the proportion of genes in the dataset associated with each pathway.

doi:10.6342/NTU202500809

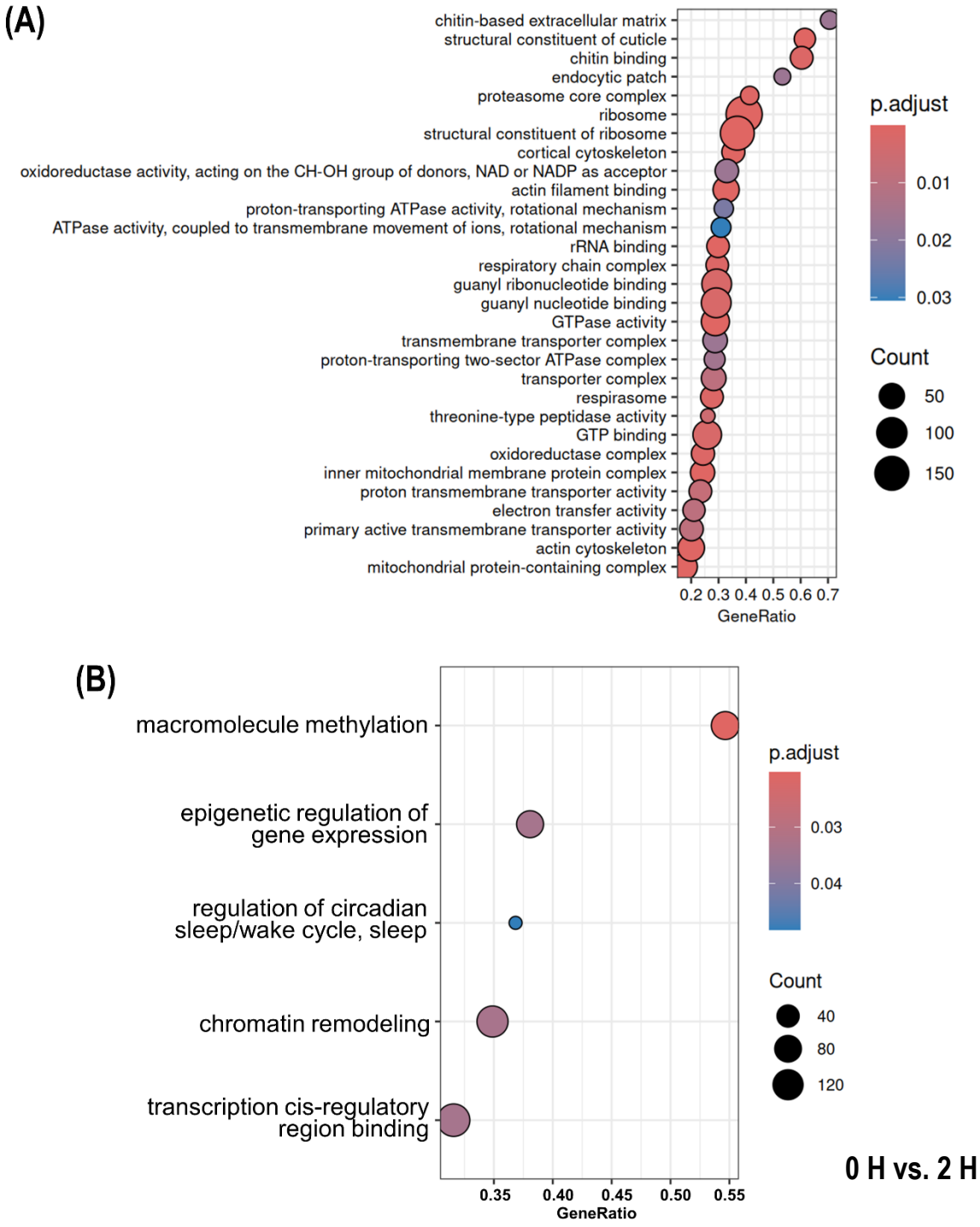

Figure 29. Gene Set Enrichment Analysis (GSEA) based on DEG results between the 0H and 2H groups. Enriched upregulated (A) and downregulated (B) pathways, with dot size representing the number of genes associated with each pathway and color indicating the adjusted *p*-value (p.adjust). The GeneRatio represents the proportion of genes in the dataset associated with each pathway.

doi:10.6342/NTU202500809

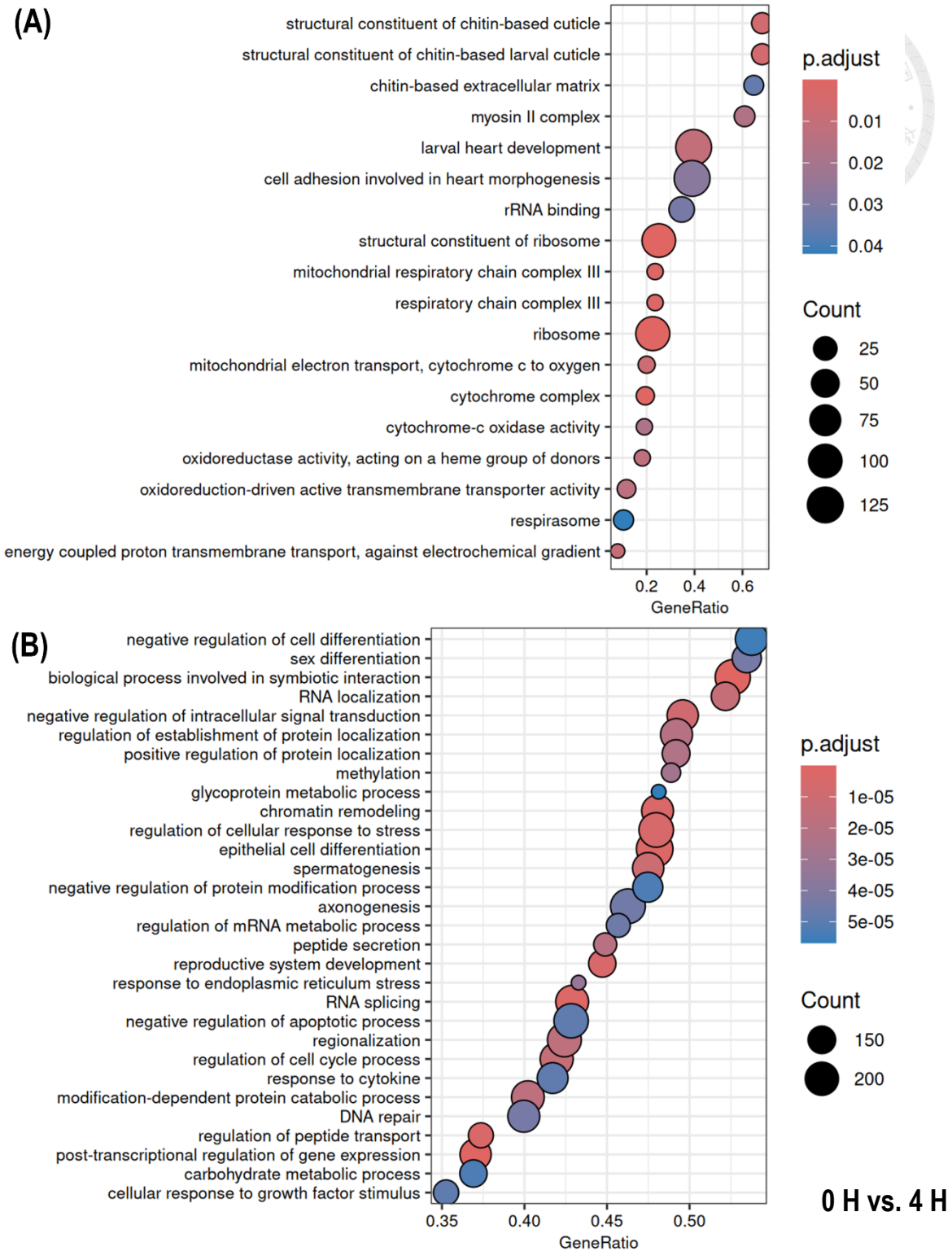

Figure 30. Gene Set Enrichment Analysis (GSEA) based on DEG results between the 0H and 4H groups. Enriched upregulated (A) and downregulated (B) pathways, with dot size representing the number of genes associated with each pathway and color indicating the adjusted *p*-value (p.adjust). The GeneRatio represents the proportion of genes in the dataset associated with each pathway.

doi:10.6342/NTU202500809

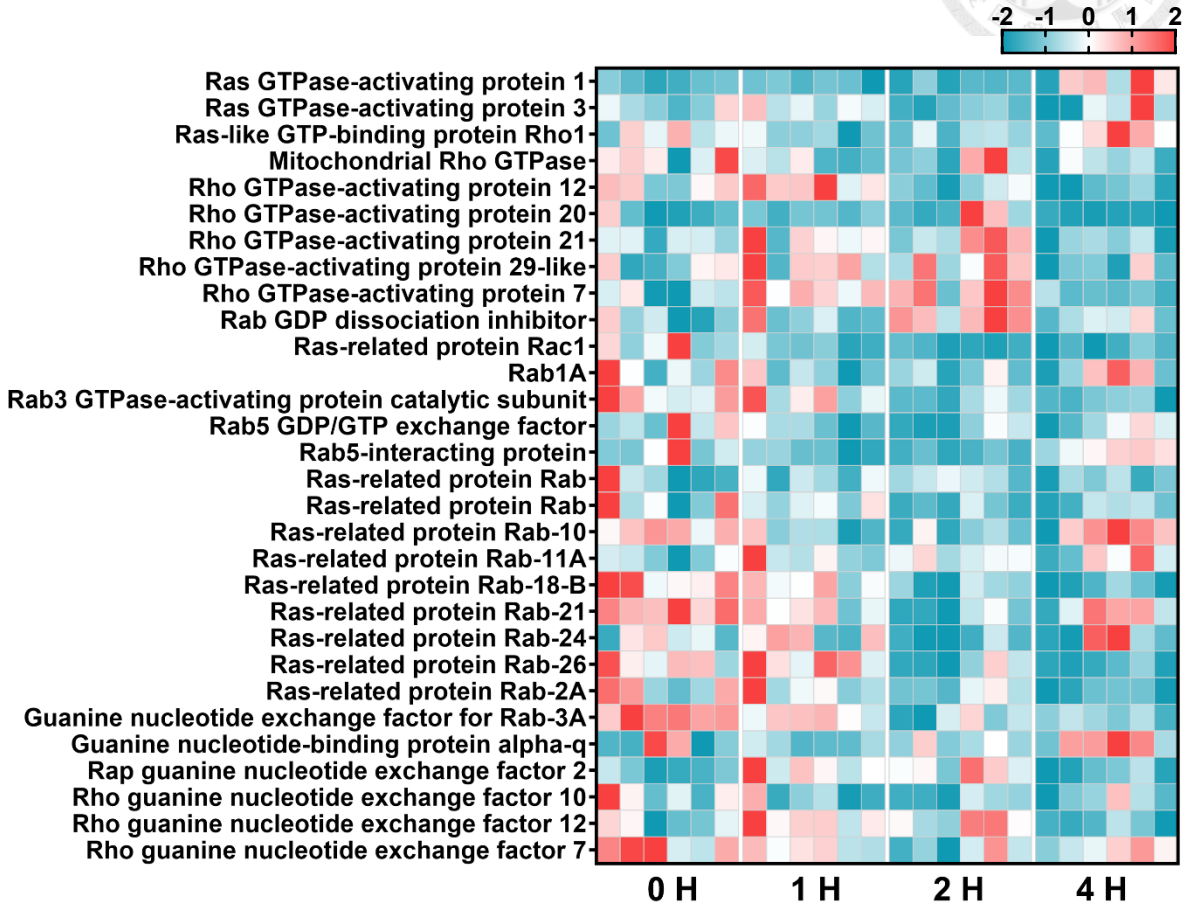

Figure 31. Expression of genes related to GTPase activity, visualized as a heatmap with Z-score normalization. The color scale ranges from -2 (blue) to 2 (red), with intermediate values represented in shades of blue, white, and red.

doi:10.6342/NTU202500809

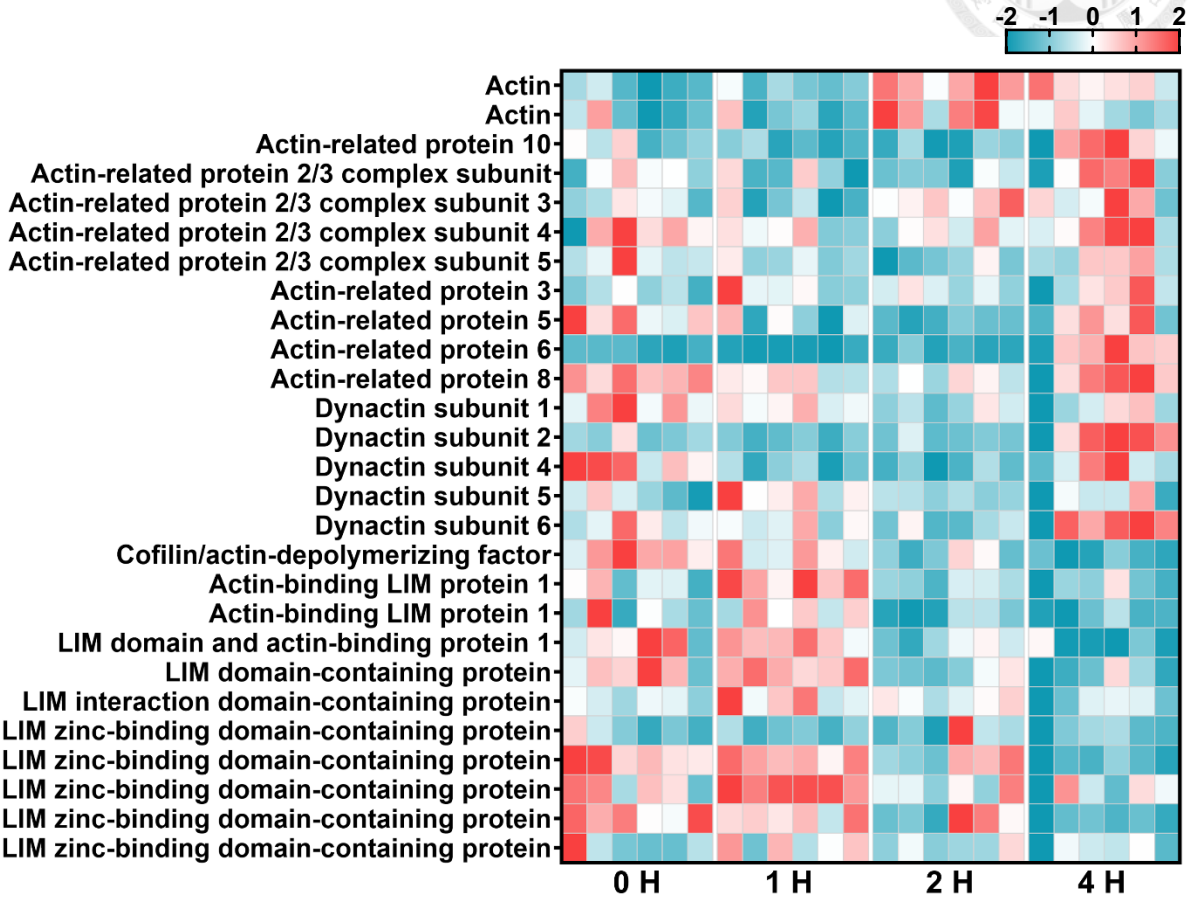

Figure 32. Expression of genes related to actin cytoskeleton, visualized as a heatmap with Z-score normalization. The color scale ranges from -2 (blue) to 2 (red), with intermediate values represented in shades of blue, white, and red.

doi:10.6342/NTU202500809

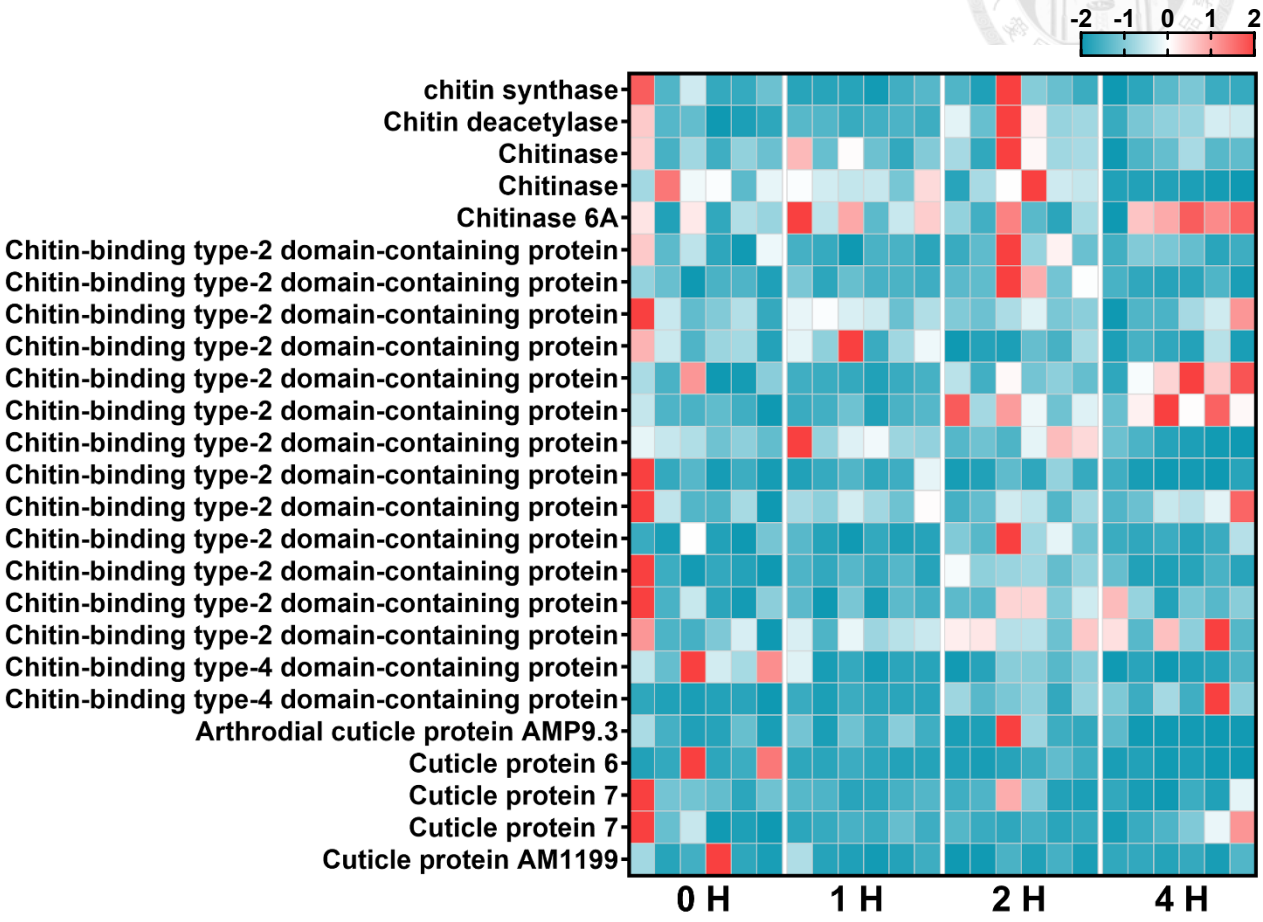

Figure 33. Expression of genes related to chitin and cuticle formation, visualized as a heatmap with Z-score normalization. The color scale ranges from -2 (blue) to 2 (red), with intermediate values represented in shades of blue, white, and red.

doi:10.6342/NTU202500809

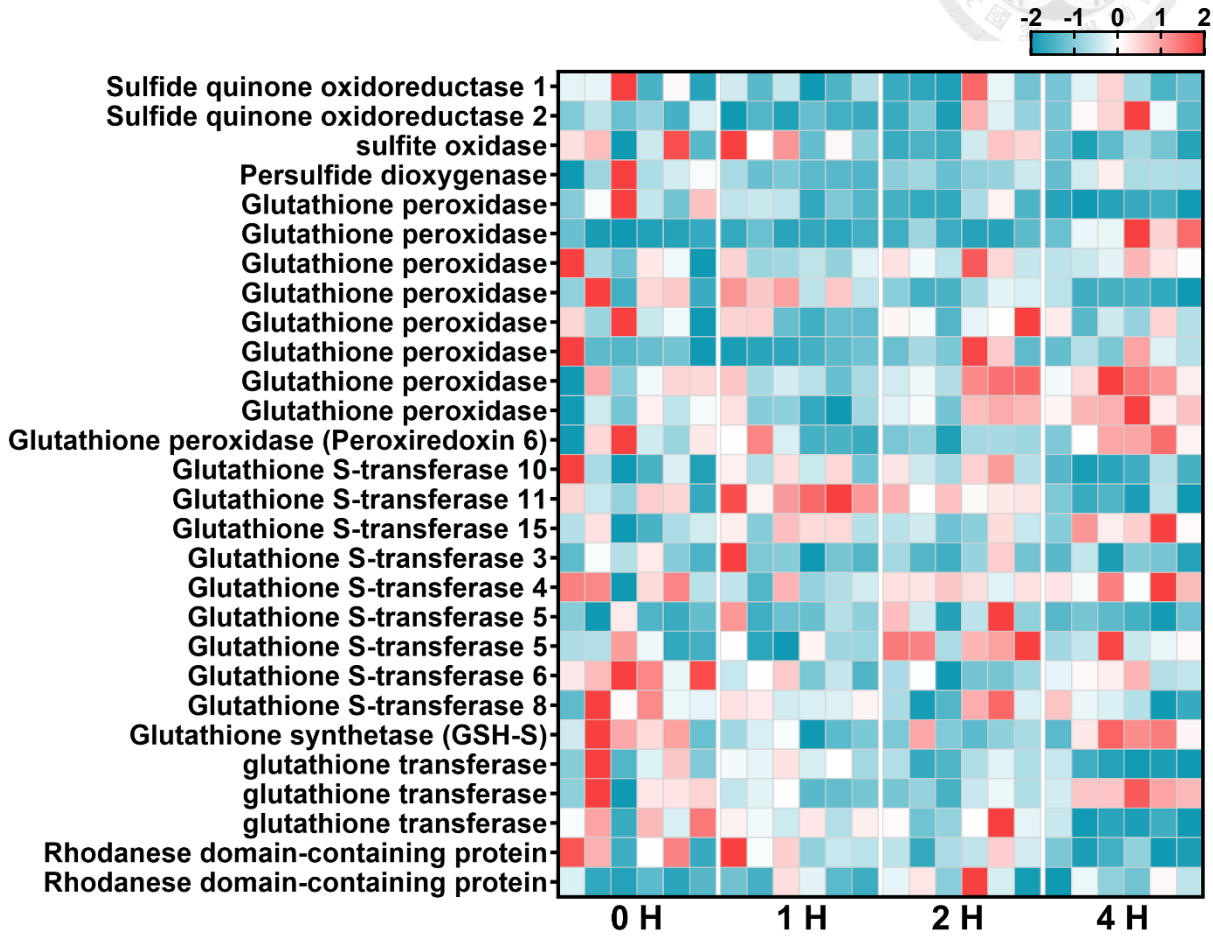

Figure 34. Expression of genes related to sulfide metabolism, visualized as a heatmap with Z-score normalization. The color scale ranges from -2 (blue) to 2 (red), with intermediate values represented in shades of blue, white, and red.

doi:10.6342/NTU202500809

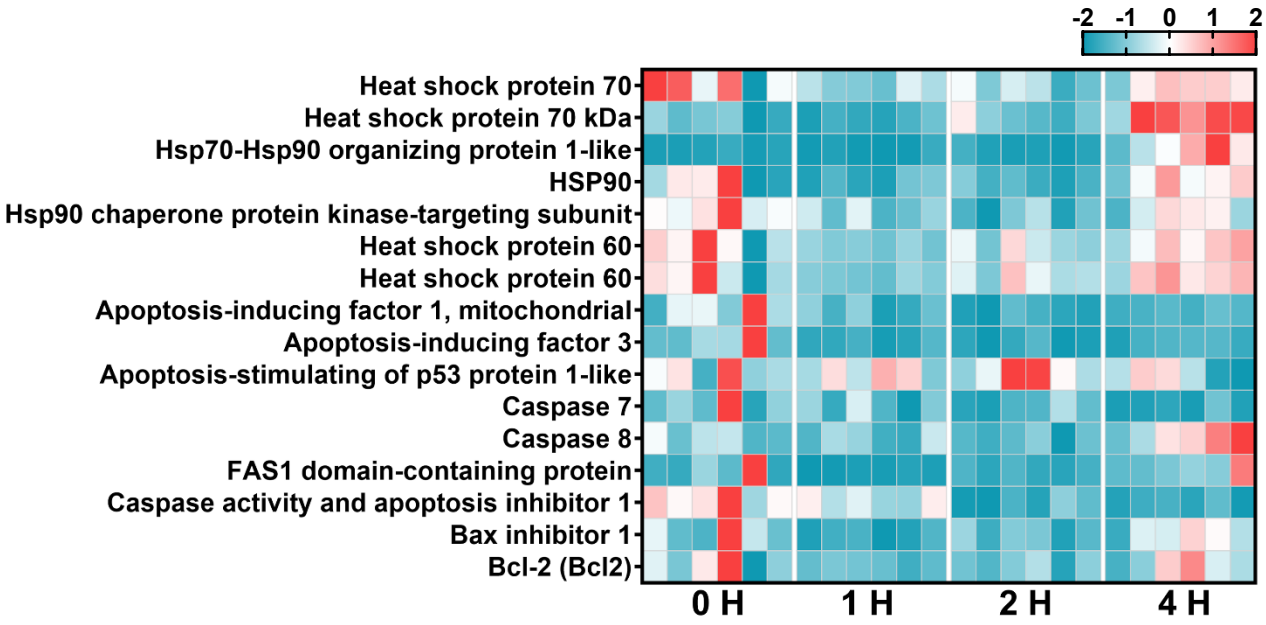

Figure 35. Expression of genes related to stress and apoptosis, visualized as a heatmap with Z-score normalization. The color scale ranges from -2 (blue) to 2 (red), with intermediate values represented in shades of blue, white, and red.

doi:10.6342/NTU202500809

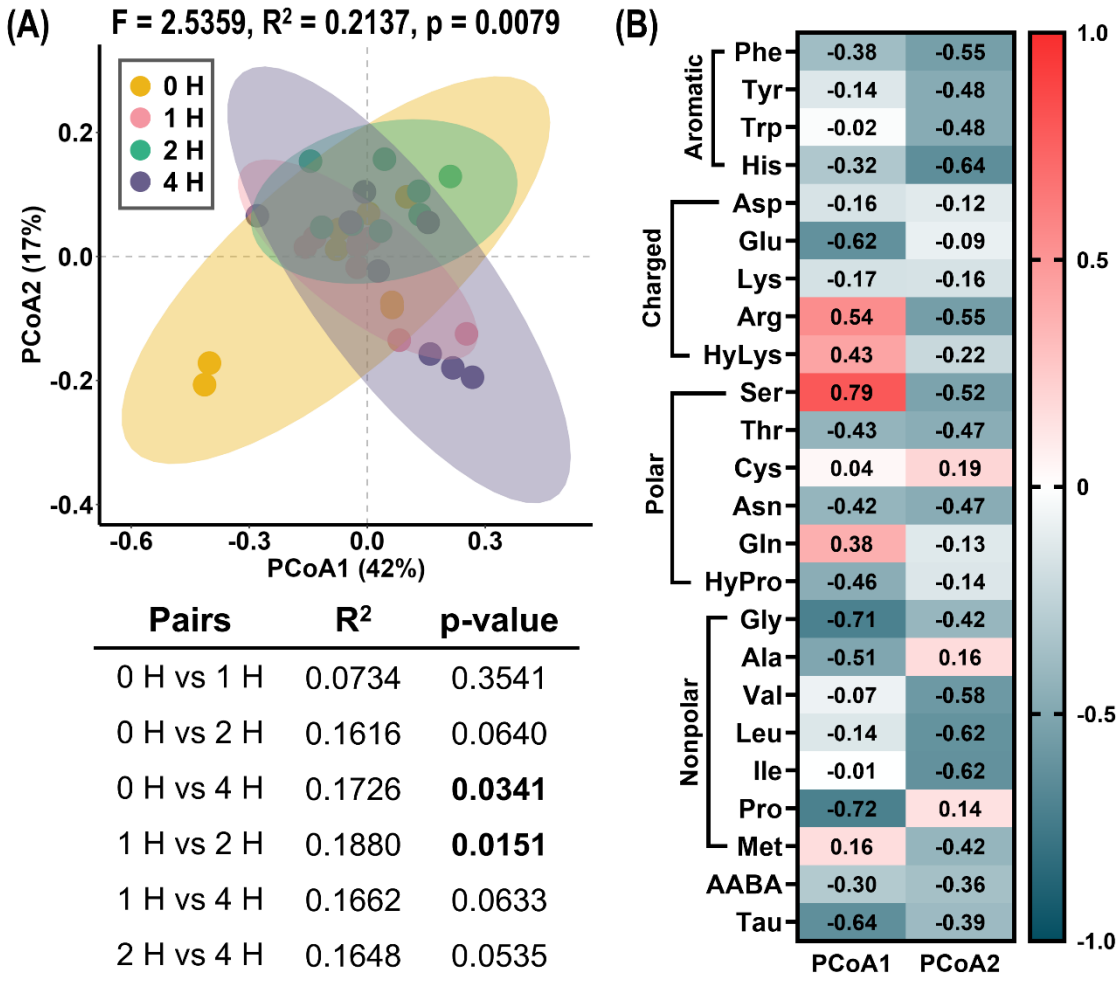

Pairs	R^2	p-value
0 H vs 1 H	0.0734	0.3541
0 H vs 2 H	0.1616	0.0640
0 H vs 4 H	0.1726	**0.0341**
1 H vs 2 H	0.1880	**0.0151**
1 H vs 4 H	0.1662	0.0633
2 H vs 4 H	0.1648	0.0535

Figure 36. PCoA for the free amino acid (FAA) profile in the gills of *X. testudinatus* after reintroduction. PERMANOVA was performed with 9999 permutations, and the pairwise comparison table is included (A). The contributed correlation (B) of each amino acid to PCoA1 and PCoA2 is shown as a heatmap using a color scale ranging from 0.79 (red) to -72 (blue).

doi:10.6342/NTU202500809

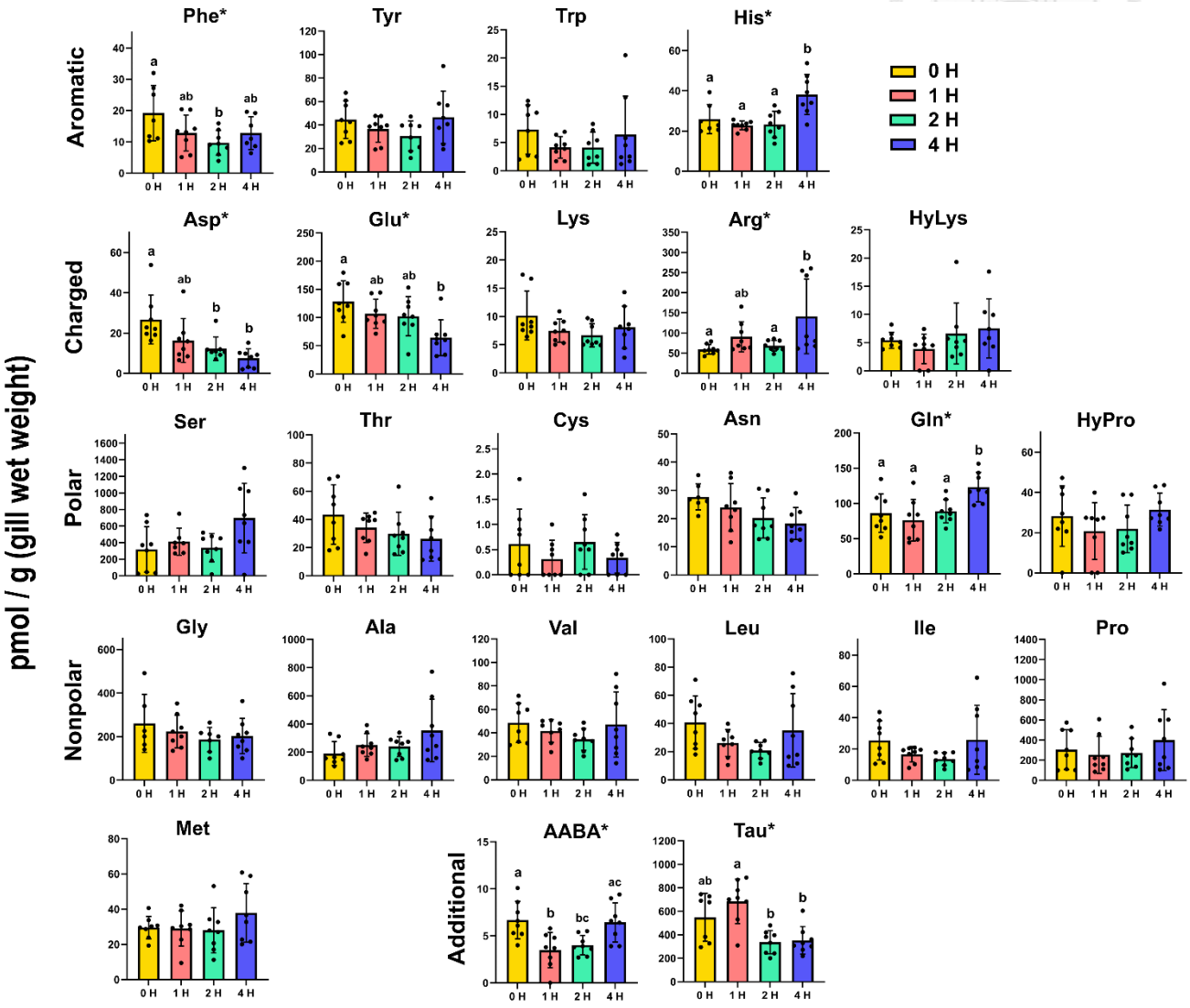

Figure 37. Bar charts of free amino acid (FAA) content, grouped as aromatic, charged, polar, nonpolar, and additional categories. Values are presented as mean ± SD (n = 8). Statistical significance was determined using one-way ANOVA followed by Bonferroni post hoc analysis ($p < 0.05$).

doi:10.6342/NTU202500809

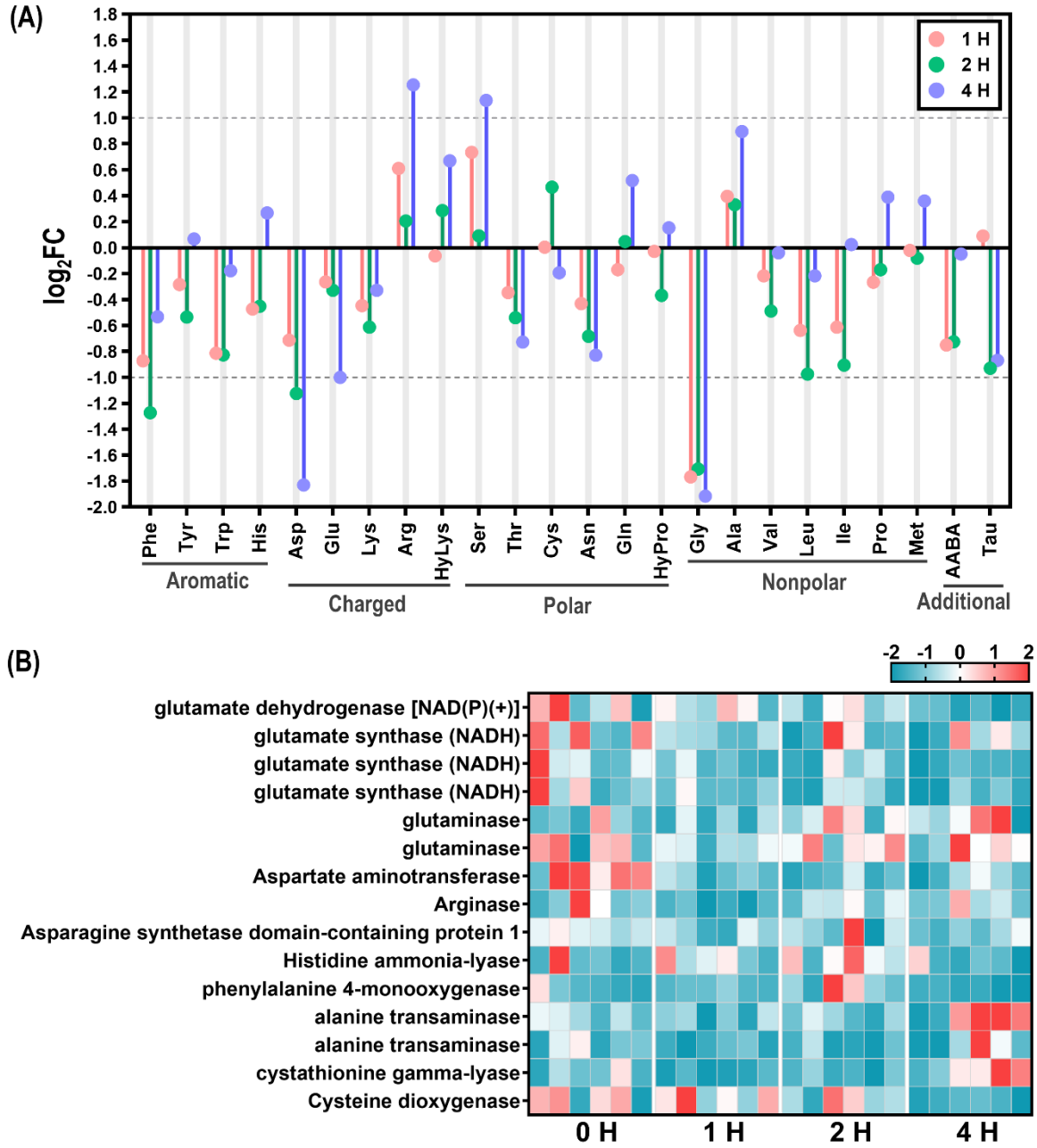

Figure 38. Fold change (FC) in free amino acid (FAA) levels 1H, 2H, and 4H post-reintroduction, relative to 0H. FC values were log2-transformed. A faint gray background line aligns each FAA, with 1H, 2H, and 4H represented by pink, green, and purple dots, respectively (A). Expression of genes related to amino acid metabolism was visualized as a heatmap with Z-score normalization (B).

doi:10.6342/NTU202500809

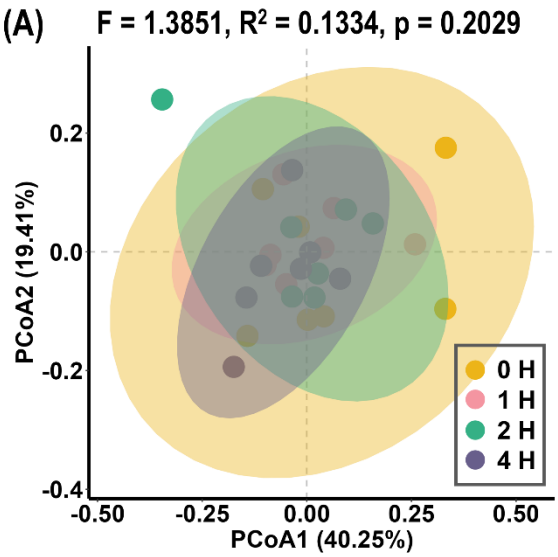

Pairs	R^2	p-value
0 H vs 1 H	0.1000	0.2269
0 H vs 2 H	0.1411	0.0921
0 H vs 4 H	0.0882	0.3082
1 H vs 2 H	0.0755	0.3251
1 H vs 4 H	0.0791	0.3050
2 H vs 4 H	0.0547	0.4254

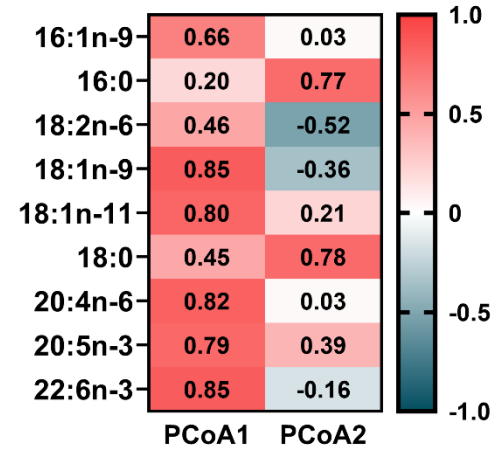

Figure 39. PCoA of the fatty acid (FA) profile in the gills of *X. testudinatus* after reintroduction. PERMANOVA was performed with 9999 permutations, and the pairwise comparison table is included (A). The contributed correlation (B) of each FA to PCoA1 and PCoA2 is shown as a heatmap using a color scale ranging from 0.85 (red) to -0.52 (blue).

doi:10.6342/NTU202500809

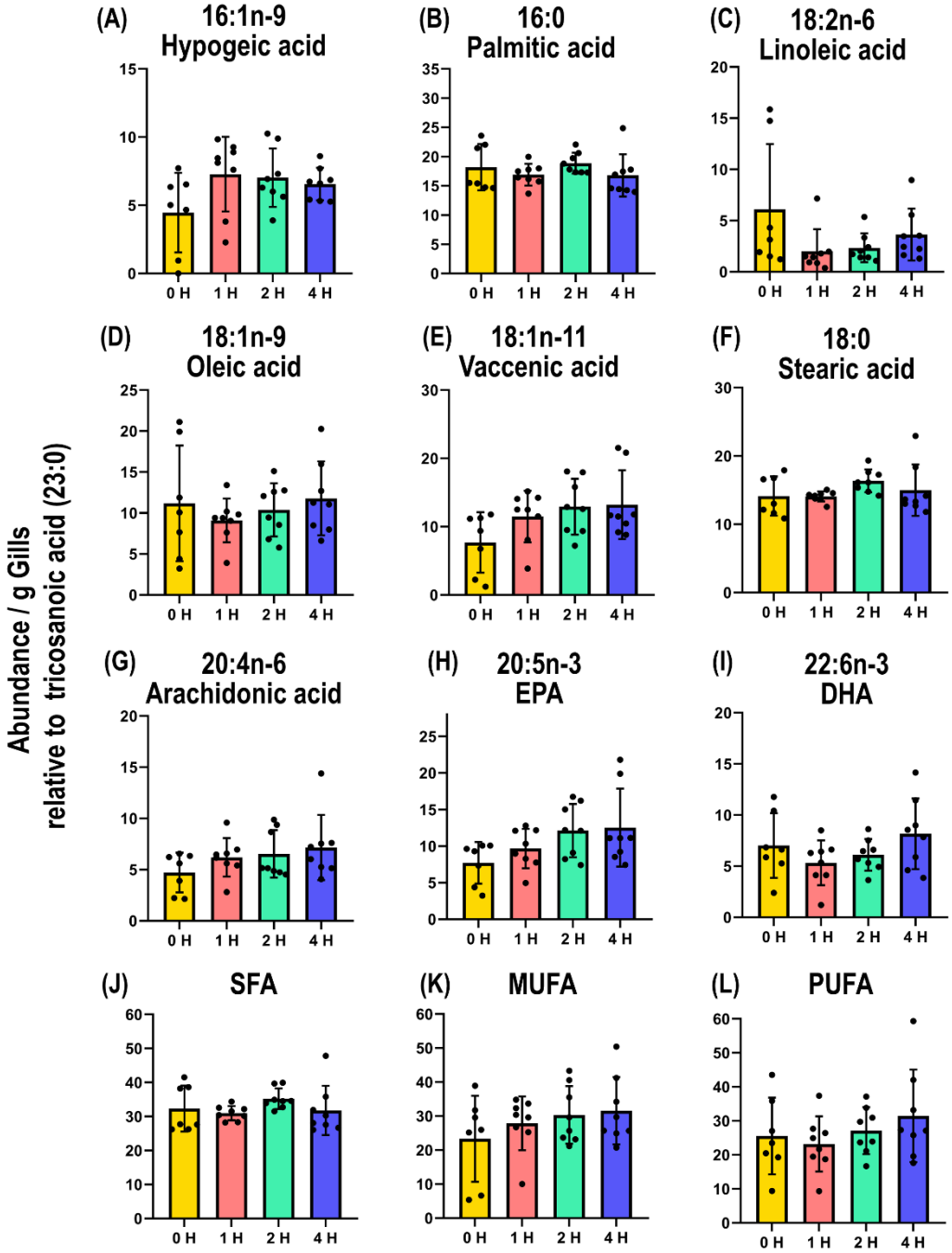

Figure 40. Bar charts of fatty acid (FA) content. Fatty acid names are labeled with their chain length and saturation. Values are presented as mean ± SD (n = 8). Statistical significance was determined using one-way ANOVA followed by Bonferroni post hoc analysis ($p < 0.05$); however, no significant differences were observed. EPA, eicosapentaenoic acid; DHA, docosahexaenoic acid; SFA, saturated fatty acid; MUFA, monounsaturated fatty acid; PUFA, polyunsaturated fatty acid.

doi:10.6342/NTU202500809

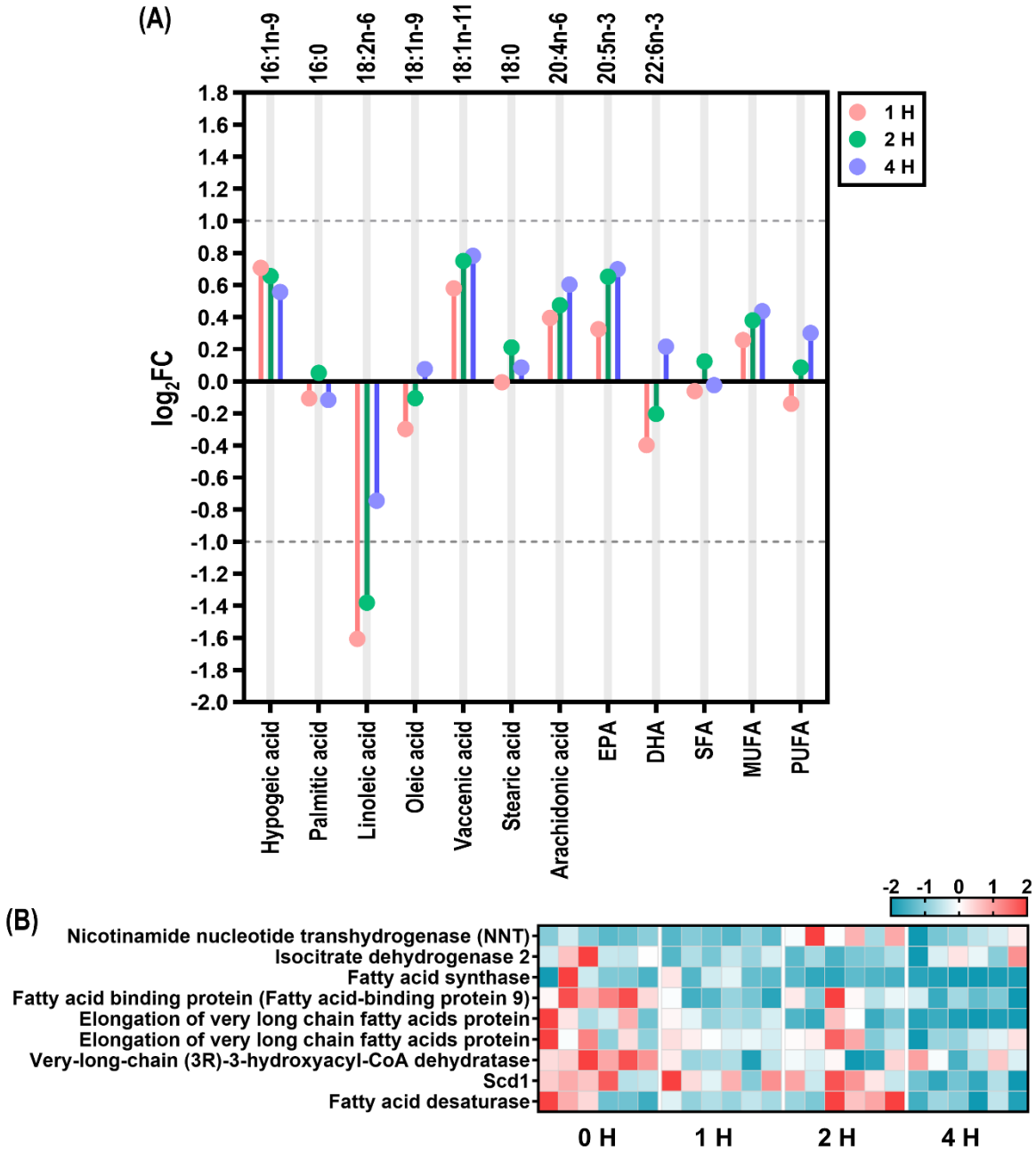

Figure 41. Fold change (FC) in fatty acid (FA) levels 1H, 2H, and 4H post-reintroduction, relative to 0H. FC values were log2-transformed. A faint gray background line aligns each FA, with 1H, 2H, and 4H represented by pink, green, and purple dots, respectively (A). Carbon chain and saturation are displayed at the top, and the corresponding fatty acids are labeled at the bottom. EPA, eicosapentaenoic acid; DHA, docosahexaenoic acid; SFA, saturated fatty acid; MUFA, monounsaturated fatty acid; PUFA, polyunsaturated fatty acid. Expression of genes related to fatty acid metabolism was visualized as a heatmap with Z-score normalization (B).

doi:10.6342/NTU202500809

Conclusions and Perspectives

Our research demonstrates the adaptation of *X. testudinatus* holobiont to the shallow-water hydrothermal vent system at Kueishan Island by examining the interactions between environmental conditions, bacterial communities, and the crustacean host (Fig. 42). The shallow-water hydrothermal vents create one of the most extreme and dynamic marine environments, exerting spatiotemporal influences on adjacent coral ecosystems. Physicochemical indicators, primarily sulfide, pH, DIC, and pCO_2, reflect fluctuations in hydrothermal activity and its impact on the surrounding environments. This hydrothermal system serves as an ideal platform for studying biological responses to environmental perturbations derived from vent fluids. Among the hydrothermal-associated bacterial class Campylobacteria, sulfur-reducing *Thioreductor* dominates the bacterioplankton to maintain environmental sulfur compounds in their reduced form (HS^-/H_2S), which can be oxidized by chemoautotrophic sulfur-oxidizing *Sulfurovum* predominantly symbiotic in the gills and carapace of *X. testudinatus*, contributing to essential sulfur cycling within the hydrothermal field. The gill-associated *Sulfurovum* may have co-evolved with *X. testudinatus*, facilitating sulfide detoxification and organic energy production to sustain the holobiont under resource-limited conditions imposed by the chemically enriched extreme environments.

A key aspect of this adaptation lies in the metabolic interactions between *X. testudinatus* and its microbial symbiont. The host's ion-regulatory mechanisms appear to have evolved not only to cope with environmental pH fluctuations but also to leverage microbial metabolism for mutual benefit. Moreover, *X. testudinatus* exhibits an early stress response by stabilizing cellular structures and suppressing non-essential metabolic processes to minimize the impacts of chemicals and oxidants derived from

doi:10.6342/NTU202500809

hydrothermal fluids. Changes in metabolite profiles are potentially involved in cellular maintenance, sulfide oxidation, and reactive oxygen species (ROS) detoxification, ensuring internal homeostasis when the holobiont is facing hydrothermal exposure. These observations suggest that *X. testudinatus* holobiont may have undergone selective pressures favoring physiological plasticity and metabolic integration. This potentially mutualistic strategy represents an evolutionary convergence among hydrothermal vent organisms, where metazoan-microbe co-evolution enables survival in extreme habitats. This reveals how life can thrive under persistent environmental stress through biochemical cooperation and physiological specialization.

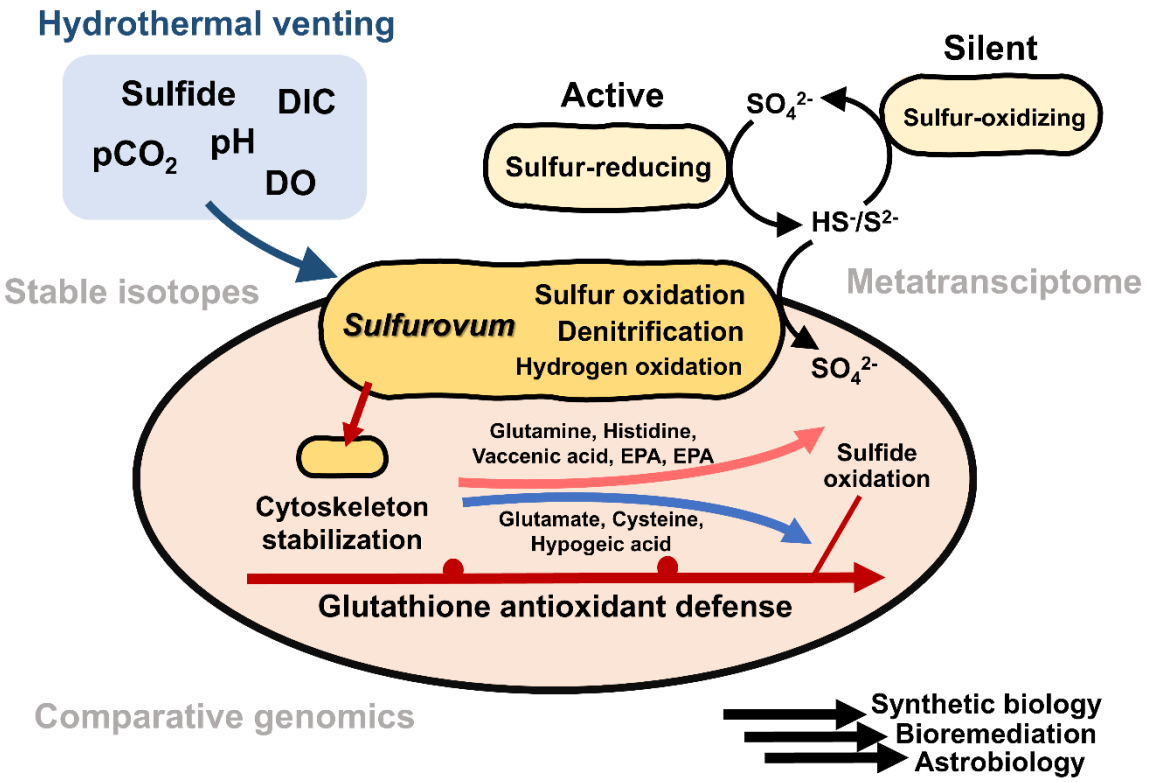

Figure 42. Environmental interactions and the adaptive strategies of the *X. testudinatus* holobiont in the Kueishan Island shallow-water hydrothermal fields.

doi:10.6342/NTU202500809

This study provides insight into the interactive dynamics between *X. testudinatus* and hydrothermal-associated microorganisms. Future research should integrate multi-omics approaches to elucidate the genetic, metabolic, and ecological mechanisms driving microbe-host interactions in hydrothermal vent environments. Comparative genomics can reveal adaptative mechanisms that facilitate the transition of free-living microbes to symbiosis (Wang et al., 2023), while metatranscriptomics and metabolomics can identify metabolite crosstalk between the hosts and their symbionts (Aguiar-Pulido et al., 2016). Microelectrode and biochemical measurements can further quantify the gradients of pH, oxygen, sulfide, chemicals and metal ions, clarifying microbial metabolic niches within the holobiont (Vitvitsky et al., 2012; Shih et al., 2022). Stable isotope analysis can confirm microbial contributions to biogeochemical cycles, underlying carbon, nitrogen, oxygen, and sulfur, as well as their role in host nutrient assimilation (Ke et al., 2024). Considering the current climate and ecological crisis, understanding extremophile adaptation not only satisfies our fascination with the origins of life but also has broader implications for bioremediation, biodegradation, and synthetic biology, aiding in the reduction of environmental contamination and the development of sustainable resources (Krüger et al., 2018). Furthermore, their survival mechanisms and inherent evolutionary processes contribute to astrobiology, providing information on the limits of life for habitat exploration in extreme environments, both on and even beyond our planet (Nandhini et al., 2021).

doi:10.6342/NTU202500809

References

Abele, D., and S. Puntarulo (2004). Formation of reactive species and induction of antioxidant defence systems in polar and temperate marine invertebrates and fish. *Comp Biochem Physiol A: Mol Integr Physiol* 138(4), 405-415. Doi: 10.1016/j.cbpb.2004.05.013.

Adigun, O. A., M. Nadeem, T. H. Pham, L. E. Jewell, M. Cheema, and R. Thomas (2021). Recent advances in bio-chemical, molecular and physiological aspects of membrane lipid derivatives in plant pathology. *Plant Cell Environ* 44(1), 1-16. Doi: 10.1111/pce.13904.

Aguiar-Pulido, V., W. Huang, V. Suarez-Ulloa, T. Cickovski, K. Mathee, and G. Narasimhan (2016). Metagenomics, metatranscriptomics, and metabolomics approaches for microbiome analysis: supplementary issue: bioinformatics methods and applications for big metagenomics data. *Evol Bioinform* 12, EBO-S36436. Doi: 10.4137/EBO.S36436.

Akerman, N. H., D. A. Butterfield and J. A. Huber (2013). Phylogenetic diversity and functional gene patterns of sulfur-oxidizing subseafloor Epsilonproteobacteria in diffuse hydrothermal vent fluids. *Front Microbiol* 4, 185. Doi: 10.3389/fmicb.2013.00185.

Allen, G. J. P., P. L. Kuan, Y. C. Tseng, P. P. Hwang, A. R. Quijada-Rodriguez and D. Weihrauch (2020). Specialized adaptations allow vent-endemic crabs (*Xenograpsus testudinatus*) to thrive under extreme environmental hypercapnia. *Sci Rep-Uk* 10(1). Doi: 10.1038/s41598-020-68656-1.

Allen, G. J. P., M.-C. Wang, Y.-C. Tseng and D. Weihrauch (2021). Effects of emersion on acid–base regulation, osmoregulation, and nitrogen physiology in the semi-terrestrial mangrove crab, *Helice formosensis*. *J Comp Physiol B* 191(3), 455-468. Doi: 10.1007/s00360-021-01354-0.

Amann, R. I., B. J. Binder, R. J. Olson, S. W. Chisholm, R. Devereux and D. A. Stahl (1990). Combination of 16S rRNA-targeted oligonucleotide probes with flow cytometry for analyzing mixed microbial populations. *Appl Environ Microbiol* 56(6), 1919-1925. Doi: 10.1128/aem.56.6.1919-1925.1990.

Amend, J. P., T. M. McCollom, M. Hentscher, and W. Bach (2011). Catabolic and anabolic energy for chemolithoautotrophs in deep-sea hydrothermal systems hosted in different rock types. *Geochim Cosmochim Acta* 75(19), 5736-5748.

doi:10.6342/NTU202500809

Doi: 10.1016/j.gca.2011.07.041.

Amores-Sánchez, M. I., and M. Á. Medina (1999). Glutamine, as a precursor of glutathione, and oxidative stress. *Mol Genet Metab* 67(2), 100-105. Doi: 10.1006/mgme.1999.2857.

Arakane, Y., and S. Muthukrishnan (2010). Insect chitinase and chitinase-like proteins. *Cell Mol Life Sci* 67, 201-216. Doi: 10.1007/s00018-009-0161-9.

Araki, S., T. Takata, K. Ono, T. Sawa, S. Kasamatsu, H. Ihara, Y. Kumagai, T. Akaike, Y. Watanabe, and Y. Tsuchiya (2023). Cystathionine γ-lyase self-inactivates by polysulfidation during cystine metabolism. *Int J Mol Sci* 24(12), 9982. Doi: 10.3390/ijms24129982.

Araseki, M., K. Yamamoto, and K. Miyashita (2002). Oxidative stability of polyunsaturated fatty acid in phosphatidylcholine liposomes. *Biosci Biotechnol Biochem* 66(12), 2573-2577. Doi: 10.1271/bbb.66.2573.

Arcadi, E., E. Buschi, E. Rastelli, M. Tangherlini, P. De Luca, V. Esposito, R. Calogero, F. Andaloro, T. Romeo, and R. Danovaro (2023). Novel insights on the bacterial and archaeal diversity of the Panarea shallow-water hydrothermal vent field. *Microorganisms* 11(10), 2464. Doi: 10.3390/microorganisms11102464.

Bang, C., T. Dagan, P. Deines, N. Dubilier, W. J. Duschl, S. Fraune, U. Hentschel, H. Hirt, N. Hülter, T. Lachnit, and D. Picazo. (2018). Metaorganisms in extreme environments: do microbes play a role in organismal adaptation? *Zoology* 127, 1-19. Doi: 10.1016/j.zool.2018.02.004.

Barosa, B., A. Ferrillo, M. Selci, M. Giardina, A. Bastianoni, M. Correggia, L. di Iorio, G. Bernardi, M. Cascone, R. Capuozzo, and M. Intoccia (2023). Mapping the microbial diversity associated with different geochemical regimes in the shallow-water hydrothermal vents of the Aeolian archipelago, Italy. *Front Microbiol* 14, 1134114. Doi: 10.3389/fmicb.2023.1134114.

Becker, J., and E. A. Craig (1994). Heat-shock proteins as molecular chaperones. *Eur J Biochem* 219(1-2), 11-23. Doi: 10.1111/j.1432-1033.1994.tb19910.x.

Bement, W. M., A. B. Goryachev, A. L. Miller, and G. von Dassow (2024). Patterning of the cell cortex by Rho GTPases. *Nat Rev Mol Cell Biol* 25, 290–308. Doi: 10.1038/s41580-023-00682-z.

Bender, R. A. (2012). Regulation of the histidine utilization (hut) system in bacteria. *Microbiol Mol Biol Rev* 76(3), 565-584. Doi: 10.1128/mmbr.00014-12.

doi:10.6342/NTU202500809

Bertucci, F., E. Parmentier, G. Lecellier, A. D. Hawkins and D. Lecchini (2016). Acoustic indices provide information on the status of coral reefs: an example from Moorea Island in the South Pacific. *Sci Rep-Uk* 6(1), 33326. Doi: 10.1038/srep33326.

Bermúdez, M. A., L. Pereira, C. Fraile, L. Valerio, M. A. Balboa, and J. Balsinde (2022). Roles of palmitoleic acid and its positional isomers, hypogeic and sapienic acids, in inflammation, metabolic diseases and cancer. *Cells* 11(14), 2146. Doi: 10.3390/cells11142146.

Bettencourt, R., V. Costa, M. Laranjo, D. Rosa, L. Pires, A. Colaço, H. Lopes, and R. Serrão Santos (2011). Out of the deep sea into a land-based aquarium environment: investigating physiological adaptations in the hydrothermal vent mussel *Bathymodiolus azoricus*. *ICES J Mar Sci* 68(2), 357-364. Doi: 10.1093/icesjms/fsq119.

Blewett, H. J., C. A. Gerdung, M. R. Ruth, S. D. Proctor, and C. J. Field (2009). Vaccenic acid favourably alters immune function in obese JCR: LA-cp rats. *Br J Nutr* 102(4), 526-536. Doi: 10.1017/S0007114509231722.

Blow, F., N. Y. Ankrah, N. Clark, I. Koo, E. L. Allman, Q. Liu, M. Anitha, A. D. Patterson, and A. E. Douglas (2020). Impact of facultative bacteria on the metabolic function of an obligate insect-bacterial symbiosis. *mBio* 11(4), e00402-20. Doi: 10.1128/mBio.00402-20.

Bordenstein, S. R., and K. R. Theis (2015). Host biology in light of the microbiome: ten principles of holobionts and hologenomes. *PLoS Biol* 13(8), e1002226. Doi: 10.1371/journal.pbio.1002226.

Breusing, C., M. Genetti, S. L. Russell, R. B. Corbett-Detig, and R. A. Beinart (2022). Horizontal transmission enables flexible associations with locally adapted symbiont strains in deep-sea hydrothermal vent symbioses. *Proc Natl Acad Sci USA* 119(14), e2115608119. Doi: 10.1073/pnas.2115608119.

Brooks, A. W., K. D. Kohl, R. M. Brucker, E. J. van Opstal, and S. R. Bordenstein (2017). Correction: Phylosymbiosis: Relationships and functional effects of microbial communities across host evolutionary history. *PLoS Biol* 15(1), e1002587. Doi: 10.1371/journal.pbio.1002587.

Brosnan, M. E., and J. T. Brosnan (2020). Histidine metabolism and function. *J Nutr 150*, 2570S-2575S. Doi: 10.1093/jn/nxaa079.

doi:10.6342/NTU202500809

Butterfield, D. A., G. J. Massoth, R. E. Mcduff, J. E. Lupton and M. D. Lilley (1990). Geochemistry of hydrothermal fluids from axial seamount hydrothermal emissions study vent field, Juan De Fuca Ridge: subseafloor boiling and subsequent fluid-rock interaction. *J Geophys Res-Solid* 95(B8), 12895-12921. Doi:10.1029/JB095iB08p12895.

Burgin, A. J., W. H. Yang, S. K. Hamilton, and W. L. Silver. (2011). Beyond carbon and nitrogen: how the microbial energy economy couples elemental cycles in diverse ecosystems. *Front Ecol Environ*, 9(1), 44-52. Doi: 10.1890/090227.

Cady and J. T. Staley (2004). Subfreezing growth of the sea ice bacterium "*Psychromonas ingrahamii*". *Microb Ecol* 47(3), 300-304. Doi: 10.1007/s00248-0031040-9.

Campbell, B. J., A. S. Engel, M. L. Porter and K. Takai (2006). The versatile epsilon-proteobacteria: key players in sulphidic habitats. *Nat Rev Microbiol* 4(6), 458-468. Doi: 10.1038/nrmicro1414.

Canion, A., O. Prakash, S. J. Green, L. Jahnke, M. M. M. Kuypers and J. E. Kostka (2013). Isolation and physiological characterization of psychrophilic denitrifying bacteria from permanently cold Arctic fjord sediments (Svalbard, Norway). *Environ Microbiol* 15(5), 1606-1618. Doi: 10.1111/1462-2920.12110.

Cao, M. and H. Goodrich-Blair. (2017). Ready or not: microbial adaptive responses in dynamic symbiosis environments. *J Bacteriol*, 199(15), 10-1128. Doi: 10.1128/jb.00883-16.

Carballal, S., V. Vitvitsky, R. Kumar, D. A. Hanna, M. Libiad, A. Gupta, J. W. Jones and R. Banerjee (2021). Hydrogen sulfide stimulates lipid biogenesis from glutamine that is dependent on the mitochondrial NAD(P)H pool. *J Biol Chem* 292, 100950. Doi: 10.1016/j.jbc.2021.100950.

Cardoso, R. B., R. Sierra-Alvarez, P. Rowlette, E. R. Flores, J. Gomez, and J. A. Field (2006). Sulfide oxidation under chemolithoautotrophic denitrifying conditions. *Biotechnol Bioeng* 95(6), 1148-1157. Doi: 10.1002/bit.21084.

Carlson, M. and H. Pagès (2024). *AnnotationForge: Tools for building SQLite-based annotation data packages*. R package version 1.48.0. https://bioconductor.org/packages/AnnotationForge.

Cerqueira, T., D. Pinho, H. Froufe, R. S. Santos, R. Bettencourt and C. Egas (2017). Sediment microbial diversity of three deep-sea hydrothermal vents southwest of the Azores. *Microb Ecol* 74(2), 332-349. Doi: 10.1007/s00248-017-0943-9.

doi:10.6342/NTU202500809

Chan, B. K. K., T. W. Wang, P. C. Chen, C. W. Lin, T. Y. Chan and L. M. Tsang (2016). Community structure of macrobiota and environmental parameters in shallow water hydrothermal vents off Kueishan Island, Taiwan. *Plos One* 11(2), e0148675. Doi: 10.1371/journal.pone.0148675.

Chang, N. N., L. H. Lin, T. H. Tu, M. S. Jeng, Y. Chikaraishi and P. L. Wang (2018). Trophic structure and energy flow in a shallow-water hydrothermal vent: Insights from a stable isotope approach. *Plos One* 13(10), e0204753. Doi: 10.1371/journal.pone.0204753.

Chaston, J., and H. Goodrich-Blair (2010). Common trends in mutualism revealed by model associations between invertebrates and bacteria. *FEMS Microbiol Rev* 34(1), 41-58. Doi: 10.1111/j.1574-6976.2009.00193.x.

Chen, C., T. Y. Chan and B. K. K. Chan (2018a). Molluscan diversity in shallow water hydrothermal vents off Kueishan Island, Taiwan. *Mar Biodivers* 48(1), 709-714. Doi: 10.1007/s12526-017-0804-2.

Chen, C., T. H. Lin, H. K. Watanabe, T. Akamatsu and S. Kawagucci (2021). Baseline s oundscapes of deep-sea habitats reveal heterogeneity among ecosystems and sensitivity to anthropogenic impacts. *Limnol Oceanogr* 66(10), 3714-3727. Doi: 10.1002/lno.11911.

Chen, C., G. C. Wu, Y. T. Chung, H. W. Li, P. H. Chou, Y. C. Tseng, C. J. Chen, S. Dufour and C. F. Chang (2023). Duplicated paralog of sulfide: quinone oxidoreductase contributes to the adaptation to hydrogen sulfide-rich environment in the hydrothermal vent crab, *Xenograpsus testudinatus*. *Sci Total Environ* 890, 164257. Doi: 10.1016/j.scitotenv.2023.164257.

Chen, J., C. S. Robb, F. Unfried, L. Kappelmann, S. Markert, T. Song, J. Harder, B. Avci, D. Becher, P. Xie, R. I. Amann, J. H. Hehemann, T. Schweder and H. Teeling (2018b). Alpha- and beta-mannan utilization by marine Bacteroidetes. *Environ Microbiol* 20(11), 4127-4140. Doi: 10.1111/1462-2920.14414.

Chiu, L., M. C. Wang, K. Y. Tseng, C. L. Wei, H. T. Lin, S. H. Yang, and Y. C. Tseng (2022). Shallow-water hydrothermal vent system as an extreme proxy for discovery of microbiome significance in a crustacean holobiont. *Front Mar Sci* 9, 976255. Doi: 10.3389/fmars.2022.976255.

Chiu, L., M. C. Wang, C. L. Wei, T. H. Lin, and Y. C. Tseng (2024). A two-year physicochemical and acoustic observation reveals spatiotemporal effects of

doi:10.6342/NTU202500809

earthquake-induced shallow-water hydrothermal venting on the surrounding environments. *Limnol Oceanogr Lett* 9(4), 423-432. Doi: 10.1002/lol2.10412.

Clare, J., M. R. Lindley, and E. Ratcliffe (2024). The Antimicrobial and Antibiofilm Abilities of Fish Oil Derived Polyunsaturated Fatty Acids and Manuka Honey. *Microorganisms* 12(4), 778. Doi: 10.3390/microorganisms12040778.

Cline, J. D. (1969). Spectrophotometric Determination of Hydrogen Sulfide in Natural Waters. *Limnol Oceanogr* 14(3), 454. Doi: 10.4319/lo.1969.14.3.0454.

Cruaud, P., C. Decker, K. Olu, S. Arnaud-Haond, C. Papot, J. Le Baut, A. Vigneron, A. Khripounoff, N. Gayet, C. Cathalot, J. C. Caprais, P. Pignet, A. Godfroy and M. A. Cambon-Bonavita (2019). Ecophysiological differences between vesicomyid species and metabolic capabilities of their symbionts influence distribution patterns of the deep-sea clams. *Mar Ecol-Evol Persp* 40(3). Doi: 10.1111/maec.12541.

Cuellar-Gempeler, C. and M. A. Leibold (2019). Key colonist pools and habitat filters mediate the composition of fiddler crab-associated bacterial communities. *Ecology* 100(4). Doi: 10.1002/ecy.2628.

Dahms, H.-U., N. V. Schizas, R. A. James, L. Wang and J.-S. Hwang (2018). Marine hydrothermal vents as templates for global change scenarios. *Hydrobiologia* 818(1), 1-10. Doi: 10.1007/s10750-018-3598-8.

Dahms, H. U., L. C. Tseng and J. S. Hwang (2017). Are vent crab behavioral preferences adaptations for habitat choice? *Plos One* 12(9). Doi: 10.1371/journal.pone.0182649.

Dana, R., T. L. Leto, H. L. Malech, and R. Levy (1998). Essential requirement of cytosolic phospholipase A2 for activation of the phagocyte NADPH oxidase. *J Biol Chem* 273(1), 441-445. Doi: 10.1074/jbc.273.1.441.

Dando, P. R., J. A. Hughes, Y. Leahy, L. J. Taylor and S. Zivanovic (1995). Earthquakes increase hydrothermal venting and nutrient inputs into the Aegean. *Cont Shelf Res* 15(6), 655-662. Doi: Doi 10.1016/0278-4343(94)E0031-G.

Deane, E. E., S. P. Kelly, J. C. Luk, and N. Y. Woo (2002). Chronic salinity adaptation modulates hepatic heat shock protein and insulin-like growth factor I expression in black sea bream. *Mar Biotechnol* 4, 193-205. Doi: 10.1007/s1012602-0091-5.

Deffontaines, B., K. J. Chang, P. C. Huang, H. H. Hsu, S. K. Hsu, C. S. Liu, C. T. Lee, S. Magalhaes and G. Fortunato (2022). Neotectonics of the volcanic Kuei-Shan

doi:10.6342/NTU202500809

Tao island, and geodynamic implications (NE Taiwan-SW Okinawa Trough). *Tectonophysics* 832. Doi: 10.1016/j.tecto.2022.229362.

Dickson, A. G. and F. J. Millero (1987). A comparison of the equilibrium-constants for the dissociation of carbonic-acid in Sseawater media. *Deep-Sea Res I: Oceanogr Res Pap* 34(10), 1733-1743. Doi: 10.1016/0198-0149(87)90021-5.

Dick, G. J. (2019). The microbiomes of deep-sea hydrothermal vents: distributed globally, shaped locally. *Nat Rev Microbiol* 17(5), 271-283. Doi: 10.1038/s41579-019-0160-2.

Dixon, P. (2003). VEGAN: A package of R functions for community ecology. *J Veg Sci* 14(6), 927-930. Doi: 10.1658/1100-9233(2003)014[0927:VAPORF]2.0.CO;2.

Doering, T., K. Tandon, S. H. Topa, S. J. Pidot, L. L. Blackall, and M. J. van Oppen. (2023). Genomic exploration of coral-associated bacteria: identifying probiotic candidates to increase coral bleaching resilience in *Galaxea fascicularis*. *Microbiome*, 11(1), 185. Doi: 10.1186/s40168-023-01622-x.

Dray, S., and A. B. Dufour (2007). The ade4 package: Implementing the duality diagram for ecologists. *J Stat Softw* 22, 1-20. Doi: 10.18637/jss.v022.i04.

Duarte, C. M., L. Chapuis, S. P. Collin, D. P. Costa, R. P. Devassy, V. M. Eguiluz, C. Erbe, T. A. C. Gordon, B. S. Halpern, H. R. Harding, M. N. Havlik, M. Meekan, N. D. Merchant, J. L. Miksis-Olds, M. Parsons, M. Predragovic, A. N. Radford, C. A. Radford, S. D. Simpson, H. Slabbekoorn, E. Staaterman, I. C. Van Opzeeland, J. Winderen, X. L. Zhang and F. Juanes (2021). The soundscape of the anthropocene ocean. *Science* 371(6529), eaba4658. Doi: 0.1126/science.aba4658.

Duperron, S., A. Quiles, K. M. Szafranski, N. Léger and B. Shillito (2016). Estimating symbiont abundances and gill surface areas in specimens of the hydrothermal vent mussel *Bathymodiolus puteoserpentis* maintained in pressure vessels. *Front Mar Sci* 3, 16. Doi: 10.3389/fmars.2016.00016.

Dworkin, J. (2018). Detection of fungal and bacterial carbohydrates: Do the similar structures of chitin and peptidoglycan play a role in immune dysfunction?. *PLoS Pathog* 14(10), e1007271. Doi: 10.1371/journal.ppat.1007271.

Elderfield, H. and A. Schultz (1996). Mid-ocean ridge hydrothermal fluxes and the chemical composition of the ocean. *Annu Rev Earth Pl Sc* 24, 191-224. Doi: 10.1146/annurev.earth.24.1.191.

doi:10.6342/NTU202500809

Erfanian, M., A. J. Mitchell, J. Kang and F. Aletta (2019). The psychophysiological implications of soundscape: a systematic review of empirical literature and a research agenda. *Int J Env Res Pub He* 16(19), 3533. Doi: 10.3390/ijerph16193533.

Evans, D. H., P. M. Piermarini and K. P. Choe (2005). The multifunctional fish gill: Dominant site of gas exchange, osmoregulation, acid-base regulation, and excretion of nitrogenous waste. *Physiol Rev* 85(1), 97-177. Doi: 10.1152/physrev.00050.2003.

Falkowski, P. G., T. Fenchel, and E. F. Delong (2008). The microbial engines that drive Earth's biogeochemical cycles. *Science* 320(5879), 1034-1039. Doi: 10.1126/science.1153213

Felbeck, H. and G. N. Somero (1982). Primary production in deep-sea hydrothermal vent organisms: Roles of sulfide-oxidizing bacteria. *Trends Biochem Sci* 7(6), 201-204. Doi: 10.1016/0968-0004(82)90088-3.

Feder, M. E., and G. E. Hofmann (1999). Heat-shock proteins, molecular chaperones, and the stress response: evolutionary and ecological physiology. *Annu Rev Physiol* 61(1), 243-282. Doi: 10.1146/annurev.physiol.61.1.243.

Feder, M. E., T. L. Karr, W. Yang, J. M. Hoekstra, and A. C. James (1999). Interaction of Drosophila and its endosymbiont Wolbachia: natural heat shock and the overcoming of sexual incompatibility. *Am Zool* 39(2), 363-373. Doi: 10.1093/icb/39.2.363.

Fialamedioni, A., C. Metivier, A. Herry and M. Lepennec (1986). Ultrastructure of the gill of the hydrothermal-Vent mytilid Bathymodiolus Sp. *Mar Biol* 92(1), 65-72. Doi: 10.1007/Bf00392747.

Fisher, C. R., K. Takai and N. Le Bris (2007). Hydrothermal Vent Ecosystems. *Oceanography* 20(1), 14-23. Doi: 10.5670/oceanog.2007.75.

Fornari, D. J., T. Shank, K. L. Von Damm, T. K. P. Gregg, M. Lilley, G. Levai, A. Bray, R. M. Haymon, M. R. Perfit and R. Lutz (1998). Time-series temperature measurements at high-temperature hydrothermal vents, East Pacific Rise 9°49′–51′N: evidence for monitoring a crustal cracking event. *Earth Planet Sc Lett* 160(3-4), 419-431. Doi: 10.1016/S0012-821x(98)00101-0.

Fortunato, C. S., B. Larson, D. A. Butterfield, and J. A. Huber (2018). Spatially distinct, temporally stable microbial populations mediate biogeochemical cycling at and

doi:10.6342/NTU202500809

below the seafloor in hydrothermal vent fluids. *Environ Microbiol* 20(2), 769-784. Doi: 10.1111/1462-2920.14011.

François-Étienne, S., L. Nicolas, N. Eric, C. Jaqueline, P. L. Pierre-Luc, B. Sidki, H. Aleicia, B. Danilo, V. A. Luis, and D. Nicolas (2023). Important role of endogenous microbial symbionts of fish gills in the challenging but highly biodiverse Amazonian blackwaters. *Nat Commun* 14(1), 3903. Doi: 10.1038/s41467-023-39461-x.

Freitas, E. T. F., A. M. S. Moreira, R. S. de Paula, G. R. Andrade, M. D. de Carvalho, P. S. Assis, E. C. Jorge, and A. V. Cardoso (2022). Ultrastructure of the gill ciliary epithelium of Limnoperna fortunei (Dunker 1857), the invasive golden mussel. *BMC Zool* 7(1), 6. Doi: 10.1186/s40850-022-00107-y.

Fukunaga, Y., M. Kurahashi, K. Tanaka, K. Yanagi, A. Yokota and S. Harayama (2006). *Pseudovibrio ascidiaceicola* sp. nov., isolated from ascidians (sea squirts). *Int J Syst Evol Micr* 56(2), 343-347. Doi: 10.1099/00207713-56-4-923.

Fujita, Y., H. Matsuoka, and K. Hirooka (2007). Regulation of fatty acid metabolism in bacteria. *Mol Microbiol* 66(4), 829-839. Doi: 10.1111/j.1365-2958.2007.05947.x.

Galand, P. E., O. Pereira, C. Hochart, J. C. Auguet, and D. Debroas (2018). A strong link between marine microbial community composition and function challenges the idea of functional redundancy. *ISME J* 12(10), 2470-2478. Doi: 10.1038/s41396-018-0158-1.

Garg, N. (2021). Metabolomics in functional interrogation of individual holobiont members. *mSystems, 6*(4), 10-1128. Doi: 10.1128/msystems.00841-21.

Giovannelli, D., G. d'Errico, E. Manini, M. Yakimov and C. Vetriani (2013). Diversity and phylogenetic analyses of bacteria from a shallow-water hydrothermal vent in Milos island (Greece). *Front Microbiol* 4, 184. Doi: 10.3389/fmicb.2013.00184.

Girija, G. K., L. C. Tseng, P. Muthu, Y. L. Chen, Y. N. Ho, and J. S. Hwang. (2024). Microbiome flexibility enhances the resilience of the potentially invasive coral *Tubastraea aurea* to abrupt environmental changes: Insights from a shallow water hydrothermal vent transplantation study. *Sci Total Environ*, 954, 176792. Doi: 10.1016/j.scitotenv.2024.176792.

Glowka, L. (2003). Putting marine scientific research on a sustainable footing at hydrothermal vents. *Marine Policy* 27(4), 303-312. Doi: 10.1016/S0308597x(03)00042-3.

doi:10.6342/NTU202500809

Goffredi, S. K. and J. P. Barry (2002). Species-specific variation in sulfide physiology between closely related Vesicomyid clams. *Mar Ecol Prog Ser* 225, 227-238. Doi: 10.3354/meps225227.

Goffredi, S. K., W. J. Jones, H. Erhlich, A. Springer and R. C. Vrijenhoek (2008). Epibiotic bacteria associated with the recently discovered Yeti crab, Kiwa hirsuta. *Environ Microbiol* 10(10), 2623-2634. Doi: 10.1111/j.1462-2920.2008.01684.x.

Goffredi, S. K. (2010). Indigenous ectosymbiotic bacteria associated with diverse hydrothermal vent invertebrates. *Env Microbiol Rep* 2(4), 479-488. Doi: 10.1111/j.1758-2229.2010.00136.x.

Gonzalez, F. J., B. Rincon-Tomas, L. Somoza, E. Santofimia, T. Medialdea, P. Madureira, E. Lopez-Pamo, J. R. Hein, E. Marino, C. de Ignacio, J. Reyes, M. Hoppert and J. Reitner (2020). Low-temperature, shallow-water hydrothermal vent mineralization following the recent submarine eruption of Tagoro volcano (El Hierro, Canary Islands). *Mar Geol* 430. Doi: 10.1016/j.margeo.2020.106333.

Gorjão, R., A. K. Azevedo-Martins, H. G. Rodrigues, F. Abdulkader, M. Arcisio-Miranda, J. Procopio, and R. Curi (2009). Comparative effects of DHA and EPA on cell function. *Pharmacol Ther* 122(1), 56-64. Doi:10.1016/j.pharmthera.2009.01.004.

Grabovich, M. Y., M. S. Muntyan, V. Y. Lebedeva, V. S. Ustiyan and G. A. Dubinina (1999). Lithoheterotrophic growth and electron transfer chain components of the filamentous gliding bacterium *Leucothrix mucor* DSM 2157 during oxidation of sulfur compounds. *Fems Microbiol Lett* 178(1), 155-161. Doi: 10.1111/j.15746968.1999.tb13772.x.

Hahnke, R. L. and J. Harder (2013). Phylogenetic diversity of *Flavobacteria* isolated from the North Sea on solid media. *Syst Appl Microbiol* 36(7), 497-504. Doi: 10.1016/j.syapm.2013.06.006.

Halary, S., V. Riou, F. Gaill, T. Boudier and S. Duperron (2008). 3D FISH for the quantification of methane- and sulphur-oxidizing endosymbionts in bacteriocytes of the hydrothermal vent mussel *Bathymodiolus azoricus*. *ISME J* 2(3), 284-292. Doi: 10.1038/ismej.2008.3.

Hamer, B., D. P. Hamer, W. E. G. Müller, and R. Batel (2004). Stress-70 proteins in marine mussel Mytilus galloprovincialis as biomarkers of environmental pollution: a field study. *Environ Int* 30(7), 873-882. Doi: 10.1016/j.envint.2004.02.008.

doi:10.6342/NTU202500809

Han, C. H., Y. Ye, Y. W. Pan, H. W. Qin, G. H. Wu and C. T. A. Chen (2014). Spatial distribution pattern of seafloor hydrothermal vents to the southeastern Kueishan Tao offshore Taiwan Island. *Acta Oceanologica Sinica* 33(4), 37-44. Doi: 10.1007/s13131014-0405-x.

Han, J. R., M. Q. Ye, C. Wang, and Z. J. Du. (2019). *Halioglobus sediminis* sp. nov., isolated from coastal sediment. *Int J Syst Evol Microbiol*, 69(6), 1601-1605. Doi: 10.1099/ijsem.0.003366.

Hanna, D., R. Kumar and R. Banerjee (2023). A metabolic paradigm for hydrogen sulfide signaling electron transport chain plasticity. *Antioxid Redox Sign* 38(1-3), 57-67. Doi: 10.1089/ars.2022.0067.

Hansen, A. W., and K. V. Venkatachalam (2023). Sulfur-Element containing metabolic pathways in human health and crosstalk with the microbiome. *Biochem Biophys Rep* 35, 101529. Doi: 10.1016/j.bbrep.2023.101529.

Havlik, M. N., M. Predragovic and C. M. Duarte (2022). State of play in marine soundscape assessments. *Front Mar Sci* 9. Doi: 10.3389/fmars.2022.919418.

Hayes, J. D., and L. I. McLellan (1999). Glutathione and glutathione-dependent enzymes represent a co-ordinately regulated defence against oxidative stress. *Free Radic Res* 31(4), 273-300. Doi: 10.1080/10715769900300851.

Heberle, H., G. V. Meirelles, F. R. da Silva, G. P. Telles, and R. Minghim (2015). InteractiVenn: a web-based tool for the analysis of sets through Venn diagrams. *BMC Bioinformatics* 16, 1-7. Doi: 10.1186/s12859-015-0611-3.

Hedderich, R., O. Klimmek, A. Kröger, R. Dirmeier, M. Keller and K. O. Stetter (1998). Anaerobic respiration with elemental sulfur and with disulfides. *FEMS Microbiol Rev* 22(5), 353-381. Doi: 10.1111/j.1574-6976.1998.tb00376.x.

Henry, R. P. and M. G. Wheatly (1992). Interaction of respiration, ion regulation, and acid-base balance in the everyday life of aquatic crustaceans. *Am Zool* 32(3), 407416. Doi: 10.1093/icb/32.3.407.

Hildebrandt, T. M. and M. K. Grieshaber (2008). Three enzymatic activities catalyze the oxidation of sulfide to thiosulfate in mammalian and invertebrate mitochondria. *FEBS J* 275(13), 3352-3361. Doi: 10.1111/j.1742-4658.2008.06482.x.

Ho, T. W., J. S. Hwang, M. K. Cheung, H. S. Kwan and C. K. Wong (2015). Dietary analysis on the shallow-water hydrothermal vent crab *Xenograpsus testudinatus* using Illumina sequencing. *Mar Biol* 162(9), 1787-1798. Doi: 10.1007/s00227-015-2711-z.

doi:10.6342/NTU202500809

Hoek, T. A., K. Axelrod, T. Biancalani, E. A. Yurtsev, J. Liu and J. Gore (2016). Resource availability modulates the cooperative and competitive nature of a microbial cross-feeding mutualism. PLoS Biol 14(8), e1002540. Doi: 10.1371/journal.pbio.1002540.

Howe, B. M., J. Miksis-Olds, E. Rehm, H. Sagen, P. F. Worcester and G. Haralabus (2019). Observing the oceans acoustically. *Front Mar Sci* 6, 426. Doi: 10.3389/fmars.2019.00426.

Hu, M. Y., Y. J. Guh, Y. T. Shao, P. L. Kuan, G. L. Chen, J. R. Lee, M. S. Jeng and Y. C. Tseng (2016). Strong ion regulatory abilities enable the crab *Xenograpsus testudinatus* to inhabit highly acidified marine vent systems. *Frontiers in Physiology* 7. Doi: 10.3389/fphys.2016.00014.

Hu, M. Y. A., W. Hagen, M. S. Jeng and R. Saborowski (2012). Metabolic energy demand and food utilization of the hydrothermal vent crab *Xenograpsus testudinatus* (Crustacea: Brachyura). *Aquat Biol* 15(1), 11-25. Doi: 10.3354/ab00396.

Huang, S., Z. Zheng, Q. Wei, I. Han, and P. R. Jaffé (2019). Performance of sulfur-based autotrophic denitrification and denitrifiers for wastewater treatment under acidic conditions. *Bioresour Technol* 294, 122176. Doi: 10.1016/j.biortech.2019.122176.

Inagaki, F., K. Takai, K. H. Nealson and K. Horikoshi (2004). *Sulfurovum lithotrophicum* gen. nov., sp nov., a novel sulfur-oxidizing chemolithoautotroph within the epsilon-Proteobacteria isolated from Okinawa Trough hydrothermal sediments. *Int J Syst Evol Micr* 54, 1477-1482. Doi: 10.1099/ijs.0.03042-0.

James, A. K., L. W. Kelly, C. E. Nelson, E. G. Wilbanks, and C. A. Carlson (2019). Elevated pCO_2 alters marine heterotrophic bacterial community composition and metabolic potential in response to a pulse of phytoplankton organic matter. *Environ Microbiol* 21(2), 541-556. Doi: 10.1111/1462-2920.14484.

Jebara, F., C. Weiss, and A. Azem (2017). Hsp60 and Hsp70 chaperones: guardians of mitochondrial proteostasis. *eLS* 1-9. Doi: 10.1002/9780470015902.a0027152.

Jeng, M. S., N. K. Ng and P. K. L. Ng (2004). Feeding behaviour: Hydrothermal vent crabs feast on sea 'snow'. *Nature* 432(7020), 969-969. Doi: 10.1038/432969a.

Jiang, Y., W. Wang, Q. Xie, N. A. Liu, L. Liu, D. Wang, X. Zhang, C. Yang, X. Chen, D. Tang, and E. Wang (2017). Plants transfer lipids to sustain colonization by mutualistic mycorrhizal and parasitic fungi. *Science* 356(6343), 1172-1175.

doi:10.6342/NTU202500809

Doi: 10.1126/science.aam9970.

Johnson, H. P., M. Hutnak, R. P. Dziak, C. G. Fox, I. Urcuyo, J. P. Cowen, J. Nabelek and C. Fisher (2000). Earthquake-induced changes in a hydrothermal system on the Juan de Fuca mid-ocean ridge. *Nature* 407(6801), 174-177. Doi: 10.1038/35025040.

Johnson, P. W., A. Sastry, J. M. Sieburth, C. R. Arnold and M. S. Doty (1971). *Leucothrix mucor* infestation of benthic crustacea, fish eggs, and tropical algae. *Limnol Oceanogr* 16(6), 962-969. Doi: 10.4319/lo.1971.16.6.0962.

Jouin, C. and F. Gaill (1990). Gills of hydrothermal vent annelids: structure, ultrastructure and functional implications in 2 alvinellid species. *Progress in Oceanography* 24(1-4), 59-69. Doi: 10.1016/0079-6611(90)90019-X.

Jurenka, R. A., M. de Renobales, and G. J. Blomquist (1987). De novo biosynthesis of polyunsaturated fatty acids in the cockroach Periplaneta americana. *Arch Biochem Biophys* 255(1), 184-193. Doi: 10.1016/0003-9861(87)90309-2.

Kadko, D., J. Baross, and J. Alt (1995). The magnitude and global implications of hydrothermal flux. *Geophys Monogr Am Geophys Union* 91, 446-446.

Kappelmann, L., K. Krüger, J. H. Hehemann, J. Harder, S. Markert, F. Unfried, D. Becher, N. Shapiro, T. Schweder, R. I. Amann and H. Teeling (2019). Polysaccharide utilization loci of North Sea Flavobacteriia as basis for using SusC/D-protein expression for predicting major phytoplankton glycans. *ISME J* 13(1), 76-91. Doi: 10.1038/s41396018-0242-6.

Kalanetra, K. M., S. L. Huston, and D. C. Nelson. (2004). Novel, attached, sulfur-oxidizing bacteria at shallow hydrothermal vents possess vacuoles not involved in respiratory nitrate accumulation. *Appl Environ Microbiol* 70(12), 7487-7496. Doi: 10.1128/AEM.70.12.7487-7496.2004.

Kasaya, T., H. Machiyama, K. Kitada and K. Nakamura (2015). Trial exploration for hydrothermal activity using acoustic measurements at the North Iheya Knoll. *Geochem J* 49(6), 597-602. Doi: 10.2343/geochemj.2.0389.

Katunuma, N., M. Okada, and Y. Nishii (1966). Regulation of the urea cycle and TCA cycle by ammonia. *Adv Enzyme Regul* 4, 317-335. Doi: 10.1016/0065-2571(66)90025-2.

Ke, Z., H. Huang, D. Chen, and Y. Tan (2024). Trophic relationship between mussels and scale worms under various seepage intensities in the haima cold seep:

doi:10.6342/NTU202500809

Insights from stable isotopes (δ13C and δ15N) and C: N: P stoichiometry. *Deep Sea Res Part I: Oceanogr Res Pap* 206, 104264. Doi: 10.1016/j.dsr.2024.104264.

Khurana, T., B. Khurana, and A. A. Noegel (2002). LIM proteins: association with the actin cytoskeleton. *Protoplasma* 219, 1-12. Doi: 10.1007/s007090200000.

Kleiner, M., X. Dong, T. Hinzke, J. Wippler, E. Thorson, B. Mayer, and M. Strous (2018). Metaproteomics method to determine carbon sources and assimilation pathways of species in microbial communities. *Proc Natl Acad Sci USA* 115(24), E5576-E5584. Doi: 10.1073/pnas.1722325115.

Kohl, J. B., A. T. Mellis, and G. Schwarz (2019). Homeostatic impact of sulfite and hydrogen sulfide on cysteine catabolism. *Br J Pharmacol* 176(4), 554-570. Doi: 10.1111/bph.14464.

Koito, T., S. Saitou, T. Nagasaki, S. Yamagami, T. Yamanaka, K. Okamura, and K. Inoue (2018). Taurine-related compounds and other free amino acids in deep-sea hydrothermal vent and non-vent invertebrates. Mar Biol 165, 1-6. Doi: 10.1007/s00227-018-3442-8.

Konstantinou, K. I., C. Y. Pan and C. H. Lin (2013). Microearthquake activity around Kueishantao island, offshore northeastern Taiwan: Insights into the volcano-tectonic interactions at the tip of the southern Okinawa Trough. *Tectonophysics* 593, 20-32. Doi: 10.1016/j.tecto.2013.02.019.

Kröger, A., S. Biel, J. Simon, R. Gross, G. Unden and C. R. D. Lancaster (2002). Fumarate respiration of *Wolinella succinogenes*: Enzymology, energetics and coupling mechanism. *Biochim Biophys Acta* 1553(1-2), 23-38. Doi: 10.1016/S00052728(01)00234-1.

Krüger, A., C. Schäfers, C. Schröder, and G. Antranikian (2018). Towards a sustainable biobased industry–highlighting the impact of extremophiles. *New Biotechnol* 40, 144-153. Doi: 10.1016/j.nbt.2017.05.002.

Krafft, T., R. Gross and A. Kroger (1995). The function of *Wolinella succinogenes psr* genes in electron transport with polysulfide as the terminal electron acceptor. *Eur J Biochem* 230(2), 601-606. Doi: 10.1111/j.1432-1033.1995.0601h.x.

Kurniawan, J., K. Suga, and T. L. Kuhl (2017). Interaction forces and membrane charge tunability: Oleic acid containing membranes in different pH conditions. *Biochim Biophys Acta Biomembr* 1859(2), 211-217. Doi: 10.1016/j.bbamem.2016.11.001.

doi:10.6342/NTU202500809

Lai, K. P., P. Zhu, D. A. T. Boncan, L. Yang, C. C. T. Leung, J. C. H. Ho, X. Lin, T. F. Chan, R. Y. C. Kong, and W. K. F. Tse (2022). Integrated omics approaches revealed the osmotic stress-responsive genes and microbiota in gill of marine medaka. *mSystems* 7(2), e00047-22. Doi: 10.1128/msystems.00047-22.

Langille, M. G., J. Zaneveld, J. G. Caporaso, D. McDonald, D. Knights, J. A. Reyes, J. C. Clemente, D. E. Burkepile, R. L. Vega Thurber, R. Knight, and R. G. Beiko (2013). Predictive functional profiling of microbial communities using 16S rRNA marker gene sequences. *Nat Biotechnol* 31(9), 814-821. Doi: 10.1038/nbt.2676.

Lebrato, M., Y. V. Wang, L. C. Tseng, E. P. Achterberg, X. G. Chen, J. C. Molinero, K. Bremer, U. Westernstroer, E. Soding, H. U. Dahms, M. Kuter, V. Heinath, J. Johnck, K. I. Konstantinou, Y. J. Yang, J. S. Hwang and D. Garbe-Schonberg (2019). Earthquake and typhoon trigger unprecedented transient shifts in shallow hydrothermal vents biogeochemistry. *Sci Rep-Uk* 9. Doi: 10.1038/s41598-019-53314-y.

Lee, J. M., H. Lee, S. Kang, and W. J. Park (2016). Fatty acid desaturases, polyunsaturated fatty acid regulation, and biotechnological advances. *Nutrients* 8(1), 23. Doi: 10.3390/nu8010023.

Leek, J. T., W. E. Johnson, H. S. Parker, A. E. Jaffe, and J. D. Storey (2012). The *sva* package for removing batch effects and other unwanted variation in high-throughput experiments. *Bioinformatics* 28(6), 882-883. Doi: 10.1093/bioinformatics/bts034.

Leinberger, J., F. Milke, M. Christodoulou, A. Poehlein, J. Caraveo-Patiño, A. Teske and T. Brinkhoff (2022). Microbial epibiotic community of the deep-sea galatheid squat lobster *Munidopsis alvisca*. *Sci Rep-Uk* 12(1), 2675. Doi: 10.1038/s41598-022-06666x.

Levin, L. A., A. R. Baco, D. A. Bowden, A. Colaco, E. E. Cordes, M. R. Cunha, A. W. Demopoulos, J. Gobin, B. M. Grupe, J. Le, and A. Metaxas (2016). Hydrothermal vents and methane seeps: rethinking the sphere of influence. *Front Mar Sci* 3, 72. Doi: 10.3389/fmars.2016.00072

Liang, W. D., T. Y. Tang, Y. J. Yang, M. T. Ko and W. S. Chuang (2003). Upper-ocean currents around Taiwan. *Deep Sea Res Part II Top Stud Oceanogr* 50(6-7), 1085-1105. Doi: 10.1016/S0967-0645(03)00011-0.

doi:10.6342/NTU202500809

Libiad, M., P. K. Yadav, V. Vitvitsky, M. Martinov, and R. Banerjee (2014). Organization of the human mitochondrial hydrogen sulfide oxidation pathway. *J Biol Chem* 289(45), 30901-30910.

Libiad, M., V. Vitvitsky, T. Bostelaar, D. W. Bak, H. J. Lee, N. Sakamoto, E. Fearon, C. A. Lyssiotis, E. Weerapana and R. Banerjee (2019). Hydrogen sulfide perturbs mitochondrial bioenergetics and triggers metabolic reprogramming in colon cells. *J Biol Chem* 294(32), 12077-12090. Doi: 10.1074/jbc.RA119.009442.

Lilley, M. D., D. A. Butterfield, J. E. Lupton and E. J. Olson (2003). Magmatic events can produce rapid changes in hydrothermal vent chemistry. *Nature* 422(6934), 878-881. Doi: 10.1038/nature01569.

Lin, T. H., T. Akamatsu, F. Sinniger and S. Harii (2021). Exploring coral reef biodiversity via underwater soundscapes. *Biol Conserv* 253. Doi: 10.1016/j.biocon.2020.108901.

Lin, T. H., C. Chen, H. K. Watanabe, S. Kawagucci, H. Yamamoto and T. Akamatsu (2019). Using soundscapes to assess deep-sea benthic ecosystems. *Trends Ecol Evol* 34(12), 1066-1069. Doi: 10.1016/j.tree.2019.09.006.

Little, C. T. and R. C. Vrijenhoek (2003). Are hydrothermal vent animals living fossils? *Trends Ecol Evol* 18(11), 582-588. Doi: 10.1016/j.tree.2003.08.009.

Liu, X., L. Jiang, Q. Hu, J. Lyu, and Z. Shao (2020). *Thiomicrorhabdus indica* sp. nov., an obligately chemolithoautotrophic, sulfur-oxidizing bacterium isolated from a deep-sea hydrothermal vent environment. *Int J Syst Evol Micr* 70(1), 234-239. Doi: 10.1099/ijsem.0.003744.

Lonsdale, P. (1977). Structural geomorphology of a fast-spreading rise crest: the East Pacific Rise near 3° 25′S. *Mar Geophys Res* 3(3), 251-293. Doi: 10.1007/BF00285656.

Louca, S., L. W. Parfrey, and M. Doebeli (2016). Decoupling function and taxonomy in the global ocean microbiome. *Science* 353(6305), 1272-1277. Doi: 10.1126/science.aaf4507.

Louca, S., M. F. Polz, F. Mazel, M. B. Albright, J. A. Huber, M. I. O'Connor, M. Ackermann, A. S. Hahn, D. S. Srivastava, S. A. Crowe, and M. Doebeli (2018). Function and functional redundancy in microbial systems. *Nat Ecol Evol* 2(6), 936-943. Doi: 10.1038/s41559-018-0519-1.

Lough, A. J. M., D. P. Connelly, W. B. Homoky, J. A. Hawkes, V. Chavagnac, A. Castillo, M. Kazemian, K. Nakamura, T. Araki, B. Kaulich and R. A. Mills

doi:10.6342/NTU202500809

(2019). Diffuse hydrothermal venting: A hidden source of iron to the oceans. *Front Mar Sci* 6, 329. Doi: 10.3389/fmars.2019.00329.

Love, M. I., W. Huber, and S. Anders (2014). Moderated estimation of fold change and dispersion for RNA-seq data with DESeq2. *Genome Biol* 15, 550. Doi: 10.1186/s13059-014-0550-8.

Macy, J. M., I. Schroder, R. K. Thauer and A. Kroger (1986). Growth the *Wolinella succinogenes* on H_2S plus fumarate and on formate plus sulfur as energy sources. *Arch Microbiol* 144(2), 147-150. Doi: 10.1007/Bf00414725.

Mantha, G., A. K. Awasthi, A. M. Al-Aidaroos and J. S. Hwang (2013). Diversity and abnormalities of cyclopoid copepods around hydrothermal vent fluids, Kueishantao Island, north-eastern Taiwan. *J Nat Hist* 47(5-12), 685-697. Doi: 10.1080/00222933.2012.747638.

Martens-Habbena, W., P. M. Berube, H. Urakawa, J. R. de La Torre, and D. A. Stahl (2009). Ammonia oxidation kinetics determine niche separation of nitrifying Archaea and Bacteria. *Nature* 461(7266), 976-979. Doi: 10.1038/nature08465.

Martín-Díaz, J. P., A. González-Vega, T. Barreyre, B. Cornide, J. M. Arrieta, J. T. Vázquez, D. Palomino, J. A. L. Rodríguez, J. Escánez-Pérez, C. Presas-Navarro, and E. Fraile-Nuez (2024). Unveiling the inherent physical-chemical dynamics: Direct measurements of hydrothermal fluid flow, heat, and nutrient outflow at the Tagoro submarine volcano (Canary Islands, Spain). *Sci Total Environ* 918, 170565. Doi: 10.1016/j.scitotenv.2024.170565.

Marty, L., W. Siala, M. Schwarzländer, M. D. Fricker, M. Wirtz, L. J. Sweetlove, Y. Meyer, A. J. Meyer, J. P. Reichheld, and R. Hell (2009). The NADPH-dependent thioredoxin system constitutes a functional backup for cytosolic glutathione reductase in Arabidopsis. Proc Natl Acad Sci U S A 106(22), 9109-9114. Doi: 10.1073/pnas.0900206106.

Matabos, M., T. Barreyre, S. K. Juniper, M. Cannat, D. Kelley, J. M. Alfaro-Lucas, V. Chavagnac, A. Colaço, J. Escartin, E. Escobar, and D. Fornari (2022). Integrating multidisciplinary observations in vent environments (IMOVE): decadal progress in deep-sea observatories at hydrothermal vents. *Front Mar Sci* 9, 866422. Doi: 10.3389/fmars.2022.866422.

Maugeri, T. L., V. Lentini, C. Gugliandolo, F. Italiano, S. Cousin and E. Stackebrandt (2009). Bacterial and archaeal populations at two shallow hydrothermal vents off Panarea Island (Eolian Islands, Italy). *Extremophiles* 13(1), 199-212.

doi:10.6342/NTU202500809

Doi: 10.1007/s00792-0080210-6.

McCollom, T. M. and E. L. Shock (1998). Fluid-rock interactions in the lower oceanic crust: Thermodynamic models of hydrothermal alteration. *J Geophys Res Solid Earth* 103(B1), 547-575.

McCutcheon, J. P., and N. A. Moran (2007). Parallel genomic evolution and metabolic interdependence in an ancient symbiosis. *Proc Natl Acad Sci USA* 104(49), 19392-19397. Doi: 10.1073/pnas.0708855104.

McDermott, J. M., S. P. Sylva, S. Ono, C. R. German and J. S. Seewald (2020). Abiotic redox reactions in hydrothermal mixing zones: Decreased energy availability for the subsurface biosphere. *P Natl Acad Sci USA* 117(34), 20453-20461. Doi: 10.1073/pnas.2003108117.

McGonigle, J. M., S. Q. Lang, and W. J. Brazelton (2020). Genomic evidence for formate metabolism by Chloroflexi as the key to unlocking deep carbon in Lost City microbial ecosystems. *Appl Environ Microbiol* 86(8), e02583-19. Doi: 10.1128/AEM.02583-19.

McInnes, L., J. Healy and J. Melville (2018). Umap: Uniform manifold approximation and projection for dimension. *arXiv preprint arXiv*, 1802.03426. Doi: 10.48550/arXiv.1802.03426.

McKenna, M. F., S. Baumann-Pickering, A. C. M. Kok, W. K. Oestreich, J. D. Adams, J. Barkowski, K. M. Fristrup, J. A. Goldbogen, J. Joseph, E. B. Kim, A. Kugler, M. O. Lammers, T. Margolina, L. E. P. Reeves, T. J. Rowell, J. A. Stanley, A. K. Stimpert, E. J. Zang, B. L. Southall, C. C. Wall, S. Van Parijs and L. T. Hatch (2021). Advancing the Interpretation of Shallow Water Marine Soundscapes. *Front Mar Sci* 8, 719258. Doi: 10.3389/fmars.2021.719258.

Mehrbach, C., C. H. Culberson, J. E. Hawley and R. M. Pytkowicx (1973). Measurement of the apparent dissociation constants of carbonic acid in seawater at atmospheric pressure. *Limnol Oceanogr* 18(6), 897-907. Doi: 10.4319/lo.1973.18.6.0897.

Miller, S. L. (1953). A production of amino acids under possible primitive earth conditions. *Science*, 117(3046), 528-529. Doi: 10.1126/science.117.3046.52.

Miller, S. L. and Urey, H. C. (1959). Organic compound synthesis on the primitive Earth: Several questions about the origin of life have been answered, but much remains to be studied. *Science*, 130(3370), 245-251. Doi: 10.1126/science.130.3370.24.

doi:10.6342/NTU202500809

Minello, M., L. Calado and F. C. Xavier (2021). Ecoacoustic indices in marine ecosystems: a review on recent developments, challenges, and future directions. *Ices J Mar Sci* 78(9), 3066-3074. Doi: 10.1093/icesjms/fsab193.

Moi, I. M., A. T. C. Leow, M. S. M. Ali, R. N. Z. R. A. Rahman, A. B. Salleh, and S. Sabri (2018). Polyunsaturated fatty acids in marine bacteria and strategies to enhance their production. *Appl Microbiol Biotechnol* 102, 5811-5826. Doi: 10.1007/s00253-018-9063-9.

Moran, M. A., R. Belas, M. A. Schell, J. M. González, F. Sun, S. Sun, B. J. Binder, J. Edmonds, W. Ye, B. Orcutt, E. C. Howard, C. Meile, W. Palefsky, A. Goesmann, Q. Ren, I. Paulsen, L. E. Ulrich, L. S. Thompson, E. Saunders and A. Buchan (2007). Ecological genomics of marine *Roseobacters*. *Appl Environ Microbiol* 73(14), 4559-4569. Doi: 10.1128/Aem.02580-06.

Monroig, Ó., D. R. Tocher, and J. C. Navarro (2013). Biosynthesis of polyunsaturated fatty acids in marine invertebrates: recent advances in molecular mechanisms. *Mar Drugs* 11(10), 3998-4018. Doi: 10.3390/md11103998.

Morris Jr, S. M. (2002). Regulation of enzymes of the urea cycle and arginine metabolism. *Annu Rev Nutr* 22(1), 87-105. Doi: 10.1146/annurev.nutr.22.110801.140547.

Moyer, C. L., F. C. Dobbs, and D. M. Karl. (1995). Phylogenetic diversity of the bacterial community from a microbial mat at an active, hydrothermal vent system, Loihi Seamount, Hawaii. *Appl Environ Microbiol* 61(4), 1555-1562. Doi: 10.1128/aem.61.4.1555-1562.1995.

Nandhini, B., A. Ramesh, M. Monisha, and K. S. Krishna (2021). An overview of astrobiology and microbial survival in space. *Int J Innov Sci Res Technol (IJISRT)* 6(3), 21-28.

Nagasaki, T., Y. Hongo, T. Koito, I. Nakamura-Kusakabe, S. Shimamura, Y. Takaki, T. Yoshida, T. Maruyama and K. Inoue (2015). Cysteine dioxygenase and cysteine sulfinate decarboxylase genes of the deep-sea mussel *Bathymodiolus septemdierum*: possible involvement in hypotaurine synthesis and adaptation to hydrogen sulfide. *Amino Acids* 47(3), 571-578. Doi: 10.1007/s00726-014-1891-z.

Nakagawa, S., F. Inagaki, K. Takai, K. Horikoshi and Y. Sako (2005). *Thioreductor micantisoli* gen. nov., sp. nov., a novel mesophilic, sulfur-reducing chemolithoautotroph within the ε-Proteobacteria isolated from hydrothermal sediments in the Mid-Okinawa Trough. Int J Syst Evol Micr 55(2), 599-605.

doi:10.6342/NTU202500809

Doi: 10.1099/ijs.0.63351-0.

Nakagawa, S., Y. Takaki, S. Shimamura, A. L. Reysenbach, K. Takai and K. Horikoshi (2007). Deep-sea vent ε-proteobacterial genomes provide insights into emergence of pathogens. *P Natl Acad Sci USA* 104(29), 12146-12150. Doi: 10.1073/pnas.0700687104.

Nelson, D. C., K. D. Hagen and D. B. Edwards (1995). The gill symbiont of the hydrothermal vent mussel *Bathymodiolus Thermophilus* is a psychrophilic, chemoautotrophic, sulfur bacterium. *Mar Biol* 121(3), 487-495. Doi: 10.1007/Bf00349457.

Newsholme, P., J. Procopio, M. M. R. Lima, T. C. Pithon-Curi, and R. Curi (2003). Glutamine and glutamate—their central role in cell metabolism and function. *Cell Biochem Funct* 21(1), 1-9. Doi: 10.1002/cbf.1003.

Nikapitiya, C., W. S. Kim, K. Park, J. Kim, M. O. Lee, and I. S. Kwak (2015). Chitinase gene responses and tissue sensitivity in an intertidal mud crab (*Macrophthalmus japonicus*) following low or high salinity stress. *Cell Stress Chaperone* 20(3), 517-526. Doi: 10.1007/s12192-015-0576-1.

Nishihara, H., Y. Igarashi and T. Kodama (1991). *Hydrogenovibrio marinus* gen. nov., sp. nov., a marine obligately chemolithoautotrophic hydrogen-oxidizing bacterium. *Int J Syst Evol Micr* 41(1), 130-133. Doi: 10.1099/00207713-41-1-130.

Nishihara, H., Y. Miyashita, K. Aoyama, T. Kodama, Y. Igarashi and Y. Takamura (1997). Characterization of an extremely thermophilic and oxygen-stable membrane-bound hydrogenase from a marine hydrogen-oxidizing bacterium *Hydrogenovibrio marinus*. *Biochem Biophys Res Commun* 232(3), 766-770. Doi: 10.1006/bbrc.1997.6369.

Oda, A., H. K. Watanabe, S. Ohtsuka, S. Wada, Y. Kondo and H. Miyake (2022). Does t he Kuroshio Current transport planktonic larvae of the hydrothermal-vent crab *Xenograpsus* Takeda & Kurata, 1977 (Decapoda: Brachyura: Grapsoidea)? *J Crustacean Biol* 42(1). Doi: 10.1093/jcbiol/ruac016.

Oeschger, R. and R. D. Vetter (1992). Sulfide detoxification and tolerance in *Halicryptus Spinulosus* (Priapulida): a multiple strategy. *Mar Ecol Prog Ser* 86(2), 167-179. Doi: 10.3354/meps086167.

Olson, K. R. (2019). Hydrogen sulfide, reactive sulfur species and coping with reactive oxygen species. *Free Radic Biol Med*, 140, 74-83.

doi:10.6342/NTU202500809

Doi: 10.1016/j.freeradbiomed.2019.01.020.

Olson, K. R. (2021). A case for hydrogen sulfide metabolism as an oxygen sensing mechanism. *Antioxidants*, 10(11), 1650. Doi: 10.3390/antiox10111650.

Onuki, Y., M. Morishita, Y. Chiba, S. Tokiwa, and K. Takayama (2006). Docosahexaenoic acid and eicosapentaenoic acid induce changes in the physical properties of a lipid bilayer model membrane. *Chem Pharm Bull* 54(1), 68-71. Doi: 10.1248/cpb.54.68.

Papakonstanti, E. A., C. Stournaras (2008). Cell responses regulated by early reorganization of actin cytoskeleton. *FEBS Lett* 582(14), 2120-2127. Doi: 10.1016/j.febslet.2008.02.064.

Parsons, P. A. (2005). Environments and evolution: interactions between stress, resource inadequacy and energetic efficiency. *Biol Rev* 80(4), 589-610. Doi: 10.1017/S1464793105006822.

Park, S., S. Yoshizawa, K. Inomata, K. Kogure, and A. Yokota. (2012). *Halioglobus japonicus* gen. nov., sp. nov. and *Halioglobus pacificus* sp. nov., members of the class Gammaproteobacteria isolated from seawater. *Int J Syst Evol Microbiol*, 62(Pt_8), 1784-1789. Doi: 10.1099/ijs.0.031443-0.

Payne, M. S., M. R. Hall, L. Sly and D. G. Bourne (2007). Microbial diversity within earlystage cultured *Panulirus ornatus* phyllosomas. *Appl Environ Microbiol* 73(6), 19401951. Doi: 10.1128/Aem.02520-06.

Penesyan, A., J. Tebben, M. Lee, T. Thomas, S. Kjelleberg, T. Harder and S. Egan (2011). Identification of the antibacterial compound produced by the marine epiphytic bacterium *Pseudovibrio* sp. D323 and related sponge-associated bacteria. *Mar Drugs* 9(8), 1391-1402. Doi: 10.3390/md9081391.

Peng, S.-H., J.-J. Hung and J.-S. Hwang (2011). Bioaccumulation of trace metals in the submarine hydrothermal vent crab *Xenograpsus testudinatus* off Kueishan Island, Taiwan. *Mar Pollut Bull* 63(5-12), 396-401. Doi: 10.1016/j.marpolbul.2011.05.013.

Pérez-Pascual, D., A. Lunazzi, G. Magdelenat, Z. Rouy, A. Roulet, C. Lopez-Roques, R. Larocque, T. Barbeyron, A. Gobet, G. Michel, J. F. Bernardet and E. Duchaud (2017). The complete genome sequence of the fish pathogen *Tenacibaculum maritimum* provides insights into virulence mechanisms. *Front Microbiol* 8, 1542. Doi: 10.3389/fmicb.2017.01542.

Pérez-Barrancos, C., E. Fraile-Nuez, J. P. Martín-Díaz, A. González-Vega, J. Escánez-Pérez, M. I. Díaz-Durán, C. Presas-Navarro, M. Nieto-Cid, and J. M. Arrieta

doi:10.6342/NTU202500809

(2025). Shallow hydrothermal fluids shape microbial dynamics at the Tagoro Submarine Volcano (Canary Islands, Spain). *Environ Microbiol* 27(2), e70052. Doi: 10.1111/1462-2920.70052.

Perner, M., M. Hentscher, N. Rychlik, R. Seifert, H. Strauss and W. Bach (2011). Driving forces behind the biotope structures in two low-temperature hydrothermal venting sites on the southern Mid-Atlantic Ridge. *Env Microbiol Rep* 3(6), 727-737. Doi: 10.1111/j.1758-2229.2011.00291.x.

Petersen, J. M., A. Ramette, C. Lott, M. A. Cambon-Bonavita, M. Zbinden and N. Dubilier (2010). Dual symbiosis of the vent shrimp *Rimicaris exoculata* with filamentous gamma- and epsilonproteobacteria at four Mid-Atlantic Ridge hydrothermal vent fields. *Environ Microbiol* 12(8), 2204-2218. Doi: 10.1111/j.1462-2920.2009.02129.x.

Petersen, J. M., F. U. Zielinski, T. Pape, R. Seifert, C. Moraru, R. Amann, S. Hourdez, P. R. Girguis, S. D. Wankel, V. Barbe, E. Pelletier, D. Fink, C. Borowski, W. Bach and N. Dubilier (2011). Hydrogen is an energy source for hydrothermal vent symbioses. *Nature* 476(7359), 176-180. Doi: 10.1038/nature10325.

Phelan, V. V., W. T. Liu, K. Pogliano, and P. C. Dorrestein (2012). Microbial metabolic exchange—the chemotype-to-phenotype link. *Nat Chem Biol* 8(1), 26-35. Doi: 10.1038/nchembio.739.

Phleger, C. F., M. M. Nelson, A. K. Groce, S. C. Cary, K. Coyne, J. A. Gibson, and P. D. Nichols (2005). Lipid biomarkers of deep-sea hydrothermal vent polychaetes—*Alvinella pompejana*, *A. caudata*, *Paralvinella grasslei* and *Hesiolyra bergii*. *Deep Sea Res Part I: Oceanogr Res Pap* 52(12), 2333-2352. Doi: 10.1016/j.dsr.2005.08.001.

Pierrot, D., Lewis, E., and Wallace, D. W. R. (2006). MS Excel program developed for CO_2 system calculations. ORNL/CDIAC-105a., Carbon Dioxide Information Analysis Center, Oak Ridge National Laboratory, U.S. Department of Energy.

Pineda, M. C., X. Turon, and S. López-Legentil (2012). Stress levels over time in the introduced ascidian Styela plicata: the effects of temperature and salinity variations on hsp70 gene expression. *Cell Stress Chaperones* 17(4), 435-444. Doi: 10.1007/s12192-012-0321-y.

Pijanowski, B. C., L. J. Villanueva-Rivera, S. L. Dumyahn, A. Farina, B. L. Krause, B. M. Napoletano, S. H. Gage and N. Pieretti (2011). Soundscape ecology: the science of sound in the landscape. *Bioscience* 61(3), 203-216.

doi:10.6342/NTU202500809

Doi: 10.1525/bio.2011.61.3.6.

Ponsard, J., M. A. Cambon-Bonavita, M. Zbinden, G. Lepoint, A. Joassin, L. Corbari, B. Shillito, L. Durand, V. Cueff-Gauchard and P. Compere (2013). Inorganic carbon fixation by chemosynthetic ectosymbionts and nutritional transfers to the hydrothermal vent host-shrimp *Rimicaris exoculata*. *ISME Journal* 7(1), 96-109. Doi: 10.1038/ismej.2012.87.

Porchas-Cornejo, M. A., M. Martínez-Porchas, F. Vargas-Albores, T. Gollas-Galvan, L. R. Martínez-Córdova, R. Vazquez-Euan and E. Peña-Messina (2017). High-resolution detection of bacterial profile of ocean water, before and after being used by shrimp farms. *Aquacult Int* 25(5), 1833-1843. Doi: 10.1007/s10499-017-0160-z.

Price, R. E. and D. Giovannelli (2017). A review of the geochemistry and microbiology of marine shallow-water hydrothermal vents, 1-2. *In Reference Module in Earth Systems and Environmental Sciences*. ELSVIER.

Price, R. E., R. Lesniewski, K. S. Nitzsche, A. Meyerdierks, C. Saltikov, T. Pichler and J. P. Amend (2013). Archaeal and bacterial diversity in an arsenic-rich shallow-sea hydrothermal system undergoing phase separation. *Front Microbiol* 4, 158. Doi: 10.3389/fmicb.2013.00158.

Prodromou, C. (2016). Mechanisms of Hsp90 regulation. *Biochem J* 473(16), 2439-2452. Doi: 10.1042/BCJ20160005.

Putland, R. L., R. Constantine and C. A. Radford (2017). Exploring spatial and temporal trends in the soundscape of an ecologically significant embayment. *Sci Rep-Uk* 7(1), 5713. Doi: 10.1038/s41598-017-06347-0.

Rajasabapathy, R., C. Mohandass, R. Bettencourt, A. Colaço, J. Goulart and R. M. Meena (2018). Bacterial diversity at a shallow-water hydrothermal vent (Espalamaca) in Azores Island. *Curr Sci* 115(11), 2110-2121. Doi: 10.18520/cs/v115/i11/2110-2121

Rajasabapathy, R., C. Mohandass, A. Colaco, S. G. Dastager, R. S. Santos and R. M. Meena (2014). Culturable bacterial phylogeny from a shallow water hydrothermal vent of Espalamaca (Faial, Azores) reveals a variety of novel taxa. *Curr Sci* 106(1), 58-69.

Reveillaud, J., E. Reddington, J. McDermott, C. Algar, J. L. Meyer, S. Sylva, J. Seewald, C. R. German, and J. A. Huber (2016). Subseafloor microbial

doi:10.6342/NTU202500809

communities in hydrogen-rich vent fluids from hydrothermal systems along the Mid-Cayman Rise. *Environ Microbiol* 18(6), 1970-1987.
Doi: 10.1111/1462-2920.13173.

Revelle, W., and M. W. Revelle (2015). Package 'psych'. *Comprehensive R Archive Network 337*(338), 161-165.

Reysenbach, A. L., and E. Shock (2002). Merging genomes with geochemistry in hydrothermal ecosystems. *Science* 296(5570), 1077-1082.
Doi: 10.1126/science.107248.

Riley, M., J. T. Staley, A. Danchin, T. Z. Wang, T. S. Brettin, L. J. Hauser, M. L. Land and L. S. Thompson (2008). Genomics of an extreme psychrophile, *Psychromonas ingrahamii*. *BMC Genomics* 9(1), 1-19.
Doi: 10.1186/1471-2164-9-210.

Rocha, J., F. L. Garcia-Carreño, A. Muhlia-Almazán, A. B. Peregrino-Uriarte, G. Yépiz-Plascencia, and J. H. Córdova-Murueta (2012). Cuticular chitin synthase and chitinase mRNA of whiteleg shrimp Litopenaeus vannamei during the molting cycle. *Aquaculture* 330, 111-115. Doi: 10.1016/j.aquaculture.2011.12.024.

Romano, S. (2018). Ecology and biotechnological potential of bacteria belonging to the genus *Pseudovibrio*. *Appl Environ Microbiol* 84(8), e02516-02517.
Doi: 10.1128/AEM.02516-17.

Rypien, K. L., J. R. Ward and F. Azam (2010). Antagonistic interactions among coral-associated bacteria. *Environ Microbiol* 12(1), 28-39.
Doi: 10.1111/j.14622920.2009.02027.x.

Sachs, J. L., R. G. Skophammer, and J. U. Regus (2011). Evolutionary transitions in bacterial symbiosis. *Proc Natl Acad Sci USA* 108(Suppl. 2), 10800-10807.
Doi: 10.1073/pnas.1100304108.

Sahling, H., D. Rickert, R. W. Lee, P. Linke and E. Suess (2002). Macrofaunal community structure and sulfide flux at gas hydrate deposits from the Cascadia convergent margin, NE Pacific. *Mar Ecol Prog Ser* 231, 121-138.
Doi: 10.3354/meps231121.

Salazar, G., F. M. Cornejo-Castillo, V. Benitez-Barrios, E. Fraile-Nuez, X. A. Alvarez-Salgado, C. M. Duarte, J. M. Gasol and S. G. Acinas (2016). Global diversity and biogeography of deep-sea pelagic prokaryotes. *ISME J* 10(3), 596-608.
Doi: 10.1038/ismej.2015.137.

doi:10.6342/NTU202500809

Salinas, A. E., and M. G. Wong (1999). Glutathione S-transferases—a review. *Curr Med Chem* 6(4), 279-310.

Santos, O. C. S., P. V. M. L. Pontes, J. F. M. Santos, G. Muricy, M. Giambiagi-deMarval and M. S. Laport (2010). Isolation, characterization and phylogeny of sponge-associated bacteria with antimicrobial activities from Brazil. *Res Microbiol* 161(7), 604-612. Doi: 10.1016/j.resmic.2010.05.013.

Sarazin, G., G. Michard and F. Prevot (1999). A rapid and accurate spectroscopic method for alkalinity measurements in sea water samples. *Water Res* 33(1), 290-294. Doi: 10.1016/S0043-1354(98)00168-7.

Scherschel, M., J. O. Niemeier, L. J. Jacobs, M. D. Hoffmann, A. Diederich, C. Bell, P. Höhne, S. Raetz, J. B. Kroll, J. Steinbeck, and S. Lichtenauer (2024). A family of NADPH/$NADP^+$ biosensors reveals in vivo dynamics of central redox metabolism across eukaryotes. *Nat Commun* 15(1), 10704. Doi: 10.1038/s41467-024-55302-x.

Shaumi, A., U. C. Cheang, C. Y. Yang, C. W. Chang, S. Y. Guo, C. H. Yang, T. Y. Chan, and K. L. Pang (2021). Culturable fungi associated with the marine shallow-water hydrothermal vent crab *Xenograpsus testudinatus* at Kueishan Island, Taiwan. *Botanica Marina* 64(4), 289-300. Doi: 10.1515/bot-2021-0034

Shieh, W. Y., Y. T. Lin and W. D. Jean (2004). *Pseudovibrio denitrificans* gen. nov., sp nov., a marine, facultatively anaerobic, fermentative bacterium capable of denitrification. *Int J Syst Evol Micr* 54, 2307-2312. Doi: 10.1099/ijs.0.63107-0.

Shih, S. W., J. J. Yan, Y. L. Tsou, S. W. Lu, M. C. Wang, M. Y. Chou, and P. P. Hwang (2022). In vivo functional assay in fish gills: Exploring branchial acid-excreting mechanisms in zebrafish. *Int J Mol Sci* 23(8), 4419. Doi: 10.3390/ijms23084419.

Shu, Y., P. Hong, D. Tang, H. Qing, O. Omondi Donde, H. Wang, B. Xiao, and H. Wu (2019). Comparison of intestinal microbes in female and male Chinese concave-eared frogs (*Odorrana tormota*) and effect of nematode infection on gut bacterial communities. *MicrobiolOpen* 8(6), e00749. Doi: 10.1002/mbo3.749.

Sievert, S. M. and C. Vetriani (2012). Chemoautotrophy at deep-sea vents: past, present, and future. *Oceanography* 25(1), 218-233. Doi: 10.5670/oceanog.2012.21.

Silverman, H., J. W. Lynn, E. C. Achberger, and T. H. Dietz (1996). Gill structure in zebra mussels: bacterial-sized particle filtration. *Am Zool* 36(3), 373-384. Doi: 10.1093/icb/36.3.373.

doi:10.6342/NTU202500809

Simon, J. (2002). Enzymology and bioenergetics of respiratory nitrite ammonification. *FEMS Microbiol Rev* 26(3), 285-309. Doi: 10.1111/j.1574-6976.2002.tb00616.x.

Smith, C. J., D. B. Nedwell, L. F. Dong and A. M. Osborn (2007). Diversity and abundance of nitrate reductase genes (*narG* and *napA*), nitrite reductase genes (*nirS* and *nrfA*), and their transcripts in estuarine sediments. *Appl Environ Microbiol* 73(11), 36123622. Doi: 10.1128/Aem.02894-06.

Sokolova, I. M., M. Frederich, R. Bagwe, G. Lannig and A. A. Sukhotin (2012). Energy homeostasis as an integrative tool for assessing limits of environmental stress tolerance in aquatic invertebrates. *Mar Environ Res* 79, 1-15. Doi: 10.1016/j.marenvres.2012.04.003.

Staaterman, E., C. B. Paris, H. A. DeFerrari, D. A. Mann, A. N. Rice and E. K. D'Alessandro (2014). Celestial patterns in marine soundscapes. *Mar Ecol Prog Ser* 508, 17-32. Doi: 10.3354/meps10911.

Stein, J. L. (1984). Subtidal gastropods consume sulfur-oxidizing bacteria: evidence from coastal hydrothermal vents. *Science* 223(4637), 696-698. Doi: 10.1126/science.223.4637.6.

Strohm, T. O., B. Griffin, W. G. Zumft and B. Schink (2007). Growth yields in bacterial denitrification and nitrate ammonification. *Appl Environ Microbiol* 73(5), 1420-1424. Doi: 10.1128/Aem.02508-06.

Subramanian, A., P. Tamayo, V. K. Mootha, S. Mukherjee, B. L. Ebert, M. A. Gillette, A. Paulovich, S. L. Pomeroy, T. R. Golub, E. S. Lander, and J. P. Mesirov (2005). Gene set enrichment analysis: A knowledge-based approach for interpreting genome-wide expression profiles. *Proc Natl Acad Sci USA* 102(43), 15545-15550. Doi: 10.1073/pnas.0506580102.

Sun, Y., M. Wang, H. Chen, H. Wang, Z. Zhong, L. Zhou, L. Fu, C. Li, and S. Sun (2023). Insights into symbiotic interactions from metatranscriptome analysis of deep-sea mussel *Gigantidas platifrons* under long-term laboratory maintenance. *Mol Ecol* 32(2), 444-459. Doi: 10.1111/mec.16765.

Szafranski, K. M., B. Piquet, B. Shillito, F. H. Lallier and S. Duperron (2015). Relative abundances of methane- and sulfur-oxidizing symbionts in gills of the deep-sea hydrothermal vent mussel *Bathymodiolus azoricus* under pressure. *Deep-Sea Res I: Oceanogr Res Pap* 101, 7-13. Doi: 10.1016/j.dsr.2015.03.003. Doi: 10.1128/Aem.71.11.7310-7320.2005.

doi:10.6342/NTU202500809

Takai, K., F. Inagaki, S. Nakagawa, H. Hirayama, T. Nunoura, Y. Sako, K. H. Nealson and K. Horikoshi (2003). Isolation and phylogenetic diversity of members of previously uncultivated ε-proteobacteria in deep-sea hydrothermal fields. *Fems Microbiol Lett* 218(1), 167-174. Doi: 10.1111/j.1574-6968.2003.tb11514.x.

Takai, K., H. Hirayama, T. Nakagawa, Y. Suzuki, K.H. Nealson, and K. Horikoshi (2005). *Lebetimonas acidiphila* gen. nov., sp. nov., a novel thermophilic, acidophilic, hydrogen-oxidizing chemolithoautotroph within the 'Epsilonproteobacteria', isolated from a deep-sea hydrothermal fumarole in the Mariana Arc. *Int J Syst Evol Micr* 55(1), 183-189. Doi: 10.1099/ijs.0.63330-0.

Tarasov, V. G., A. V. Gebruk, A. N. Mironov and L. I. Moskalev (2005). Deep-sea and shallow-water hydrothermal vent communities: Two different phenomena? *Chem Geol* 224(1-3), 5-39. Doi: 10.1016/j.chemgeo.2005.07.021.

Thiermann, F., I. Akoumianaki, J. A. Hughes and O. Giere (1997). Benthic fauna of a shallow-water gaseohydrothermal vent area in the Aegean Sea (Milos, Greece). *Mar Biol* 128(1), 149-159. Doi: 10.1007/s002270050078.

Tivey, M. K. (2007). Generation of seafloor hydrothermal vent fluids and associated mineral Ddeposits. *Oceanography* 20(1), 50-65. Doi: 10.5670/oceanog.2007.80.

Toft, C., and S. G. Andersson (2010). Evolutionary microbial genomics: insights into bacterial host adaptation. *Nat Rev Genet* 11(7), 465-475. Doi: 10.1038/nrg2798.

Tokuda, G., A. Yamada, K. Nakano, N. O. Arita and H. Yamasaki (2008). Colonization of *Sulfurovum* sp. on the gill surfaces of *Alvinocaris longirostris*, a deep-sea hydrothermal vent shrimp. *Mar Ecol-Evol Persp* 29(1), 106-114. Doi: 10.1111/j.14390485.2007.00211.x.

Trembath-Reichert, E., D. A. Butterfield, and J. A. Huber (2019). Active subseafloor microbial communities from Mariana back-arc venting fluids share metabolic strategies across different thermal niches and taxa. *ISME J* 13(9), 2264-2279. Doi: 10.1038/s41396-019-0431-y.

Truchot, J. P. (1976). Carbon dioxide combining properties of the blood of the shore crab *Carcinus maenas* (L): carbon dioxide solubility coefficient and carbonic acid dissociation constants. *J Exp Biol* 64(1), 45-57.

Tsuchida, S., Y. Suzuki, Y. Fujiwara, M. Kawato, K. Uematsu, T. Yamanaka, C. Mizota and H. Yamamoto (2011). Epibiotic association between filamentous bacteria and the vent-associated galatheid crab, *Shinkaia crosnieri* (Decapoda: Anomura). *J Mar Biol Assoc UK* 91(1), 23-32. Doi: 10.1017/S0025315410001827.

doi:10.6342/NTU202500809

Tunnicliffe, V. (1991). The biology of hydrothermal vents: Ecology and Evolution. *Oceanogr Mar Biol Ann Rev* 29, 319-407.

Tüzün, N., M. De Block, and R. Stoks (2020). Live fast, die old: oxidative stress as a potential mediator of an unexpected life-history evolution. *Oikos* 129(9), 1330-1340. Doi: 10.1111/oik.07183.

Umam, K., H. J. Chuang, L. Chiu, W. K. Yang, Y. C. Wang, W. Y. Wu, and T. H. Lee (2020). Potential osmoprotective roles of branchial heat shock proteins towards Na^+, K^+-ATPase in milkfish (*Chanos chanos*) exposed to hypotonic stress. *Comp Biochem Physiol A Mol Integr Physiol* 248, 110749. Doi: 10.1016/j.cbpa.2020.110749.

Urnavicius, L., K. Zhang, A. G. Diamant, C. Motz, M. A. Schlager, M. Yu, N. A. Patel, C. V. Robinson, and A. P. Carter (2015). The structure of the dynactin complex and its interaction with dynein. *Science* 347(6229), 1441-1446. Doi: 10.1126/science.aaa4080.

Valentin-Alvarado, L. E., S. C. Fakra, A. J. Probst, J. R. Giska, A. L. Jaffe, L. M. Oltrogge, J. West-Roberts, J. Rowland, M. Manga, D. F. Savage, and C. Greening. (2024). Autotrophic biofilms sustained by deeply sourced groundwater host diverse bacteria implicated in sulfur and hydrogen metabolism. *Microbiome* 12(1), 1-20. Doi: 10.1186/s40168-023-01704-w.

Valenzuela-González, F., M. Martínez-Porchas, E. Villalpando-Canchola and F. Vargas-Albores (2016). Studying long 16S rDNA sequences with ultrafast-metagenomic sequence classification using exact alignments (Kraken). *J Microbiol Meth* 122, 38-42. Doi: 10.1016/j.mimet.2016.01.011.

Valero-Mora, P. M. (2010). ggplot2: Elegant graphics for data analysis. *J Stat Softw* 35, 1-3. Doi: 10.18637/jss.v035.i01.

Van den Heuvel, R. H. H., B. Curti, M. A. Vanoni, and A. Mattevi (2004). Glutamate synthase: a fascinating pathway from L-glutamine to L-glutamate. *Cell Mol Life Sci* 61, 669-681. Doi: 10.1007/s00018-003-3316-0.

Van Dover, C. L. and J. L. Trask (2000). Diversity at deep-sea hydrothermal vent and intertidal mussel beds. *Mar Ecol Prog Ser* 195, 169-178. Doi: 10.3354/meps195169.

Vaucher, R., S. E. Dashtgard, C. S. Horng, C. Zeeden, A. Dillinger, Y. Y. Pan, R. A. Setiaji, W. R. Chi and L. Lowemark (2021). Insolation-paced sea level and

doi:10.6342/NTU202500809

sediment flux during the early Pleistocene in Southeast Asia. *Sci Rep-Uk* 11(1), 16707. Doi: 10.1038/s41598-021-96372-x.

Vetriani, C., J. W. Voordeckers, M. Crespo-Medina, C. E. O'Brien, D. Giovannelli and R. A. Lutz (2014). Deep-sea hydrothermal vent Epsilonproteobacteria encode a conserved and widespread nitrate reduction pathway (Nap). *ISME J* 8(7), 1510-1521. Doi: 10.1038/ismej.2013.246.

Vitvitsky, V., Kabil, O. and Banerjee, R., 2012. High turnover rates for hydrogen sulfide allow for rapid regulation of its tissue concentrations. Antioxidants & redox signaling, 17(1), 22-31. Doi: 10.1089/ars.2011.4310.

Vitvitsky, V., R. Kumar, M. Libiad, A. Maebius, A. P. Landry and R. Banerjee (2021). The mitochondrial NADH pool is involved in hydrogen sulfide signaling and stimulation of aerobic glycolysis. *J Biol Chem* 296, 100736. Doi: 10.1016/j.jbc.2021.100736.

Von Damm, K. L., M. D. Lilley, W. C. Shanks III, M. Brockington, A. M. Bray, K. M. O'Grady, E. Olson, A. Graham, and G. Proskurowski (2003). Extraordinary phase separation and segregation in vent fluids from the southern East Pacific Rise. *Earth Planet Sci Lett* 206(3-4), 365-378. Doi: 10.1016/S0012-821X(02)01081-6.

Yu, G., L. G. Wang, Y. Han, and Q. Y. He (2012). clusterProfiler: An R package for comparing biological themes among gene clusters. *Omics J Integr Biol* 16(5), 284-287. Doi: 10.1089/omi.2011.0118.

Wang, L., M. K. Cheung, H. S. Kwan, J. S. Hwang and C. K. Wong (2015). Microbial diversity in shallow-water hydrothermal sediments of Kueishan Island, Taiwan as revealed by pyrosequencing. *J Basic Microb* 55(11), 1308-1318. Doi: 10.1002/jobm.201400811.

Wang, L., M. K. Cheung, R. L. Liu, C. K. Wong, H. S. Kwan and J. S. Hwang (2017). Diversity of total bacterial communities and chemoautotrophic populations in sulfur-rich sediments of shallow-water hydrothermal vents off Kueishan Island, Taiwan. *Microb Ecol* 73(3), 571-582. Doi: 10.1007/s00248-016-0898-2.

Wang, T. W., T. Y. Chan and B. K. K. Chan (2014). Trophic relationships of hydrothermal vent and non-vent communities in the upper sublittoral and upper bathyal zones off Kueishan Island, Taiwan: a combined morphological, gut content analysis and stable isotope approach. *Mar Biol* 161(11), 2447-2463. Doi: 10.1007/s00227-014-2479-6.

doi:10.6342/NTU202500809

Wang, T. W., D. C. P. Lau, T. Y. Chan and B. K. K. Chan (2022). Autochthony and isotopic niches of benthic fauna at shallow-water hydrothermal vents. *Sci Rep-Uk* 12(1). Doi: 10.1038/s41598-022-09839-w.

Wang, J., Q. Zheng, S. Wang, J. Zeng, Q. Yuan, Y. Zhong, L. Jiang, and Z. Shao (2023). Characterization of two novel chemolithoautotrophic bacteria of *Sulfurovum* from marine coastal environments and further comparative genomic analyses revealed species differentiation among deep-sea hydrothermal vent and non-vent origins. *Front Mar Sci* 10, 1222526. Doi: 10.3389/fmars.2023.1222526.

Watsuji, T., S. Nakagawa, S. Tsuchida, T. Toki, A. Hirota, U. Tsunogai and K. Takai (2010). Diversity and function of epibiotic microbial communities on the galatheid crab. *Microbes Environ* 25(4), 288-294. Doi: 10.1264/jsme2.ME10135.

Wächtershäuser, G. U. N. T. E. R. (1998). The case for a hyperthermophilic, chemolithoautotrophic origin of life in an iron-sulfur world. *Thermophiles: the keys to molecular evolution and the origin of life*, pp.47-57.

Wei, T., V. Simko, M. Levy, Y. Xie, Y. Jin, and J. Zemla (2017). *Package 'corrplot'. Statistician* 56(316), e24.

Wickham, H. (2020). reshape2: Flexibly reshape data: A reboot of the reshape package. R Package Version 1(4)

Wills, C. and Bada, J., 2001. *The spark of life: Darwin and the primeval soup*. Oxford University Press, USA.

Wittinghofer, A., K. Scheffzek, and M. R. Ahmadian (1997). The interaction of Ras with GTPase-activating proteins. *FEBS Lett* 410(1), 63-67. Doi: 10.1016/S0014-5793(97)00321-9.

Yamamoto, M. and K. Takai (2011). Sulfur metabolisms in epsilon- and gamma-Proteobacteria in deep-sea hydrothermal fields. *Front Microbiol* 2, 192. Doi: 10.3389/fmicb.2011.00192.

Yang, S. H., P. W. Chiang, T. C. Hsu, S. J. Kao and S. L. Tang (2016). Bacterial community associated with organs of shallow hydrothermal vent crab *Xenograpsus testudinatus* near Kuishan Island, Taiwan. *Plos One* 11(3), e0150597. Doi: 10.1371/journal.pone.0150597.

Yoo, H., M. R. Antoniewicz, G. Stephanopoulos and J. K. Kelleher (2008). Quantifying reductive carboxylation flux of glutamine to lipid in a brown adipocyte cell line. *J Biol Chem* 283(30), 20621-20627. Doi: 10.1074/jbc.M706494200.

doi:10.6342/NTU202500809

Joyner-Matos, J., B. L. Predmore, J. R. Stein, C. Leeuwenburgh, and D. Julian (2010). Hydrogen sulfide induces oxidative damage to RNA and DNA in a sulfide-tolerant marine invertebrate. *Physiol Biochem Zool* 83(2), 356-365. Doi: 10.1086/597529.

Yucel, M., S. M. Sievert, C. Vetriani, D. I. Foustoukos, D. Giovannell and N. Le Bris (2013). Eco-geochemical dynamics of a shallow-water hydrothermal vent system at Milos Island, Aegean Sea (Eastern Mediterranean). *Chem Geol* 356, 11-20. Doi: 10.1016/j.chemgeo.2013.07.020.

Yurgel, S. N., M. Nadeem, and M. Cheema (2022). Microbial consortium associated with crustacean shells composting. *Microorganisms* 10(5), 1033. Doi: 10.3390/microorganisms10051033.

Zbinden, M., B. Shillito, N. Le Bris, C. D. de Montlaur, E. Roussel, F. Guyot, F. Gaill and M. A. Cambon-Bonavita (2008). New insigths on the metabolic diversity among the epibiotic microbial community of the hydrothermal shrimp *Rimicaris exoculata*. *J Exp Mar Biol Ecol* 359(2), 131-140. Doi: 10.1016/j.jembe.2008.03.009.

Zbinden, M., L. Marqué, S. M. Gaudron, J. Ravaux, N. Léger and S. Duperron (2015). Epsilonproteobacteria as gill epibionts of the hydrothermal vent gastropod *Cyathermia naticoides* (North East-Pacific Rise). *Mar Biol* 162(2), 435-448. Doi: 10.1007/s00227-014-2591-7.

Zeebe, R. E. and Wolf-Gladrow, D. (2001). *CO_2 in seawater: equilibrium, kinetics, isotopes* (Vol. 65). Gulf Professional Publishing.

Zeileis, A., F. Leisch, K. Hornik, and C. Kleiber (2002). strucchange: An R package for testing for structural change in linear regression models. *J Stat Softw* 7, 1-38. Doi: 10.18637/jss.v007.i02.

Zeppilli, D., D. Leduc, C. Fontanier, D. Fontaneto, S. Fuchs, A. J. Gooday, A. Goineau, J. Ingels, V. N. Ivanenko, R. M. Kristensen, R. C. Neves, N. Sanchez, R. Sandulli, J. Sarrazin, M. V. Sorensen, A. Tasiemski, A. Vanreusel, M. Autret, L. Bourdonnay, M. Claireaux, V. Coquille, L. De Wever, D. Rachel, J. Marchant, L. Toomey and D. Fernandes (2018). Characteristics of meiofauna in extreme marine ecosystems: a review. *Mar Biodivers* 48(1), 35-71. Doi: 10.1007/s12526-017-0815-z.

doi:10.6342/NTU202500809

Zerillo, M. M., B. N. Adhikari, J. P. Hamilton, C. R. Buell, C. A. Lévesque and N. Tisserat (2013). Carbohydrate-active enzymes in *Pythium* and their role in plant cell wall and storage polysaccharide degradation. *Plos One* 8(9), e72572. Doi: 10.1371/journal.pone.0072572.

Zhang, Z., D. Liu, B. Yi, Z. Liao, L. Tang, D. Yin, and M. He (2014). Taurine supplementation reduces oxidative stress and protects the liver in an iron-overload murine model. *Mol Med Rep* 10(5), 2255-2262. Doi: 10.3892/mmr.2014.2544

Zhang, J., Q. L. Sun, Z. D. Luan, C. Lian and L. Sun (2017). Comparative transcriptome analysis of *Rimicaris* sp. reveals novel molecular features associated with survival in deep-sea hydrothermal vent. *Sci Rep-Uk* 7, 2000. Doi: 10.1038/s41598-017-02073-9.

Zhukova, N. V. (2019). Fatty acids of marine mollusks: Impact of diet, bacterial symbiosis, and biosynthetic potential. *Biomolecules* 9(12), 857. Doi: 10.3390/biom9120857.

Zierenberg, R. A., M. W. W. Adams and A. J. Arp (2000). Life in extreme environments: Hydrothermal vents. *P Natl Acad Sci USA* 97(24), 12961-12962. Doi: 10.1073/pnas.210395997.

doi:10.6342/NTU202500809

Appendix
Relevant Publications

doi:10.6342/NTU202500809

frontiers | Frontiers in Marine Science

TYPE Original Research
PUBLISHED 02 September 2022
DOI 10.3389/fmars.2022.976255

OPEN ACCESS

EDITED BY
Jin Sun,
Ocean University of China, China

REVIEWED BY
Yan Sun,
Institute of Oceanology, Chinese Academy of Sciences (CAS), China
Benny K. K. Chan,
Academia Sinica, Taiwan

*CORRESPONDENCE
Shan-Hua Yang
shanhua@ntu.edu.tw
Yung-Che Tseng
yctseng@gate.sinica.edu.tw

†These authors have contributed equally to this work

SPECIALTY SECTION
This article was submitted to Marine Evolutionary Biology, Biogeography and Species Diversity, a section of the journal Frontiers in Marine Science

RECEIVED 24 June 2022
ACCEPTED 11 August 2022
PUBLISHED 02 September 2022

CITATION
Chiu L, Wang M-C, Tseng K-Y, Wei C-L, Lin H-T, Yang S-H and Tseng Y-C (2022) Shallow-water hydrothermal vent system as an extreme proxy for discovery of microbiome significance in a crustacean holobiont. *Front. Mar. Sci.* 9:976255. doi: 10.3389/fmars.2022.976255

Shallow-water hydrothermal vent system as an extreme proxy for discovery of microbiome significance in a crustacean holobiont

Ling Chiu[1,2†], Min-Chen Wang[2†], Kuang-Yu Tseng[3], Chih-Lin Wei[1], Huei-Ting Lin[1], Shan-Hua Yang[4*] and Yung-Che Tseng[2*]

[1]Institute of Oceanography, National Taiwan University, Taipei, Taiwan, [2]Marine Research Station, Institute of Cellular and Organismic Biology, Academia Sinica, Yilan County, Taiwan, [3]Department of Life Science, Tunghai University, Taichung, Taiwan, [4]Institute of Fisheries Science, National Taiwan University, Taipei, Taiwan

The shallow-water hydrothermal vent (HV) system off Kueishan Island lies at the end of the Okinawa Trough to the northeast of Taiwan. Near its submarine vent openings, aperiodic vent discharges generate a dynamic acidic (pH 5.5-8.1) and sulfidic (9-3000 μM) ecosystem. The dominant metazoan in this unique environment is the brachyuran vent crab, *Xenograpsus testudinatus*, which has developed robust metabolic strategies and highly adaptive acid-base regulatory mechanisms to maintain its physiological homeostasis. *X. testudinatus* is considered a holobiont, but the symbiotic mechanisms underlying acid and sulfur tolerance in the host-microbe system remain largely unclear. In this study, we used LoopSeq long-read sequencing of the full-length 16S rRNA gene to identify the bacterial communities present in the gills and carapace surface of *X. testudinatus*. The alpha diversity analysis, Venn diagram, and principal coordinate analysis (PCoA) indicated that the gills and carapace surface exhibit different bacterial constituents. Further measurements of relative abundance, coupled with functional predictions and fluorescence *in situ* hybridization (FISH), revealed a predominance of *Sulfurovum* sp. NBC37-1, a key bacterium that can perform sulfur and hydrogen oxidation to support denitrification processes. Consequently, our findings suggest that the symbiotic bacteria may play a critical role in conferring the extraordinary acid and sulfur tolerances of *X. testudinatus*, allowing the crustacean holobiont to thrive in its ecological niche within one of the most extreme marine habitats on Earth.

KEYWORDS

shallow-water hydrothermal vent, brachyuran crab, *Xenograpsus testudinatus*, sulfide-rich fluids, crustacean holobiont, detoxification, *Sulfurovum*, Kueishan Island

doi:10.6342/NTU202500809

LIMNOLOGY AND OCEANOGRAPHY
Letters

ASLO
Open Access

Limnology and Oceanography Letters 9, 2024, 423–432

doi: 10.1002/lol2.10412

LETTER

A two-year physicochemical and acoustic observation reveals spatiotemporal effects of earthquake-induced shallow-water hydrothermal venting on the surrounding environments

Ling Chiu [1,2] *Min-Chen Wang* [1,3] *Chih-Lin Wei* [2] *Tzu-Hao Lin* [4]* *Yung-Che Tseng* [1]*

[1]Marine Research Station, Institute of Cellular and Organismic Biology, Academia Sinica, Yilan County, Taiwan; [2]Institute of Oceanography, National Taiwan University, Taipei, Taiwan; [3]Institute of Physiology, Christian-Albrechts-University Kiel, Kiel, Germany; [4]Biodiversity Research Center, Academia Sinica, Taipei, Taiwan

Scientific Significance Statement

Studies of hydrothermal vents have typically been constrained to occasional observations. This approach is less effective in capturing the dynamic nature of shallow-water hydrothermal vent systems. Our 2-yr study revealed phase transitions in shallow-water hydrothermal activity associated with shallow earthquakes, specifically those occurring near the vents. These transitions are marked by shifts in physicochemical and acoustic conditions of the vent area, resulting in different impacts on the surrounding marine habitats during active and silent venting periods. These findings underscore the importance of higher temporal resolution and consideration of multiple ocean variables in monitoring shallow-water hydrothermal fields, which exhibit significant variability and are concurrently affected by anthropogenic activities, aiding researchers in developing essential strategies for better understanding, managing, and conserving these unique and precious natural resources.

Abstract

Shallow-water hydrothermal vents have gained growing attention for their intricate characteristics caused by various epipelagic factors. The shallow-water hydrothermal system offshore Kueishan Island, Taiwan, situated in an earthquake-prone area, has prompted our exploration into the relationship between hydrothermal and seismic activities. Our 2-yr observation uncovered that the hydrothermal venting entered a silent period in November 2020, followed by a resurgence of activity after September 2021, coinciding with high-frequency shallow earthquakes occurring within 5 km of the vents. The pH level, dissolved inorganic carbon, alkalinity, pCO_2, CO_3^{2-}, and sulfide served as indicators of hydrothermal activity, contributing to environmental changes in habitats

*Correspondence: lintzuhao@gate.sinica.edu.tw; yctseng@gate.sinica.edu.tw

Associate editor: Henrietta Dulai

Author Contribution Statement: LC, M-CW, T-HL, and Y-CT conceived and designed the study. LC and M-CW performed the fieldwork, sample collection, and physicochemical measurement. T-HL did the acoustic data processing. LC, M-CW, and T-HL analyzed the data. LC, M-CW, C-LW, T-HL, and Y-CT wrote the 1st draft and commented on the manuscript. All authors contributed to the article and approved the submitted version.

Data Availability Statement: We made the dataset available on the Dryad repository at https://doi.org/10.5061/dryad.j3tx95xnc (Chiu et al. 2024).

Ling Chiu and Min-Chen Wang contributed equally to this study and are listed as co-first authors.

Additional Supporting Information may be found in the online version of this article.

doi:10.6342/NTU202500809